Final Report

ADVANCED ROCKET ENGINE COOLING CONCEPT PROGRAM

By N. C. Rodewald and H. L. Burge

CASE FILE
COPY

Prepared for

NATIONAL AERONAUTICS AND SPACE ADMINISTRATION

February 1969

UNDER CONTRACT NAS 7-681

TRW
SYSTEMS GROUP

ONE SPACE PARK • REDONDO BEACH • CALIFORNIA

NOTICE

This report was prepared as an account of Government-sponsored work. Neither the United States, nor the National Aeronautics and Space Administration (NASA), nor any person acting on behalf of NASA:

A.) Makes any warranty or representation, expressed or implied, with respect to the accuracy, completeness, or usefulness of the information contained in this report, or that the use of any information, apparatus, method, or process disclosed in this report may not infringe privately owned rights; or

B.) Assumes any liabilities with respect to the use of, or for damages resulting from the use of, any information, apparatus, method or process disclosed in this report.

As used above, "person acting on behalf of NASA" includes any employee or contractor of NASA, or empolyee of such contractor, to the extent that such employee or contractor of NASA or employee of such contractor prepares, disseminates, or provides access to any information pursuant to his employment or contract with NASA, or his employment with such contractor.

Requests for copies of this report should be referred to

National Aeronautics and Space Administration
Scientific and Technical Information Facility
P.O. Box 33
College Park, Md. 20740

NASA CR-72594

Final Report

ADVANCED ROCKET ENGINE COOLING CONCEPT PROGRAM

By N. C. Rodewald and H. L. Burge

Prepared for

NATIONAL AERONAUTICS AND SPACE ADMINISTRATION

February 1969

UNDER CONTRACT NAS 7-681

TRW

SYSTEMS GROUP

ONE SPACE PARK • REDONDO BEACH • CALIFORNIA

FOREWORD

This report was prepared by the Science and Technology Division of the TRW Systems Group at One Space Park, Redondo Beach, California, under contract NAS 7-681. The contract was administered by the Lewis Research Center of the National Aeronautics and Space Administration, Cleveland, Ohio. This is the final report on activity conducted from July 1968, through January 1969. The NASA project manager was Mr. E. Edelman of the Liquid Rocket Technology Branch.

The following personnel at TRW contributed to the technical accomplishments:

Sam Van Grouw   Larry Hynek

Ken Mock   Jon Augustson

ABSTRACT

The results and evaluations of an experimental investigation of the feasibility of an advanced cooling concept using liquid foams for film cooling of a rocket engine are presented. The experimental investigation consisted of laboratory tests to confirm the high pressure existence of water fire-fighting foams and amine foams, and heat transfer tests of the concept in 3000 lb_f, 300 psia heat sink and acrylic engines. In one test, a rocket engine 25.5 inches long was completely cooled to the saturation temperature of the coolant while maintaining a high coolant efficiency. It was concluded that foam has superior anti-streaking characteristics and higher cooling capacities than its unfoamed liquid.

SUMMARY

An experimental investigation into the feasibility of a new adaptation of rocket engine liquid film cooling has been made. Liquid film cooling becomes extremely attractive for very large thrust engines where the percent coolant required reduces to less than 1 percent of the total propellant flow level and because the coolant itself may add to the overall impulse. Unfortunately, through, liquid cooling efficiencies greater than 30 percent are seldom achieved in controlled laboratory heat transfer experiments because the liquid is subjected to severe gas - liquid interface shear stress which results in wave stripping and streaking at typical rocket engine Reynolds numbers. There appears to be good potential applications for liquid film cooling if this major shortcoming can be overcome.

This investigation was directed at evaluating the feasibility of foamed liquid as a potential means of overcoming the low cooling efficiencies and streaky coverage of conventional liquids. Potential improvements in cooling efficiency and coverage could result from the unusual properties of foams:

- Thermal conductivities approaching those of the parent gas which should result in excellent thermal insulation capability

- Viscosities over an order of magnitude greater than those for the parent liquid which should minimize liquid stripping

- Improved ability to cling and spread brought about the reduced reduced surface tension of the liquid

- Significantly reduced density allowing much larger coverage per given quantity of fluid

- Improved radiation heat resistance brought about by improved reflectivity of foam.

A two-part experimental program was devised to evaluate the feasibility of foam film cooling. The first part consisted of cold flow testing and preliminary foam evaluation tests at high pressure to confirm the existence of foams under pressure. The second part of the investigation was directed at determining the efficiency, stability, and streaking characteristics of sundry foamed and nonfoamed coolants at 300 psia in the subsonic, sonic, and supersonic flow regimes of a typical 3000 lb_f rocket engine.

Preliminary evaluations of several water fire-fighting foams and a N_2H_4 foam were conducted in a glass venturi flowing 300 psia gas at typical rocket engine Reynolds numbers. The existence of a good guality foam at these pressures and the ability of a foam to persist for distances at least 25 inches in the subsonic, sonic, and supersonic regions of the glass venturi were visually confirmed.

Heat transfer tests were then conducted with several of the water fire-fighting foams in heat sink and acrylic rocket engines. The engine design was flexible so that variations could be made in chamber length, injector type, or propellant combination.

A general evaluation of the results from 41 tests indicated:

- The stable existence of foam in the hostile environment of combustion and flow regimes of a rocket engine

- Foam cooling efficiencies ranging from 50 to 70 percent could be achieved for propellant combinations having good combusion characteristics. In one test, a rocket engine 25.5 inches long was completely cooled to the saturation temperature of the coolant

- A protein fire-fighting foam at an expansion ratio of from 20 to 30 gave superior cooling efficiencies over other foaming agent types

- Foams in general possess higher effective cooling capacities and superior anti-streaking characteristics than nonfoamed liquids

- Film cooling efficiencies are strongly influenced by combustion interactions

- The coolant, even though nonreactive, did not significantly degrade the performance of the engine.

A generalized correlation for film cooling in the combustor section of a rocket was developed and used to extrapolate the results of this study to large engine sizes where it is predicted that the fraction of coolant to propellant will drop to negligible quantities.

CONTENTS

ILLUSTRATIONS

ILLUSTRATIONS (Continued)

ILLUSTRATIONS (Continued)

ILLUSTRATIONS (Continued)

ILLUSTRATIONS (Concluded)

TABLES

1. INTRODUCTION

Over the past 15 years little progress has been made in the advancement of liquid film cooling, although thrust chamber heat transfer problems have increased with the use of high engine pressures and high energy propellant combinations. Liquid film cooling becomes extremely attractive for very large thrust engines where the percent of coolant required reduces to about 1 percent of total propellant flow level.

A cursory literature search and analysis were made for conventional liquid film cooling. Cooling efficiencies greater than 30 percent are seldom achieved in controlled laboratory heat transfer experiments because the liquid film is subjected to severe shear stress which results in wave stripping at typical rocket engine Reynolds numbers. Practical liquid film cooling can only be achieved by a multiplicity of closely spaced injection ports. There appears to be good potential application for liquid film cooling if the major inefficiency can be overcome.

In early 1968 TRW Systems conducted an investigation into the use of foamed liquids as potential film coolants. The first step in evaluating foams as film coolants was to make a comprehensive literature and state-of-the-art survey. Unfortunately, only very few references of any value were found. Fire fighting foams seemed to be the predominant application area. The literature did show, however, that foams do possess many unusual properties such as:

- Thermal conductivities approaching those of the parent gas

- Viscosities over an order of magnitude greater than those for the parent liquid

- Improved ability to cling and spread brought about by the reduced surface tension

- Significantly reduced density allowing much larger surface coverage per given quantity

- Improved radiation heat resistance brought about by improved reflectivity of foam

These properties appeared to be ideally suited to the improvement of film cooling.

An in-house experimental research program was devised to demonstrate the technical feasibility of foam film cooling. The objectives of the study were to:

- Evaluate the feasibility of foam film cooling

- Investigate foam requirements

- Investigate foam stability properties

- Determine chemical sensitivity in earth storable fuels

- Investigate foam generation techniques

Experimental tests in nominal 100 lb_f 86 psia, N_2H_4 - N_2O_4 heat sink and plexiglass engines gave positive results for all the objectives:

- Foam cooling rates as low as 2 wt-percent of the total propellant flow were demonstrated to maintain engine wall temperatures throughout a coolant saturation temperature at high cooling efficiency.

- The foam film was observed in plexiglass and glass engines in subsonic and supersonic flow regions under typical cold flow and combustion temperatures and was found to be stable (no stripping).

- Typical fire fighting foaming agents were found to be compatible with the hydrazine family of fuels. In particular, hydrazine was found to form a very stable foam with a polymer agent.

- Several foam generation and injection techniques were demonstrated.

Following these highly successful investigations, the current program was initiated to provide additional feasibility evaluation of the concept in longer hardware and higher pressures.

Prior to the time the current foam program was initiated, TRW Systems was awarded a contract (FO4611-68-C-0054) from Air Force Rocket Propulsion Laboratory, Edwards, California to develop and demonstrate a 3000 lb_f thrust N_2O_4/N_2H_4 injector at a nominal 300 psia chamber pressure. For the foam feasibility study program it was proposed to conduct the foam tests, using tested and proven designs from the Air Force program. Separate hardware of identical design was fabricated for the foam tests.

In summary, the overall objective was to conduct a parametric feasibility study to determine the efficiency, stability, and streaking characteristics of sundry foamed and nonfoamed coolants at 300 psia in the subsonic, sonic, and supersonic flow regimes of a typical rocket engines. The major parameters to be investigated were: type of liquid, type of foaming agents, foam expansion, flow rate, and injection velocity.

To accomplish the overall objectives the program was divided into three tasks:

Task I   Design and fabrication of rocket engine components, foam generator, and foam injector

Task II   Cold flow testing and preliminary foam evaluation
          tests at high pressure

Task III Heat transfer tests for two chamber (L/D) variations,
          two injectors

        One injector would be a TRW coaxial injector, and the second would
be a NASA supplied injector.

2. BACKGROUND SUMMARY ON FOAMS AND LIQUID FILM COOLING

The following discussion is presented to provide descriptive terminology and background data on liquid foams as they pertain to liquid rocket engine cooling.

2.1 FOAM TECHNOLOGY STATE OF THE ART AND DISCUSSION

Foams have been defined in many colorful ways such as: "... honeycombed structure of gas in liquid, " "... millions of bubbles within a liquid, " or more scientifically as "agglomerations of gas bubbles separated from each other by thin liquid films. "

The scientific aspects of foam have been studied for many years and are set forth in several books and review articles (References 1, 2, and 3). However, the engineering state of the art of foams is not well advanced as evidenced by the fact that only a meager number of treatises dealing with foam fluid flow, heat, and mass transfer (References 4 to 9) are found in the Engineering Index under the headings of foams, fire fighting ing, and rocket cooling. Many more articles relating to the practical engineering aspects of fire-fighting foams can be found (References 10 through 19). Hence, it is readily apparent that fire fighting foams are the predominant application area. A check of the Thomas Registry under foam generators and fire extinguisher charges and recharges confirmed this first finding as five local foam fire equipment distributors were listed. Review meetings were held with several of these representatives to ascertain the hardware state of the art and to help formulate a technical approach. It was concluded that the easiest approach to evaluating foam film cooling would be to utilize as much foam fire fighting technology and equipment as practical and to concentrate on using fire fighting foam (water and foaming agent and air) rather than pursuing the detailed development of propellant foaming technology. From this survey promising commmmercial foaming agents were selected for the amine fuels.

2.1.1 Foaming Parameters

The most important foaming parameters are listed below:

- Type of applicable foaming agent: protein, detergent, and polymer

- Concentration of foaming agent

- Expansion ratio of foam $(V_g + V_L)/V_L$

- Ultimate shear stress

- Gas constituent

During the past 20 t0 30 years foam agent technology has made great strides. The predominant type of foaming agent that has evolved as the best is a protein hydrolysate made from, for example, hoof and corn meal, soybeans, animal blood, or fish meal (Reference 17). The finished product, which contains additives such as a bactericide to forestall putrefication, freezing point depressants for temperature as low as -40°F, or metal salts to increase bubble strength, becomes a concentrated liquid to be added to water at a rate of 3 or 6 percent. An excellent review of storage life and utility of protein type foaming agents under various environments is given in Reference 17. Most agents meet certain military specifications and in one instance liquids were in good condition after 15 years or more.

In the past several years many new types of foaming agents have been developed and marketed. National Foam System, Inc. (References 18 and 19), perfected a foamed polymeric film produced by agitating with air a solution of water and a linear low molecular weight polymer which is further reacted by a catalyst in the presence of air. The foam was specifically developed to combat alcohol and amine type fires. The protective inert polymeric film is resistant to solvent attack to which the protein films are not. The foaming agent is marketed in two separate containers — a 20 percent concentrate and a 3 percent catalyst. The polymeric foam may be stored as a pre-mixed solution, which has the appearance and properties of a liquid gel.

Another industrially important foaming agent is a synthetic detergent type which, when added to water, is capable of forming a truly high expansion foam of approximately 1000 parts of air by volume to 1 part of liquid. This represents approximately two-orders-of-magnitude increase in expansion over that for the conventional protein or polymeric formula. The synthetic detergent is added to water to make a 1.5 percent solution.

The concentration of the foaming agent affects the stability and heat resistance of the foam if concentrations less than those specified in the preceding paragraphs are used. The basic effect of the foaming agent is to dramatically reduce the surface tension of the water until the optimum concentration is reached. A rapid variation of surface tension with surface active agent concentration is fundamental to the ability of a liquid to foam.

The ratio of the volume of foam (gas plus liquid) to the volume of the liquid is another fundamental foam parameter and is called the "expansion factor." Expansion factor can also be expressed as foam density and primary effects of temperature and pressure of expansion factor or foam density can be estimated from the ideal gas law. Laboratory studies (References 4, 8, 14, and 16) show that physical properties such as thermal conductivity, viscosity, and drainage (stability), vary widely with expansion factor as is discussed later.

The size of the gas bubble for a given expansion ratio governs the foam's ultimate shear stress which is a measure of foam resistance to flow under no-flow conditions. This is contrasted to liquid which typically exhibits no ultimate shear stress. French (Reference 11) observed the

heat resistance of the foam to increase markedly with increased ultimate
shear stress. The optimum expansion ratio as measured by the heat
resistance index for constant values of shear stress appeared to be con-
stant at approximately 16. It is not known how bubble size affects vis-
cosity or other physical properties of the foam, but one can conjecture
that the effect will be substantial.

The type of gas constituent is not treated in any great detail in the
literature, probably because it is a secondary parameter.

2.1.2 Unique Properties of Foams

There are many properties of foams which may make them unique
as film coolants. First, an example of the thermal conductivity of foam
as a function of expansion ratio is given in Table 1 (Reference 4). Obvi-
ously, thermal conductivity of the foam is almost a function of the sum
of the respective volume fractions of air and water. Apparently, the
bubble size effect on thermal conductivity was not investigated.

Table 1. Thermal Conductivity of a Typical Foam as a Function
          of Expansion Ratio (Nominal Temperature 80°F)

Expansion Ratio*	Btu/hr °F ft	
	Exp	Theor
0 (water)	0.350	---
7.5	0.120	0.105
11.0	0.113	0.094
19.0	0.080	0.046
∞(air)	0.0156	---

* $(V_L + V_g)/V_1$

The effect of pressure (in other words, expansion ratio or foam
density) on viscosity is shown in Figure 1 as taken from Reference 8.
At an expansion ratio of approximately 6, the viscosity of the foam is
approximately 24 times greater than that for water. Grove studied only
one foaming agent type and one concentration level. He did not report
varying the bubble size (ultimate shear stress) which may be a primary
variable.

6
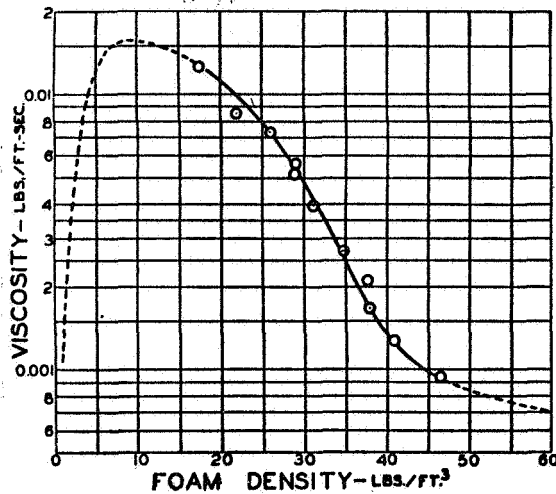
Figure 1. Effect of Pressure on Foam Viscosity

The experimental data of French (Reference 11), a measure of the radiation heat resistance of foam, was correlated by Thomas (Reference 12), as shown in Figure 2. In this dimensionless plot, the relative heat resistance of foam to water — as measured by the ratio of the time for a fixed radiated heat flux to destruct a given quantity of foam to that calculated to vaporize an equivalent quantity of water — is plotted against a multiple of the expansion factor and critical shearing strength. The ratio h is defined by

$$h' = \frac{\Theta F' \; Exp}{d\rho H_s}$$

where

Θ = Measured destruction time for the foam

Exp = Expansion of the foam (ratio, by volume, of foam to liquid)

F' = Applied radiation flux

d = Depth of foam in the sample

ρ = Density of water

H_s = Total heat (enthalpy) per unit mass of steam at 100 degrees and atmospheric pressure

Expansion × critical shearing strength = $Eq \times 10^{-8}$ dyne cm.$^{-2}$

Relative heat-resistance = $h' = \dfrac{\Theta Exp \; F'}{d\rho H_s}$

Expansion		Expansion	
o	5·7	□	13·5
×	7·2	●	19·0
+	9·0		
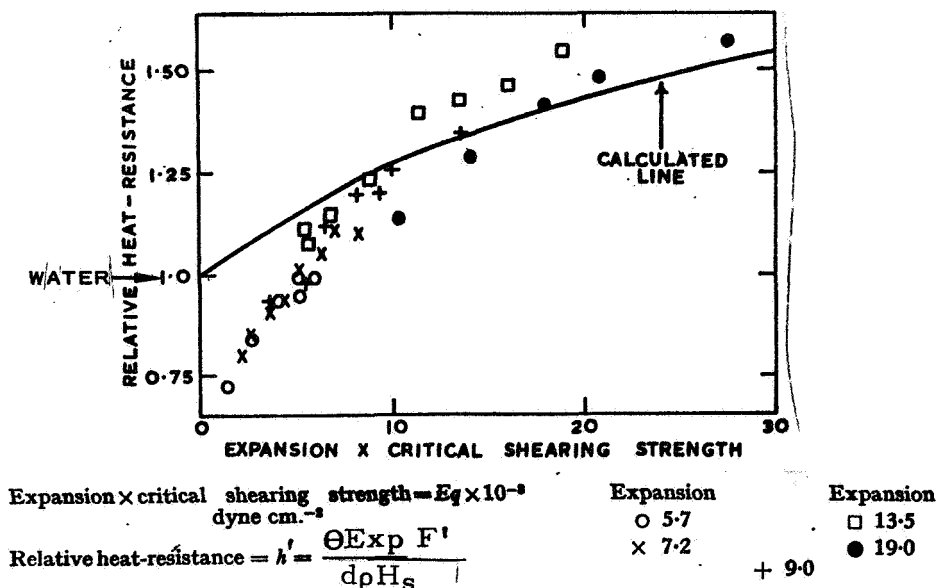
Figure 2. Heat Resistance of Foam of Different Shearing Strengths and Expansions

The increase in heat resistance can be interpreted as an improvement in reflectivity of the foam. The decrease in the heat resistance at low abscissa values was interpreted to be caused by the reduced drainage resistance of the foam.

The metastable nature of foams is illustrated in Figure 3 in the form of a plot of time versus percent liquid drained for several types of foams. Most fire fighting foams exhibit drainage behavior as-good-as or better-than that shown by curve 1. National Foam System, Inc., reports an almost infinite drainage time for their polymeric foams. However, the foam film will have a short resident time in any rocket engine application and thus drainage behavior may be insignificant.
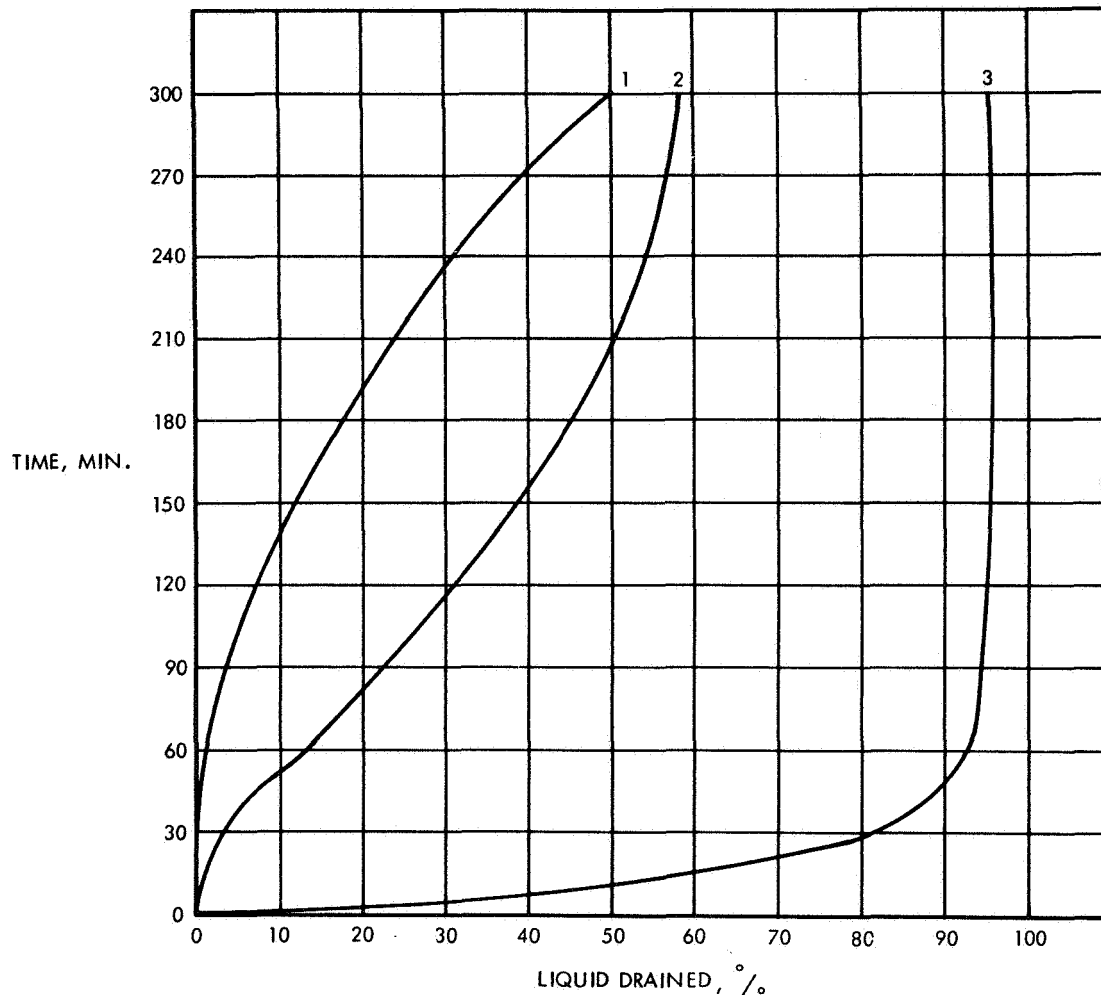
Figure 3. Drainage Behavior of Foams at 27 ±2°C (Foams Generated from 3 percent Soln at 40 lb/sq in Pressure; Foam Density 0.1 g/ml Air-Foam I; Air-Foam II, Pyrene II)

Another beneficial and unique property of a foam is its ability to cling and spread while retaining excellent thermal resistance. The ability of a foam to spread and cling is primarily because of its reduced external surface tension. The reduced external surface tension allows quick sealing of breaks (Reference 1). The external surface tension is not to be confused with the internal surface tension which is reported to vary if the foam is stretched (Reference 2). A better interpretation of the latter may be to say that foam typically exhibits a tensile strength.

Another unique property of foam which is easy to overlook is its reduced density. The lightness of the foam also adds to its ability to cling to surface and allows for a much larger surface coverage per given quantity.

2.2 METHODS OF PRODUCING FOAMS

Methods of producing foams may be classified as chemical or mechanical. Foams may be produced by the chemical reaction of two solutions — one containing a foaming agent — to form a carrier gas, which fills each tiny bubble. Chemical foam making techniques have been replaced almost completely by simpler and cheaper mechanical methods of making foam. Gas-liquid proportioning/mixing/agitating may be accomplished by aspiration or pumping, as described in Reference 19. Fry and French, Reference 14, describe a simple laboratory mechanical foam generation method which permits easy variation of foam parameters. In this method, a liquid and foaming agent are premixed and stored in a suitable pressure vessel. Compressed air serves as a pressurizing gas; flow rates were indicated by rotometers and metered by needle valves and impinged in a tee arranger, the outlet being connected to a union containing a series of screen. The size and number of screens could be varied to obtain any desired bubble size and, hence, ultimate shear stress. The bubble size was also shown to vary with liquid flow rate and ratio of air flow to liquid flow through the screen improver. This method was found to also be satisfactory by a later investigator (Reference 16).

2.3 BASIC FILM COOLING RESULTS

There are a large number of well conducted liquid film cooling studies, both in the laboratory and in rocket engine experiments. In general, these results show that the actual mechanical efficiency of the coolant is limited to 30 - 40 percent for a single injection point with the best of injection geometry designs. In Reference 20 quite detailed studies were conducted for a variety of geometries to verify this upper limit. Figure 4, taken from Reference 21 shows results for a laboratory investigation of water injection in high speed air. At the upper end of the curve the Reynolds number is approximately that of a rocket engine, and it is seen that the apparent mechanical effectiveness is 35 to 40 percent. The cause of this reduced effectiveness has been determined to be that of unstable wave cresting and stripping by gas induced shear forces, as illustrated in Figure 5. An examination of fundamental interaction forces
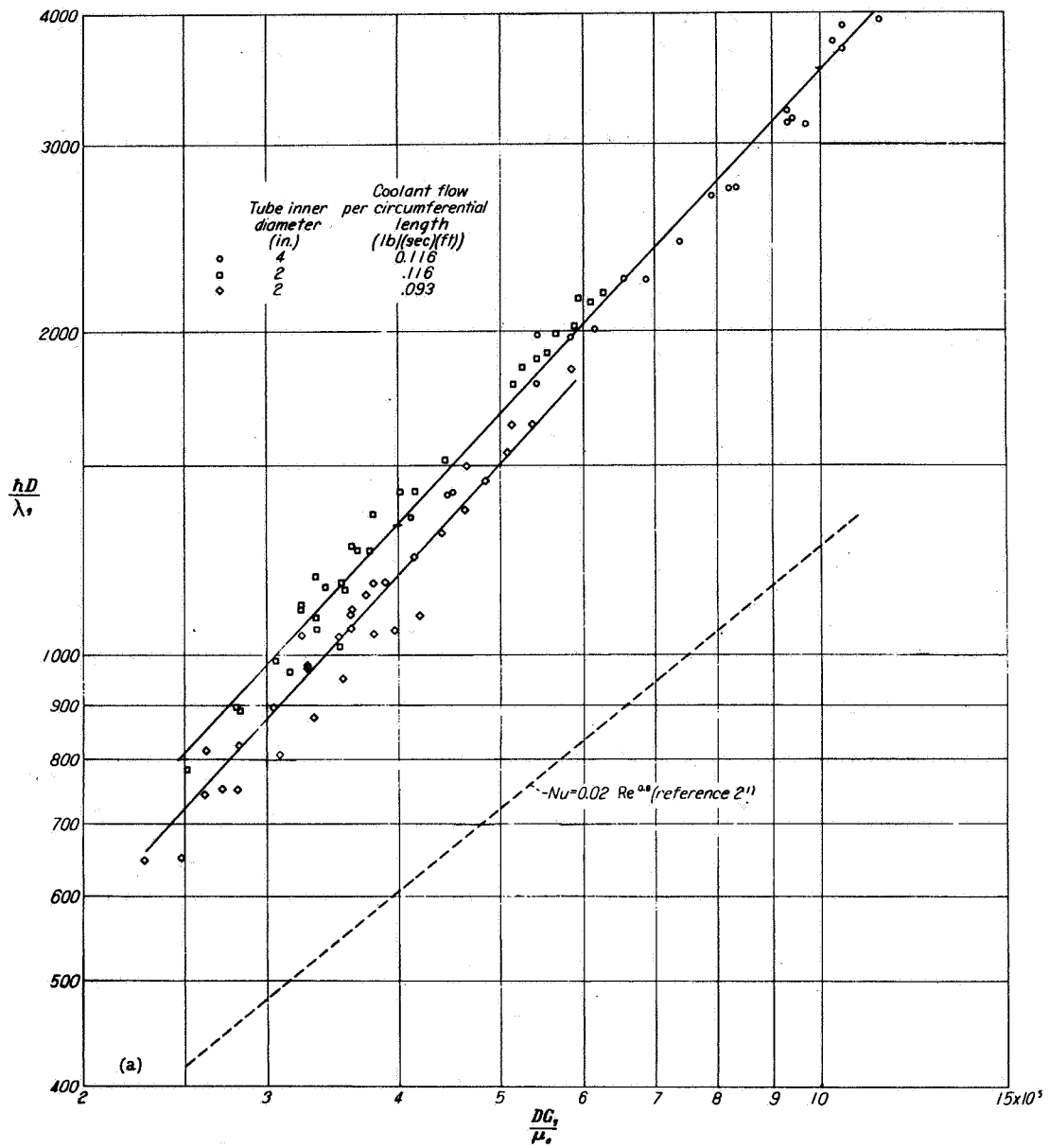
(a) Smooth-surface tubes of 2- and 4-inch diameter. Air temperatures, 800° to 2000°F; air-mass velocities, 39.4 to 81.7 pounds per second per square foot.

Figure 4. Correlation of Heat Transfer From Air Stream to Water Film at Constant Coolant Flow per Circumferential Design

10

indicates that to stabilize the liquid system its viscosity must be increased. In addition the effective bulk surface tension must be elevated to promote resistance to wave stripping, Figure 6. Foamed liquids appear to possess these qualities.

With the above discussion in mind the next sections describes the hardware design and approach to the feasibility demonstration program.

GAS VELOCITY

Heat Flux

Ideal Case

Mass Transfer

$$\int \frac{Q}{A} (x)\, dx = \dot{w}_f \left[c_p [T_s - T_i] + \Delta H_{fg} + \ell_p (T_r - T_s) \right]$$

Gas Velocity

Wave Stripping

Actual Case

$$\int \frac{Q}{A} (x)\, dx = \eta_M \, \dot{w}_f \, \Delta H$$

$\eta_M \sim 0.30 - 0.40$ Independent of Injection Scheme
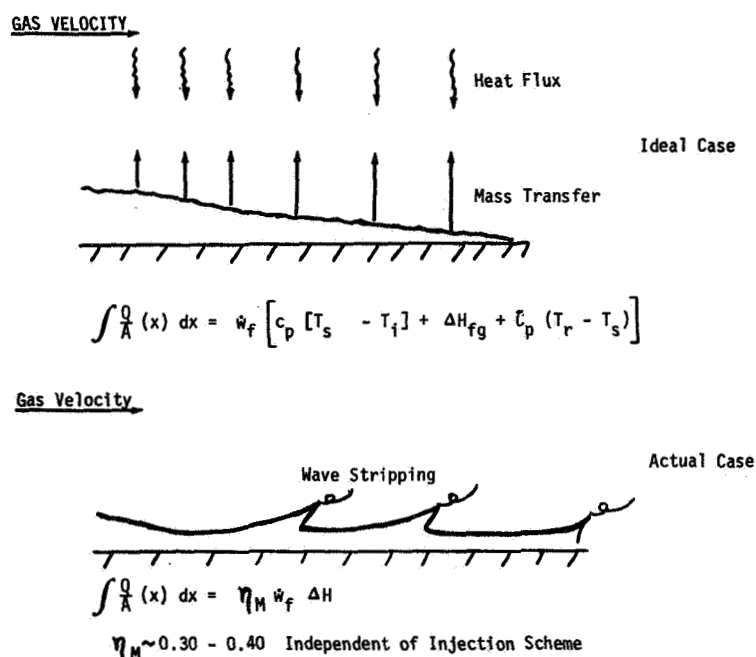
Figure 5.   Liquid Film Cooling Model

RESISTANCE TO SHEAR

Gas

Liquid
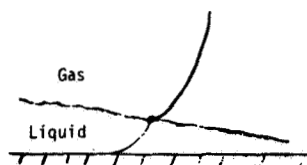
SHEAR $\sim \mu \frac{du}{dy}$ $\therefore$ Increase μ

RESISTANCE TO STRIPPING
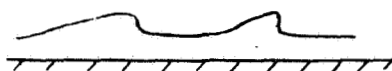
RESISTANCE $\sim \frac{v^2 b}{\sigma}$ $\therefore$ Increase σ

THERMAL RESISTANCE AND THERMAL STABILITY

WELL BEHAVED FLOW $Q \sim \lambda \frac{dT}{dy}$ $\therefore$ Decrease λ

RESPONSE $\exp[-c \alpha t] - \tau \frac{1}{c\alpha}$ $\therefore$ ESTABLISH τ AT ABOUT 10 TIMES ENGINE τ

Figure 6.   Film Stabilization Requirements

3. HARDWARE

3.1 PRELIMINARY EXPERIMENTAL DESIGN ANALYSIS

In order to properly design the scaled experimental hardware and provide a basis for component design, specification of instrumentation, and understanding of the results of the feasibility study, a preliminary analysis of scaling between the TRW 100 lb_f in-house tests and the feasibility studies was undertaken. This scaling was based on the use of available heat transfer data from the Air Force program, Contract FO 46 11-68-C-0054, from which the basic test engine configuration was developed.

3.2 HARDWARE DESIGN AND DESCRIPTION

3.2.1 Heat Transfer

The heat transfer calculations were made to investigate the expected relevant differences in foam film cooling between the 100 and the 3000 lb_f engines. Table 2 gives the nominal engine conditions for the thrust chamber built for the Air Force program. The relative difference in local heat flux for the two chambers is shown in Figure 7. Curve A represents a prediction, based on the Bartz short form technique. Experimental heat transfer data from the Air Force program confirm the theoretical predicted heat fluxes as chamber heat fluxes were observed to be constant at approximately 2.5 to 2.0 Btu/in^2-sec, while the maximum throat heat flux ranged to approximately 7 Btu/in^2-sec. Chamber recovery temperature was estimated at 3000 $\pm200^\circ$F. Table 3 gives a summary comparison of results of heat transfer areas. When the results of Table 3 and Figure 7 are considered relative to each other, order of magnitude differences in total heat load are noted. It is obvious that the planned tests in a 3000 lb_f, 300 psia engine could be expected to be a severe test of the efficiency, stability, and antistreaking resistance of the foam film. These heat fluxes were used to determine approximate required foam flow rates for the feasibility demonstration program, as well as other pertinent foam design data.

3.2.2 Liquid Foam Stability

One of the main purposes of this program was to experimentally determine the susceptibility of foam to stripping and bubble collapse (foam stability). Those major factors which affect foam stability include:

- Rate of heat transfer

- Film thickness

- Foam properties

Order-of-magnitude increases in the total rate of heat transfer are indicated from the above comparisons. It is known from visual experiments that heat will cause the temperature of the liquid and gas in the foam bubble

Table 2. Nominal 3000 lb$_f$ Engine Conditions

Chamber diameter	6 . 0 in.
Chamber length	7 . 85 in.
Chamber L*	40.
Throat diameter	2 . 7 in.
Chamber material	
Chamber	1018 hr/Lucite
Throat	OFHC Copper/Lucite
Chamber pressure	300 psia
Propellants	N_2O_4/N_2H_4
Mixture ratio	0.9 to 1.4
Total flow	~10 lb/sec

Table 3. Comparison of Relevant Heat Transfer Parameters

Engine Part	86 psia 100 lb$_f$ Engine	300.0 psia 300 lb$_f$ Engine	
	Internal Length, Inches		
Chamber	2.0	7.85	15.70*
Throat	2.45	9.75	9.75
	4.45	17.60	25.45*
	Area, In^2		
Chamber	12.6	148	296*
Throat	9.8	116	116
	22.4	264	412*

---

*Two chamber lengths
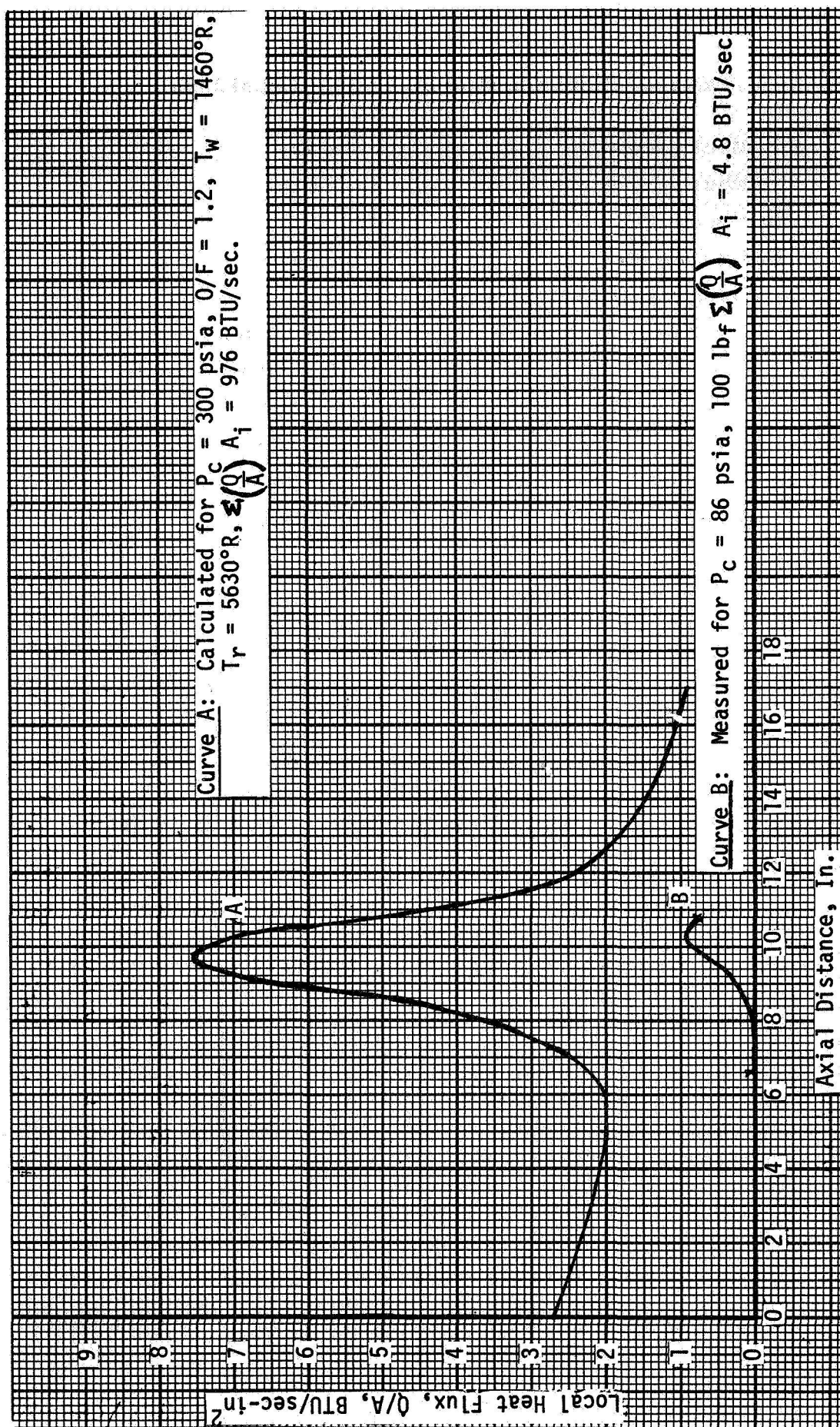
Figure 7. Comparison of Local Heat Fluxes for a 100 lb_f 86 psia
Engine and a 3000 lb_f, 300 psia Engine

14

to increase, with resulting gas expansion and liquid vaporization. Hence, the foam bubble will expand and eventually rupture, since foaming agents are capable of supporting some fixed maximum expansion. At increased heating rates it is suspected that large bubble foams will be less stable than small bubble foams; therefore, in generating foams for high heat flux applications the foams must be tailored to small bubble sizes.

Another factor of importance is the expected foam blanket thickness. What effect this will have on foam stability is unknown, although it is known that liquid cooling efficiencies decrease with film thickness for liquid film cooling. An estimate of the relative change in foam film thickness for the 100 lb_f engine versus the 3000 lb_f engine can be made as follows:

$$\frac{\dot{w}_{c1}}{\dot{w}_{c2}} = \frac{\rho_1 \, A_1 \, \nu_1}{\rho_2 \, A_2 \, \nu_2}$$

if $\nu_1 = \nu_2$ and $\rho_1 = \rho_2$

$$x_2 = x_1 \cdot \frac{D_1}{D_2} \cdot \frac{\dot{w}_{c2}}{\dot{w}_{c1}}$$

$$= x_1 \cdot \frac{2}{6} \; \frac{1.4}{.35 \, (.02)} = 67 \; x_1, \quad \dot{w}_{c2}/\dot{w}_{c1} \; \text{are evaluated from integrated heat loads.}$$

Thus, it can be seen that if other things are equal, the foam film thickness will increase more than an order of magnitude.

It is surmised that beneficial cooling properties (enhanced stabilities) are derived from the myriad properties of foams which are vastly different than the parent liquid. Little theoretical or experimental evidence appears in the literature on how such foam properties as thermal conductivity, viscosity, surface tension, and ultimate shear stress vary with pressure, temperature, bubble size, or density. It is suspected that these properties do not vary significantly with pressure with properly generated foams and thus one can expect no large change in foam stability with pressure or temperature.

3.2.3 Streaking

Streaking is the undesirable phenomenon which results when the protective film separates and exposes part of the engine to the hot gas stream. Then, unfortunately, localized hot spots can bootstrap themselves to other parts of the engine. Among the factors which are known to influence streaking are:

- Length of distance to be traveled
- Film thickness

- Coolant injector distribution characteristics
- Combustion/injector characteristics
- Coolant properties

Table 3 gives the relevant changes in flow path length and heat transfer area for the 100 and 3000 lb$_f$ hardware. No coolant streaking was observed in the previously conducted TRW in-house small engine tests, but as is readily apparent, the proposed tests could severely test the anti-streaking capabilities of the foam.

To gain some insight into film thickness as a function of expansion ratio, flow rate, and film velocity, Table 4 was prepared to aid in design. The film thickness for a liquid is extremely small and undoubtably forms the basis for streaking. It is surmised that the addition of a gas to the liquid can serve to overcome this problem. The continuity equation

$$\dot{w}_c = \rho \ A \ V$$

was used to make these calculations.

Table 4. Parametric Study of Foam Film Thickness
at 300 psia, for a 3000 lb$_f$ Engine

$$\dot{w}_{coolant} = 10\% \text{ of total propellant flow}$$

Expansion Ratio	Velocity, ft/sec			
	10	20	50	100
		inches		
1 (Liquid)	0.0123	0.00615	0.00246	0.00123
5	0.056	0.0279	0.0112	0.00559
10	0.101	0.0504	0.0201	0.0101
50	0.280	0.140	0.056	0.0280
100	0.360	0.180	0.072	0.0359

Coolant injector gaps have a marked effect on the distribution and hence streaking resistance of the coolant. Table 4 shows that the typical injector continuous annulus for unfoamed liquid will be extremely small. Because of the difficulty in maintaining precise tolerances in severe environments, it is concluded that liquid coolants are difficult to inject evenly. Experience has led to discrete holes and various spreading design geometries. The results in Table 4 show that for any expansion ratio of interest, continuous annular gaps of quite reasonable dimensions can be expected with foam injection. As such streaking due to injection geometry should be minimized.

16

It is known that foams have properties which make them streaking resistant when compared to nonfoamed coolants. These properties consist of reduced surface tension which leads to improved adhesion, greatly increased internal cohesion (tensile strength) which leads to tear resistance, and increased fluidity which means the ability to flow and seal up tears in the coolant film. In order to fully realize these properties it is necessary to consider other possible adverse effects.

As a practical design matter it is also necessary to match combustion chamber/injector interactions to the film coolant injection point, since adverse interactions at the point of injection can result in greatly diminished film cooling efficiency. In addition practical experience with rocket engine film and transpiration cooling has shown that combustion and associated injector characteristics can adversely affect film coverage by streaky combustion, wall zone turbulence, and overall combustion noise.

3.2.4 Component Design

Design and analysis for the main injector, chamber throat, and instrumentation were considerably reduced in scope because of prior effort on the Air Force program. The previous in-house effort on foam injector and generator design helped to expedite the design and fabrication of these components. Thus this effort was reduced to one of scaling up previously known viable designs.

3.2.4.1 Injector Hardware

Two injectors were utilized for this program. These were the TRW coaxial flow and a NASA-supplied flat face triplet design. The coaxial design was essentially that developed on Air Force contract FO4611-68-C-0054 for N_2O_4/N_2H_4. The NASA injector had been modified for, but had not been previously tested with, N_2H_4.

Figure 8 shows the details of the TRW coaxial injector. Thirty-six primary and secondary oxidizer streams are thrown radially outwards from the oxidizer orifice ring and impinge upon an annular sheet of fuel. Injector pressure drops control the angle of the resultant stream. Generally, the fuel propellant is in excess at the chamber wall and thus provides film cooling and a resultant low recovery temperature. With this injector it was possible to adjust the fuel and oxidizer injection characteristics.

Figure 9 is a close-up photograph of the flat face injector supplied by NASA, and Table 5 summarizes its characteristicss. This particular injector had performed quite well with NTO/50-50 for long duration. The major uncertainty in modification revolved around whether this injector could withstand the increased pressure. Hence, the injector was subsequently supported by a back-up plate.

17
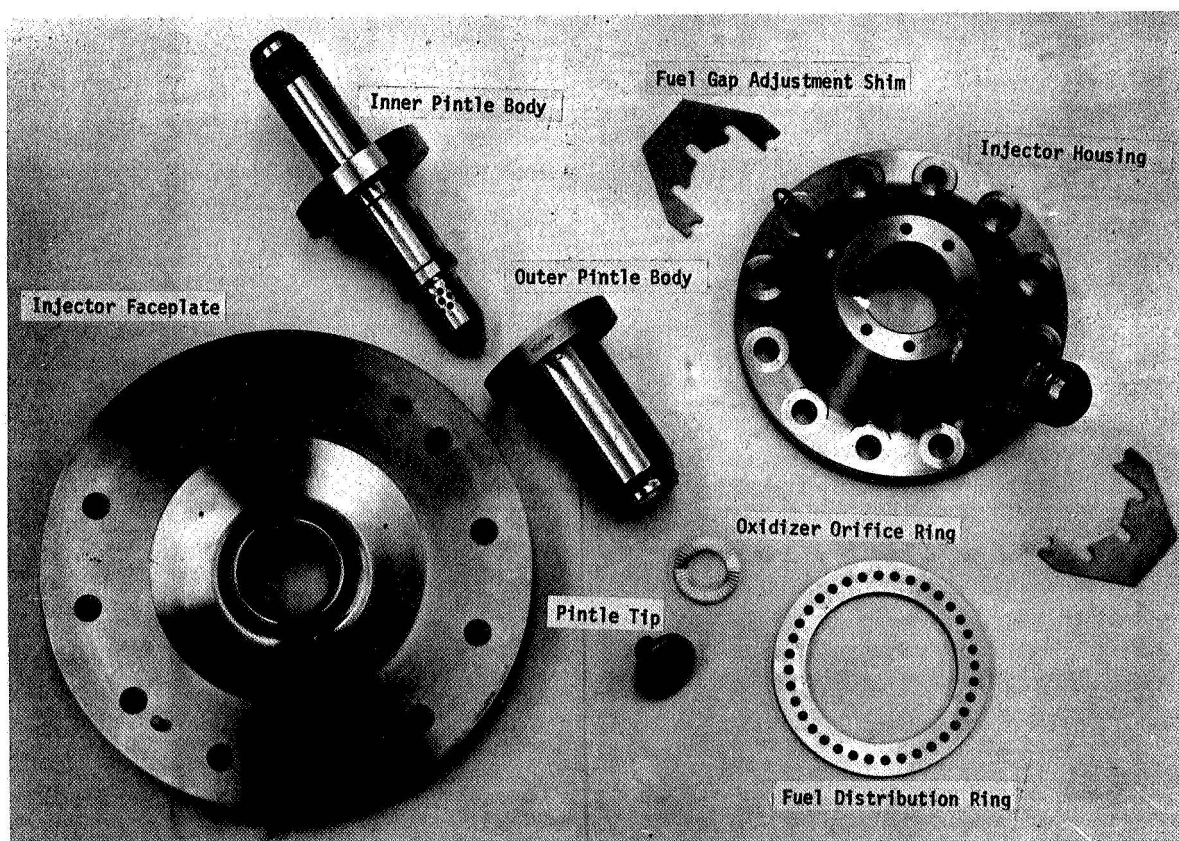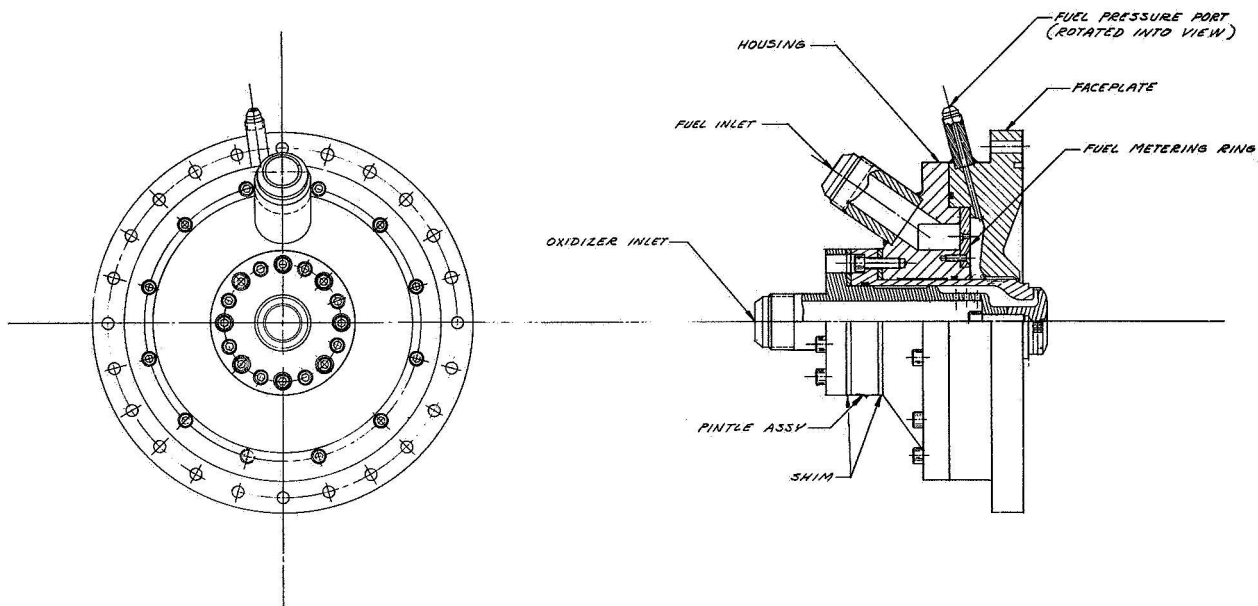
Figure 8. Views of TRW Injector

18
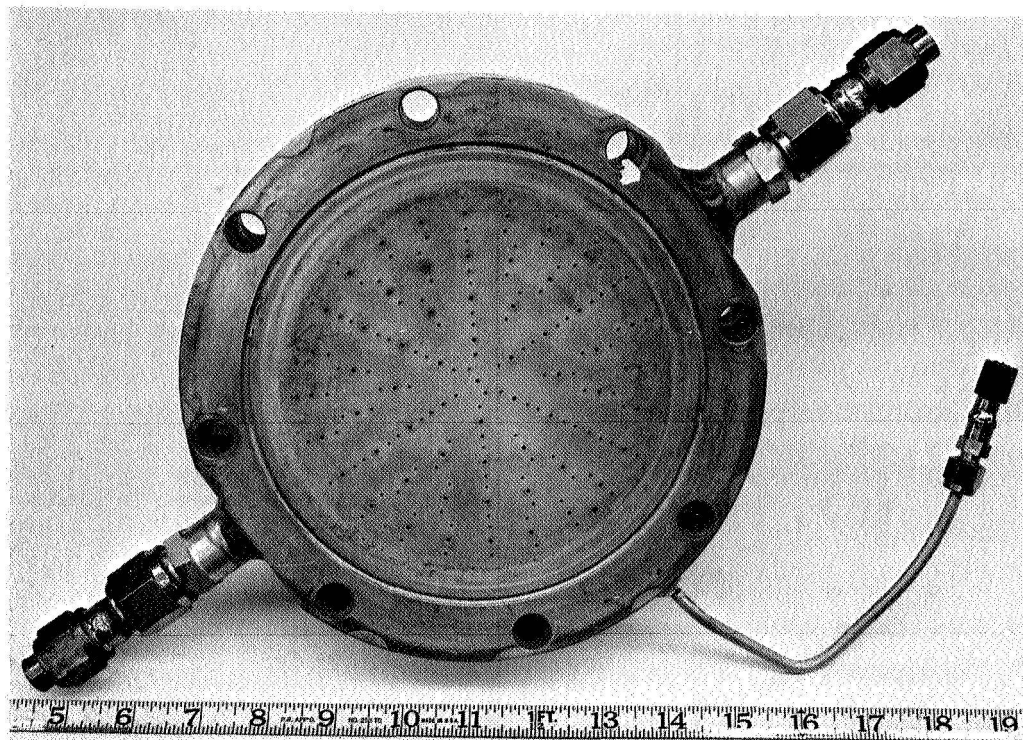
Figure 9. NASA-Supplied Flat Face Injector

Table 5. Description of NASA Supplied Flat Faced Injector

Original		Modified	
Material	- AL	Fuel Diameters	- 0.035 inch, oxidizer diameter 0.052
Pressure	- 100 psia	Pressure	- 300 psia
Thrust	- 100 lb$_f$	Thrust	- 3K
Propellants	- NTO/50-50	Propellants	- NTO/N$_2$H$_4$
Injector ΔP	- 120 psi	MR	- 1.2
Maximum pressure	- 220 psia	ΔP_f = 105 psi at 4 lb/sec H$_2$O	
Triplet	- two fuel on one oxidizer	ΔP_o = 63 psi at 4 lb/sec H$_2$O	
40 fuel orifices, 21 oxidizer orifices		Maximum operational pressure - 400 psia	
		Impingement Distance = 0.55 inch	

3.2.5 Chamber Hardware

The chamber hardware was comprised of heat sink and acrylic, transparent hardware. The heat sink hardware was designed to provide a maximum of flexibility. Interchangeable spool sections were designed to provide the capability of building up long L/D engine sections. The engine throat was machined copper.

Figure 10 is a photograph of one of the combustion chamber segments. The chamber element is 7.85 inches long and has a diameter of 6.0 inches. There are provisions for nine surface thermocouples, three longitudinal rows spaced 120 degrees apart. The L/D variation called for in the contract was accomplished by joining a duplicate chamber to the first one.

19
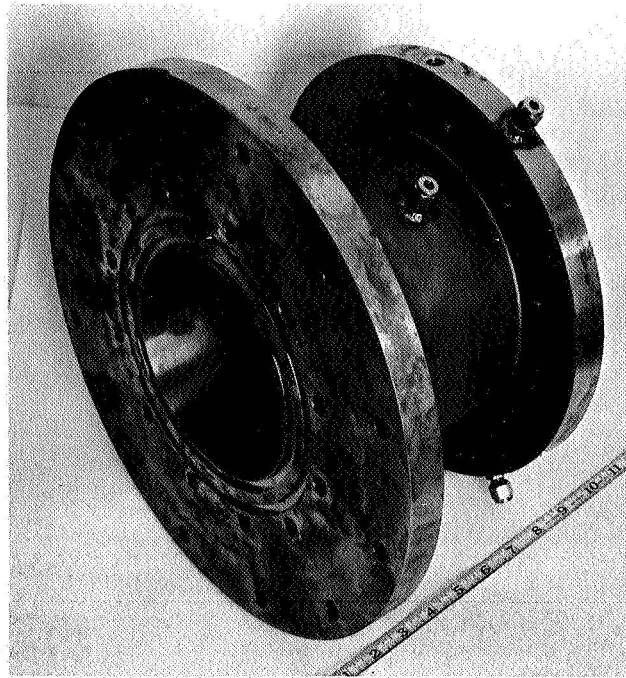
Figure 10. Combustion Chamber Segment

A photograph of the copper heat-sink throat is snown in Figure 11. The throat was designed with a 30-degree convergence angle and a 15-degree divergence angle. The throat was terminated at an area ratio of 3.5. Temperature measurements were made in three longitudinal rows spaced 120 degrees apart. The particular row seen in Figure 11 had an extra four plugs.

There was a contractual obligation to document foam film attachment in acrylic engines and/or combustion segments. Toward this end sketches of acrylic engines and combustion chamber segments having internal dimensions corresponding to the workhorse hardware were prepared and submitted to potential vendors. Because of delays of up to 3 months in obtaining specially fabricated plastic billets having diameters of 8 inches or greater, techniques for laminating plastic were considered. One local vendor has considerable experience in fabricating large, high-pressure pump housings from laminated plastic. They have built a special machine to insure excellent bonding of successive flat slabs and were able to bond 4-inch slabs of plastic perpendicular to the direction of flow to minimize bond stresses, as shown in Figure 12. Strength was added to the radial bonds by supporting the entire engine with longitudinal bolts.

Figure 11
Copper Heat Sink Throat
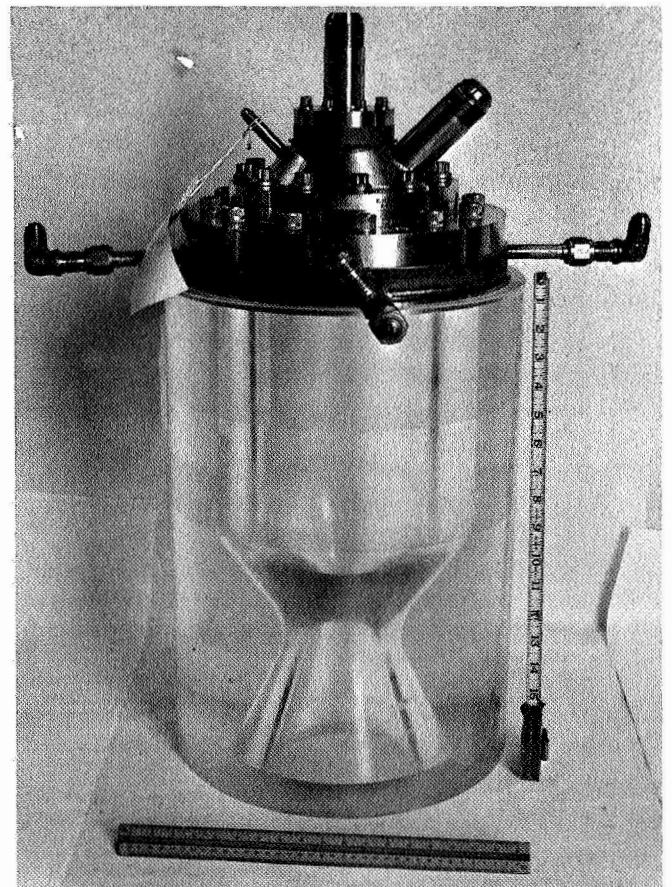
Figure 12
Acrylic Engine Setup

3.3 FOAM INJECTOR DESIGNS

Because this program was a feasibility demonstration effort, the foams were all generated external to the engine and injected into the engine through a continuous gap foam feed ring. Several designs were investigated in the program, and they are described here, along with other pertinent design data.

A sketch of the initial continuous annular foam ring used in the program is shown in Figure 13. It was basically patterned after the design found so successful in the TRW in-house feasibility study. The design incorporated easily replaceable split shims so that the injector gap could be varied without time consuming engine disassembly. The angle of foam injection was 30 degrees; thus, a gap change effected by any shim addition or subtraction was one-half the thickness of the shim. The maximum shim was approximately one-fourth inch.

A photograph of the disassembled 30-degree foam ring is shown in Figure 14. The 30-degree annular gap which was formed by the two mating pieces could be varied by inserting shims of various thickness as shown in Figure 14. In the initial experiments and in later experiments when the point of foam injection was lowered 1.5 inches, it was possible to protect the foam ring with a layer of ablative material attached to the injector face without disturbing the main injector pattern Figure 15 and 16.

Preliminary design calculations were made to determine injector gap settings and pressure drops as a function of film velocity and pure liquid or pure gas coolant flow rate and are presented in Table 6. It is obvious that it will be difficult to evenly inject nonfoamed coolants as indicated earlier. Calculations are shown for a gas since this in essence is a foam of infinite expansion and thus serves as the upper boundary.

The formula used to calculate pressure drop for both gas and liquid can be used as a first approximation for the pressure drop of foam flow. Starting with

$$\Delta P_L \cong \frac{\left(\frac{\dot{w}_L}{A}\right)^2}{\rho_L}$$

which applies to liquid pressure drop and noting the $\dot{w}_L$ changes little with the addition of gas, but the ρ_{foam} changes approximately according to

$$\rho_{foam} = \frac{\rho_L}{EXP}$$

22

6.000 DIA

1.375

2-169 GLAND

.562 DIA. 12 PLCS
½-20 UNF-2B THD
12 PLCS (RIGHT PL. ONLY)

2-367 GLAND

.250 DIA 12 PLCS
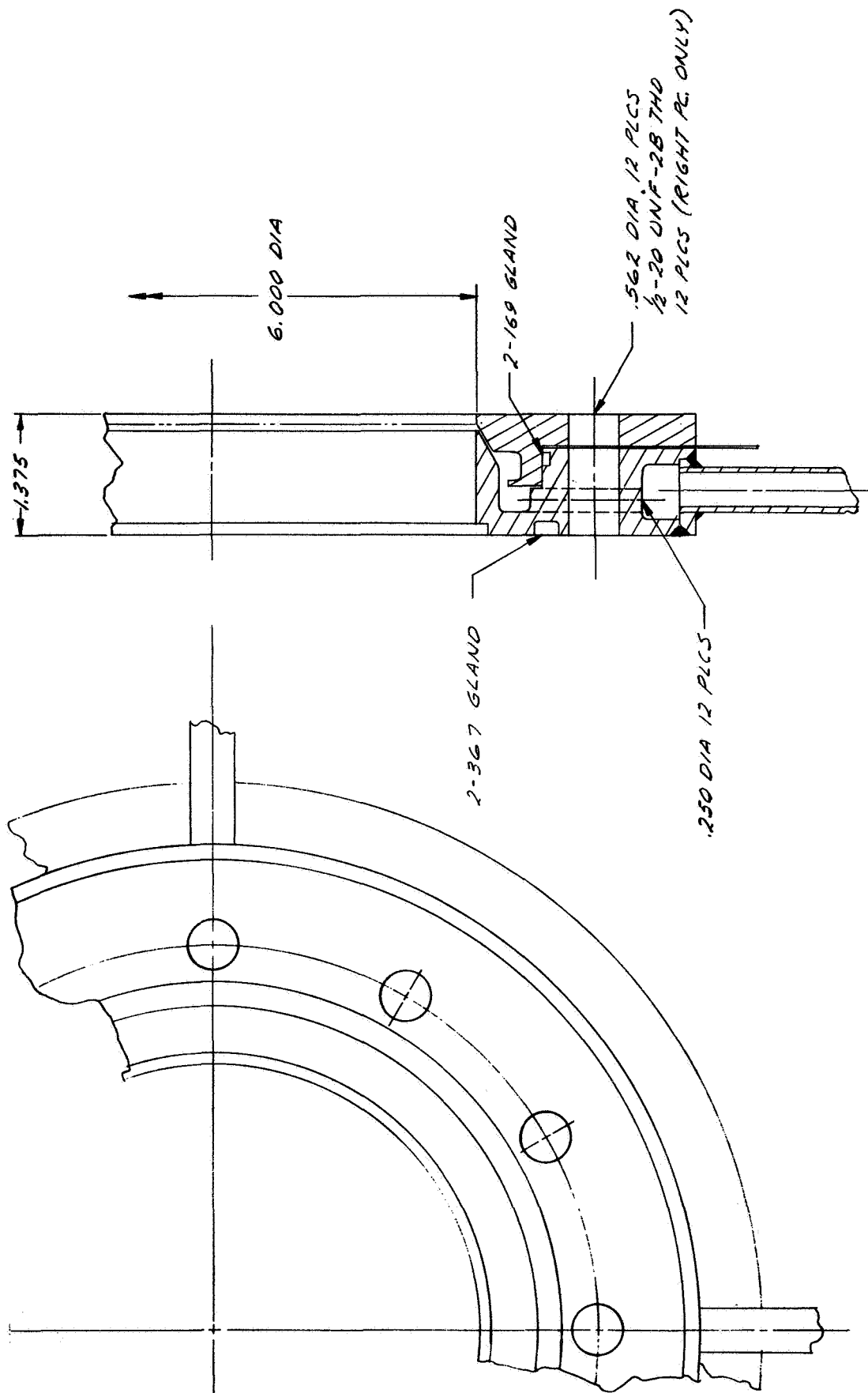
Figure 13. Sketch of Foam Ring
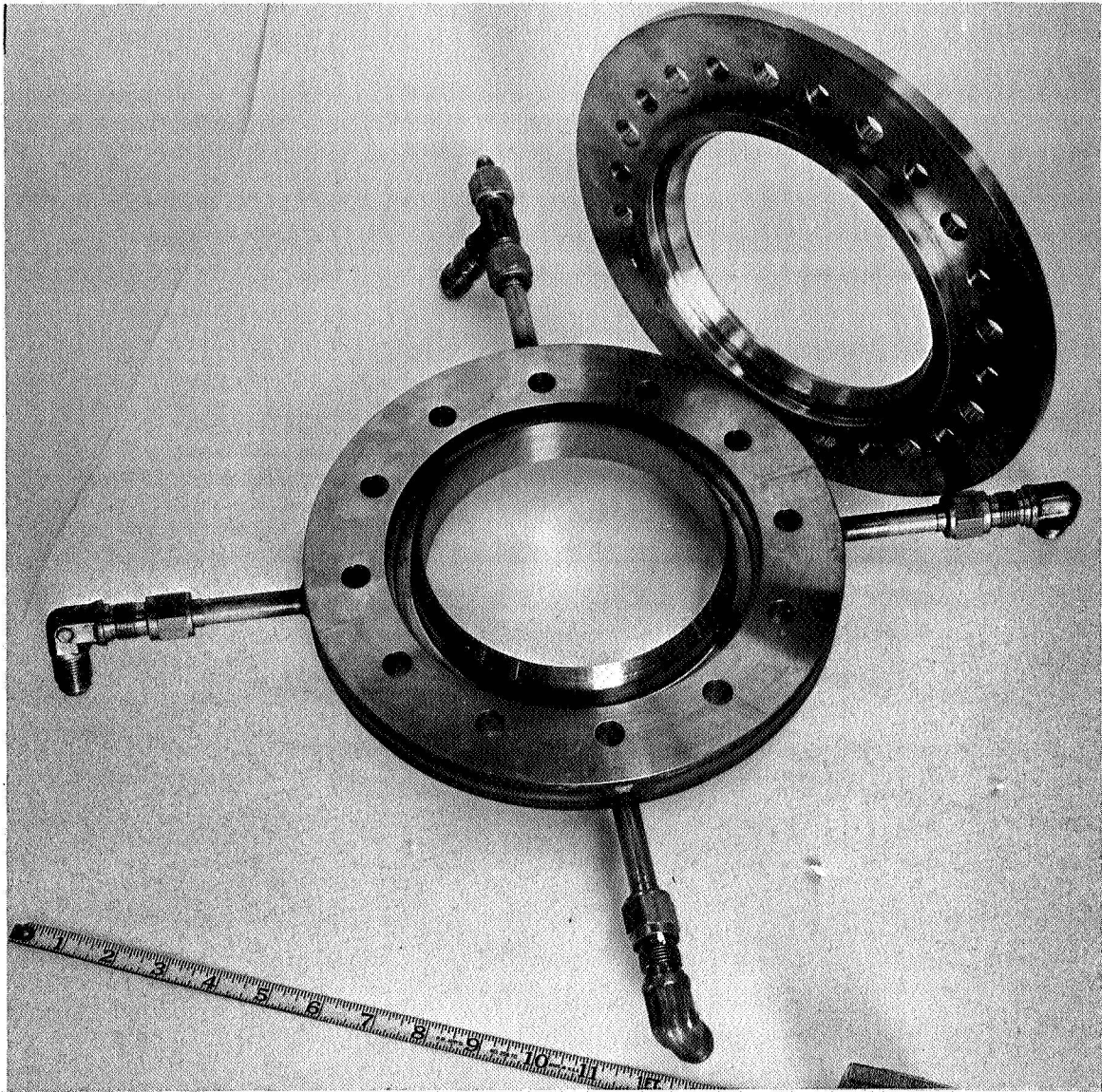
Figure 14.   Disassembled 30-Degree Foam Injector

The approximation reduces to

$$\Delta P_{foam} = \Delta P_L \text{ (EXP)}$$

For example, this approximation says that for an injector gap setting of 0.006, 10% coolant flow, and a film coolant velocity of 20 ft/sec, the pressure drop for a foam with EXP = 5.0 will be approximately 35 psi.

24
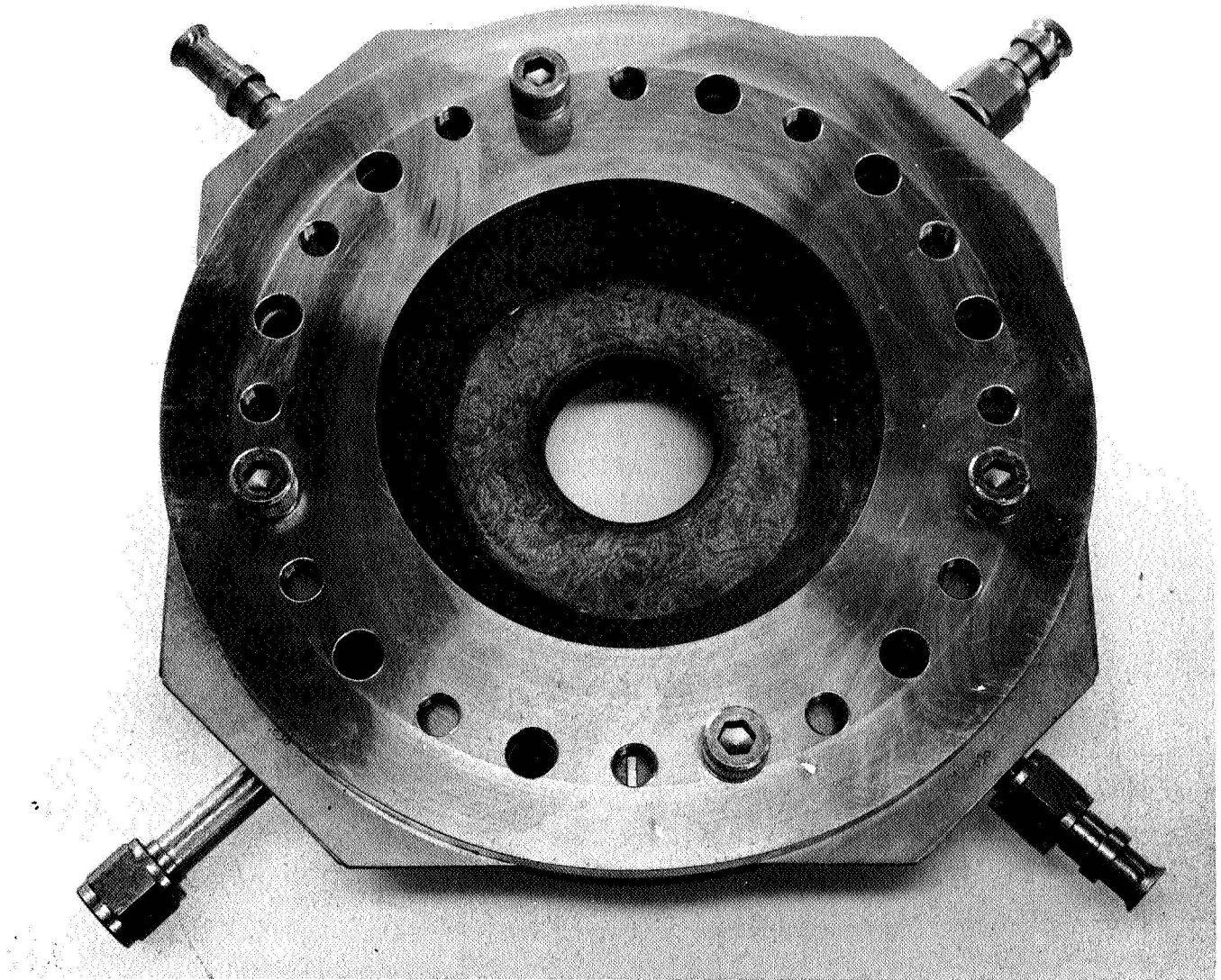
Figure 15. Assembled Foam Injector

Similarly the velocity of the foamed film coolant increases approximately with expansion ratio:

$$v_{f\ell} \ ft/sec = \frac{\dot{V}_f}{A} = \frac{\dot{V}_L \ (EXP)}{A}$$

Several additional design changes were made to the original foam injector to change the angle and velocity of foam injection.

25
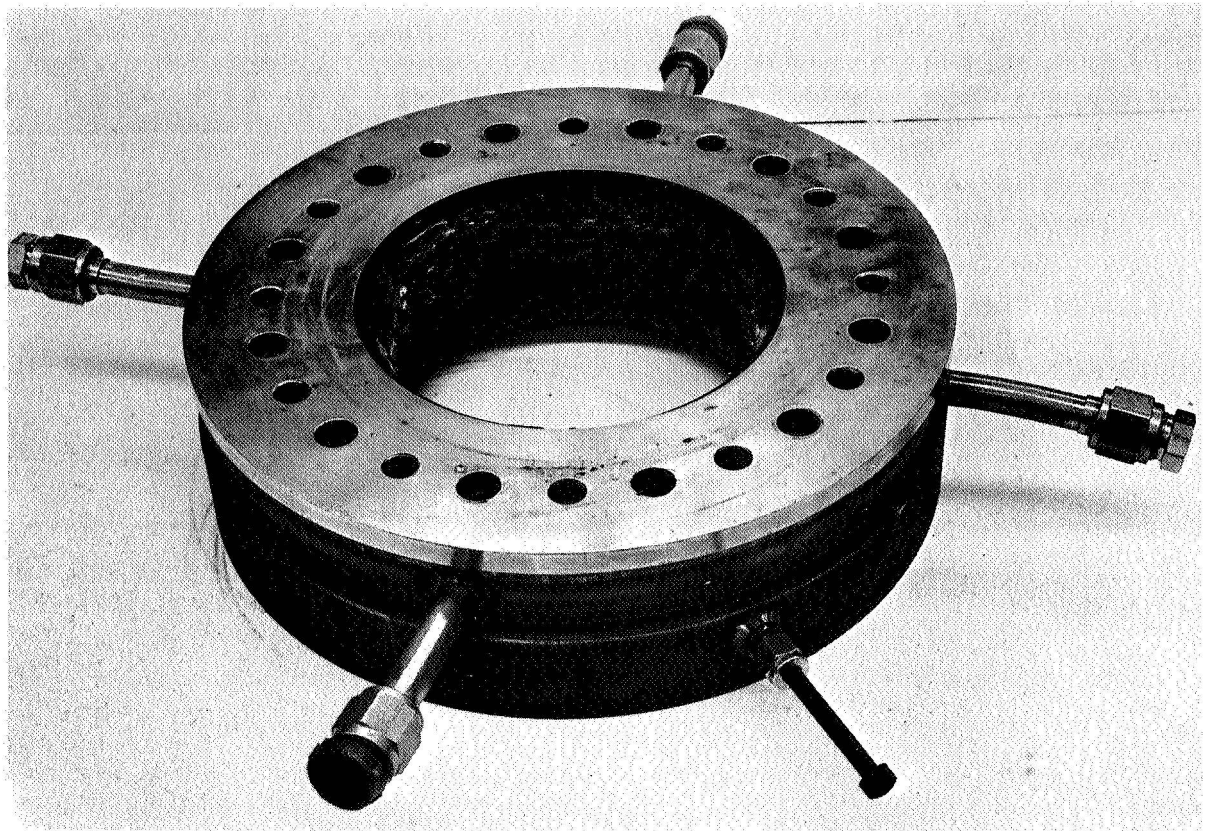
Figure 16.   Assembled Foam Injector with Point of
Foam Injection Lowered 1.5 Inches

Table 6.   Coolant Injector Gap Setting and Drop

10% coolant flow rate
300 psia, 300 lb$_f$ engine

Type of Coolant	Gas, exp = ∞			Liquid, exp = 1.0		
r, ft/sec	Gap, in.	Area, in^2	ΔP, psi	Gap, in.	Area, in^2	ΔP, psi
10	0.506	9.55	0.0452	0.0123	0.232	1.86
20	0.253	4.77	0.181	0.00615	0.116	7.44
50	0.102	1.93	1.13	0.00246	0.0464	46.5
100	0.051	0.96	4.52	0.00123	0.0213	186.
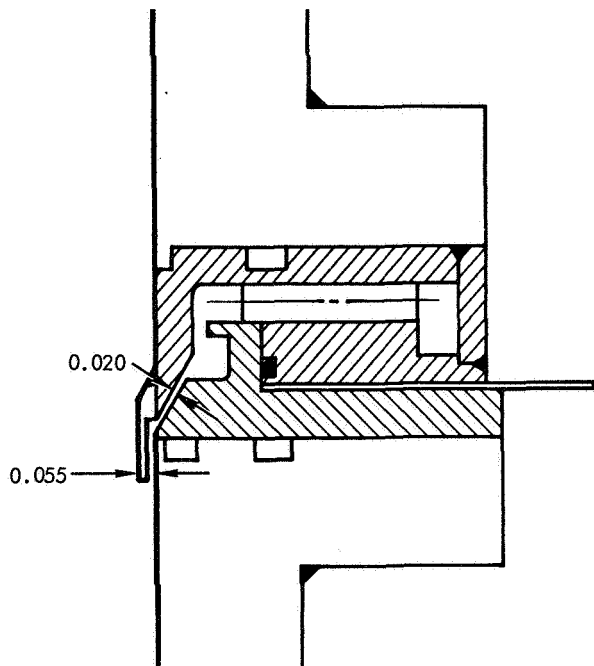
Figure 17. Schematic of Foam Ring Modification for Run 446

Figure 17 is a schematic diagram of the original injector with a deflector ring added. The purpose of the ring was to redirect the foam parallel to the wall at an increased velocity (see Run 446 in results). In conjunction with this foam injector change, the point of foam injection was lowered several inches; hence, the foam injector became exposed to the hot gas environment. A cursory heat transfer analysis was made for the injector lip to establish approximately equilibrium temperatures. Heat transfer to the wall from the gas was approximated by:

$$Q/A = 0.85 \times 10^{-3} \, (3085\,^{\circ}R - T_w)$$

And heat conduction from the outside of the injector lip to the inside wall adjacent to the foam was given by:

$$Q/A = \frac{\lambda}{x} \Delta T$$

The equilibrium point is then calculated as the wall temperature which gives a hot gas heat flux that can be conducted through the injector lip to the foam as shown in Figure 18. Based upon these results, which show that the thin part of the injector runs cool, it was conjectured that the deflector ring would run cool. Subsequent hot firings revealed a thermal expansion problem (Figure 19 and 20) with the ring moving outward sufficiently to interfere with the metering of the foam flow. The design was then modified according to Figure 21 and as described below:

(1) Reducing the angle of injection to 12 degrees

(2) Re-matching the original 30-degree gap to make two gaps - one at 30 and the other at 12 degrees

(3) Adding a 1/2-inch spacer to the bottom of the injector

(4) Adding 12 support places to prevent any mass deflection of the lip of the foam ring.

This modification to the foam ring provided the flexibility in gap setting as summarized below.

27

Shims	Gap 1	Gap 2
0	0.070 ± 0.002	0.116
0.125	0.129 ± 0.002	0.136

This configuration, used in all runs after 446, was found to operate quite satisfactorily; Figure 22 shows the unit disassembled.

3.4 FOAM GENERATION DESIGN AND SIZING

Preliminary design and analysis of the foam generator revolved around sizing, conceptual design of foaming method, response estimation, and techniques for handling potentially hazardous foams such as N_2H_4.

In order to size the generator estimated foam cooling requirements from total heat flux are determined by graphically integrating the area under Curve A, Figure 7 and the heat balance equation:

$$w\ (\Delta H)\ \eta = \Sigma \left(\frac{Q}{A}\right)_i \Delta A_i$$

CURVE A: GAS HEAT TRANSFER TO WALL

$q/A = h\ (TR - TW)$

$= 0.85 \times 10^{-3}\ (3085 - TW)$

CURVE B: HEAT CONDUCTION THROUGH INJECTOR LIP

$q/A = \frac{K2}{X}\ (TW - T\ FOAM)$

$= \frac{10}{(3600)(12)X}\ (TW - 530)$
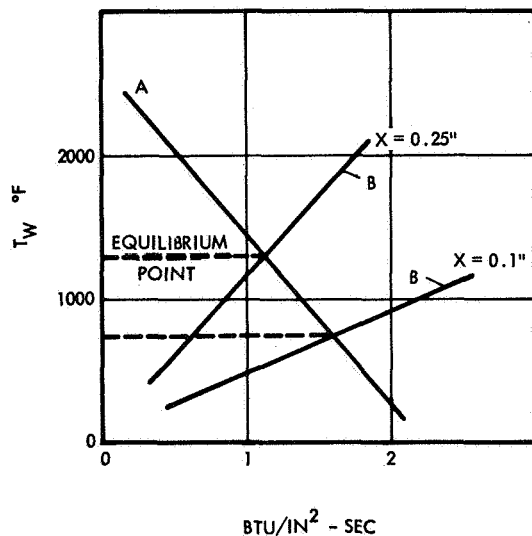
Figure 18. Surface Temperature of Unprotected Foam Ring Lip
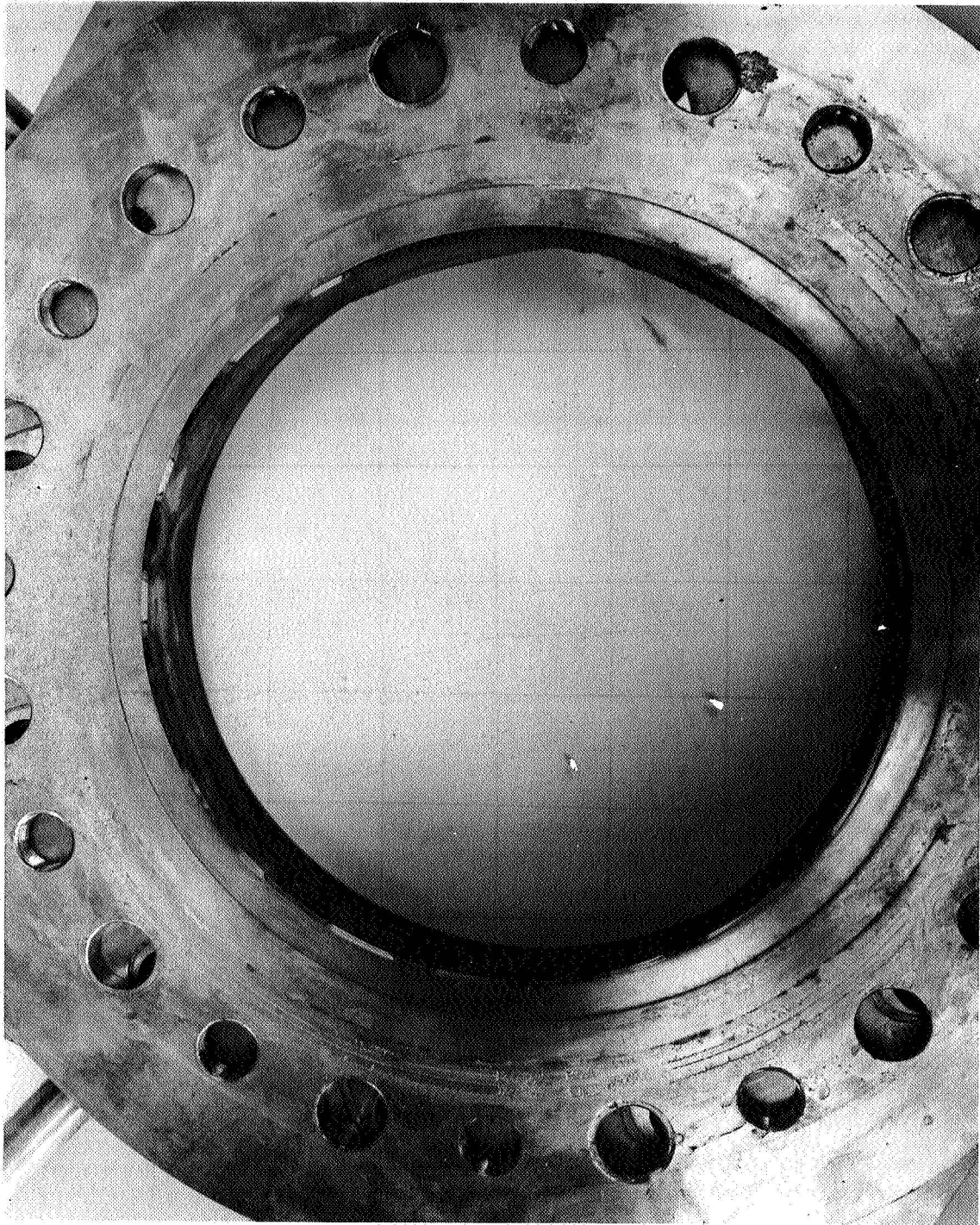
Figure 19.   Foam Ring with Deflector Modification
After Firng (Bottom View)
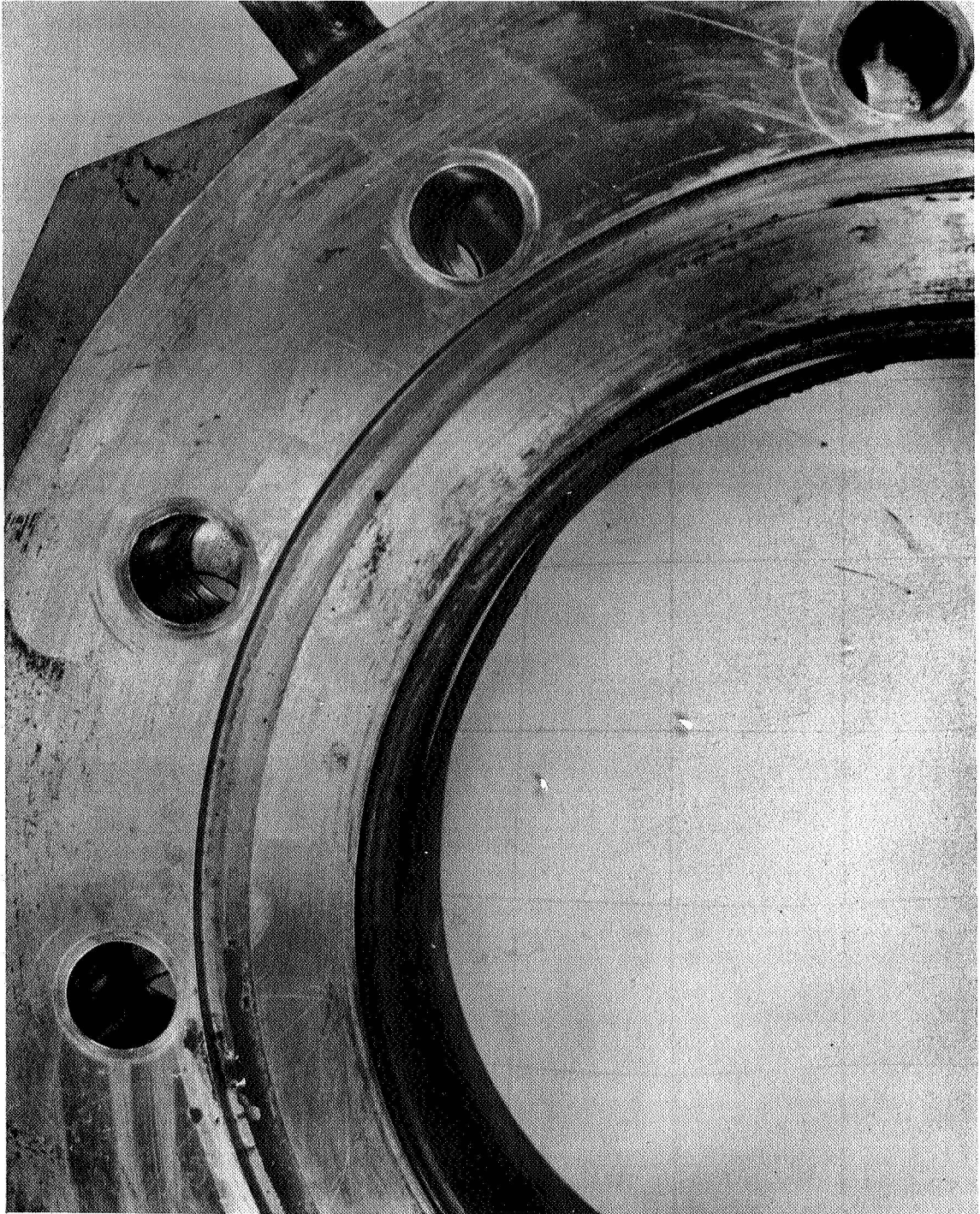
Figure 20.   Foam Ring with Deflector Modification
After Firing (Top View)

APPROXIMATE SCALE 5:1

.002 - .005
SLIP FIT
12 PLACES

.060

.020

GAP 1

GAP 2

.020

12°

1/2 IN. ADAPTER PLATE
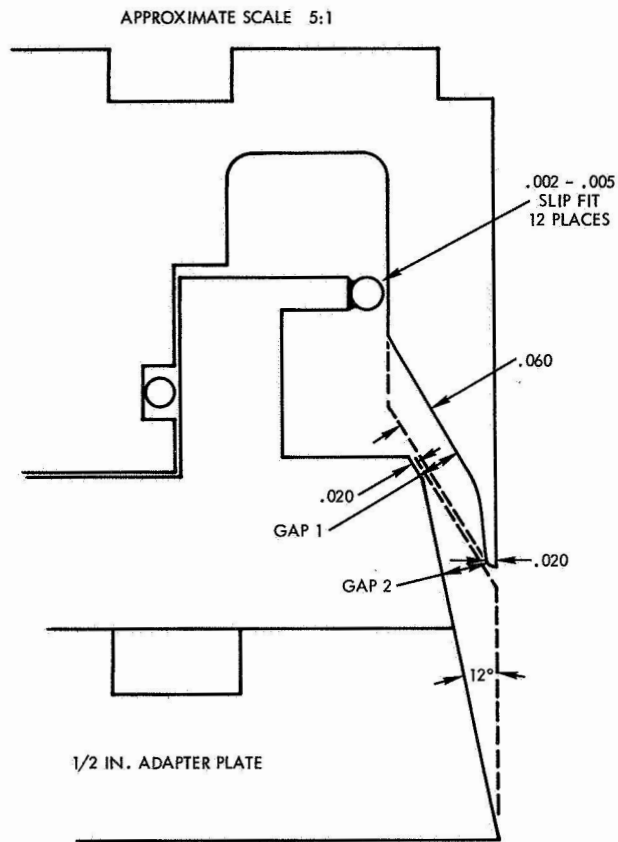
Figure 21

Sketch of Foam Ring
Modification for Runs
After 446

Figure 22. Disassembled Foam Ring Used
on all Runs After 446

31

where

$$\dot{w} = \text{foam coolant flow rate}$$

$$\Delta H = \text{foam coolant heat capacity}$$

$$= \left(c_p \Delta T\right)_L + \Delta H_{fg} + \left(T_r - T_w\right)c_{pg}$$

$$\eta = \text{cooling efficiency}$$

$$\Sigma\left(\frac{Q}{A}\right)_{T_s} A_i = \text{heat load at the coolant saturation temperature}$$

If the following assumptions are made,

(1) The wall of the engine is maintained at the saturation temperature

(2) The coolant efficiency is 100 percent

and the sensible heat of superheating the coolant vapor is ignored and the local heat adjusted to the saturation temperature of the coolant, the maximum percent coolant for the 3000 lbf engine can be estimated to be:

$$\dot{w}_{water} = \frac{1139 \text{ Btu/sec}}{(394 - 38.61) + 809.2} = \frac{1139}{1165} = 9.8\%$$

Similar calculations for the subsonic chamber give the coolant percent flow ranges of 3 to 5 percent. Based upon these calculations it was surmised that a foam generator should be built for coolant flow rates ranging from 3 to 30 percent of the main propellant flow.

Experience gained in constructing and testing foam generators in the initial TRW feasibility study and in other in-house studies led to the selection of the conceptual design shown in Figure 23. Use of cavitating venturies for flow control and measurement in conjunction with separate pressurization circuits for the foaming liquid and foaming gas allowed for absolute and relative gas/liquid flow rate control ranges from 0.1 to 3.0 lb/sec, and expansion ratios of 1 to 30. Another desirable feature of this system was that foam could be prepared over a wide range of pressure without disturbing flow rates, and would, thus, tend to be independent from the effect of engine pressure perturbations.

The function of the packed bed was to provide an improver or mixer for the gas and liquid to insure high quality foam. The purpose of the bypass system was to allow for simulation of flow through the engine under nominal back-pressure conditions to check venturi and bed pressure drops prior to engine startup.
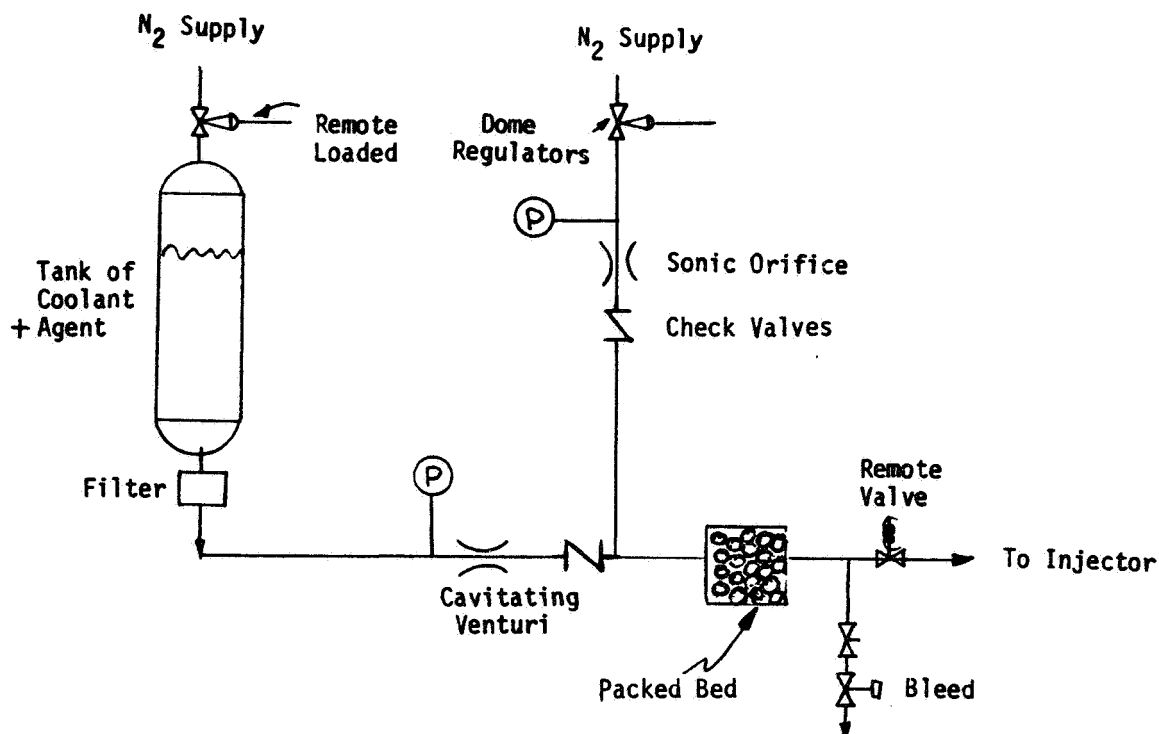
Figure 23. Foam Generator Schematic for all Runs
to and Including 331

Figure 24 shows an improved conceptual design of t he original
foam generator. In this design the bypass system has been eliminated
and the location of shutoff valves changed to improve generator response
characteristic and to facilitate the handling of potentially hazardous foam
such as N_2H_4. Table 7 gives liquid and foam volumetric flow rates as
a function of flow rate and expansion, and is helpful in estimating the foam
generator's response once the dead volume is known. In all cases the
response of the foam generator must be faster than the engine's response
otherwise hardware damage may result if combustion gas flows into the
foam generator. The arrangement of valves allowed for flexibility in valve
opening and closing sequences and the use of a purge shutdown as would
be required when hazardous foams were being handled.

Table 7. Foam Generator Response

EXP

$\dot{w}_L$ (lb/sec)	$\dot{V}$, (in^3/sec)		
	1. 0 (liquid)	5. 0	10. 0
0. 5	33. 9	69. 5	139
1. 2	33. 3	166. 0	333
3. 0	83. 1	415. 0	831

33
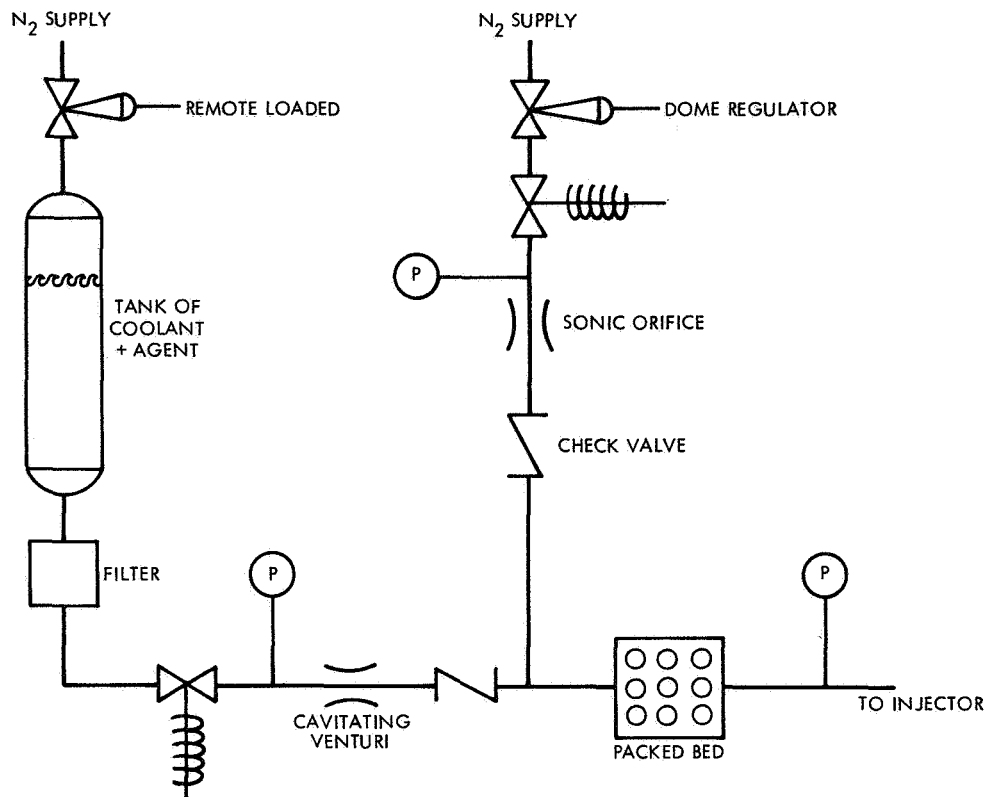
Figure 24.   Schematic of Close-Coupled Foam Generator
Used for Runs 447 Until Completion of Tests

The close-coupled version of the foam generator is shown in
Figure 25, and a close-up of the packed beds is shown in Figure 26.

3.5   TEST STAND SETUP

Numerous engine configurations and instrumentation schematics
were employed throughout the program and are summarized in Figures 27
through 32.

The initial series of testing Rums 417 to 431 was conducted with the
point of foam injection near the head end of the single L/D chamber.   The
overhead, bypass foam generator was employed in these tests as shown
in Figures 27 and 28.

The second generation of testing started with Run 446, Figure 29,
with the point of foam injection lowered by a 4.85 inch spacer and termi-
nated with Test 459.   The second generation of testing employed the close-
coupled foam generator, Figure 30.

The flat face injector was checked out in an acrylic engine as shown
in Figure 31.   This represented the start of the third generation of testing.
As shown in Figure 32, the heat sink engine setups were identical to those
of the second generation of testing since the only change was the substitution
of UDMH for N_2H_4 fuel.
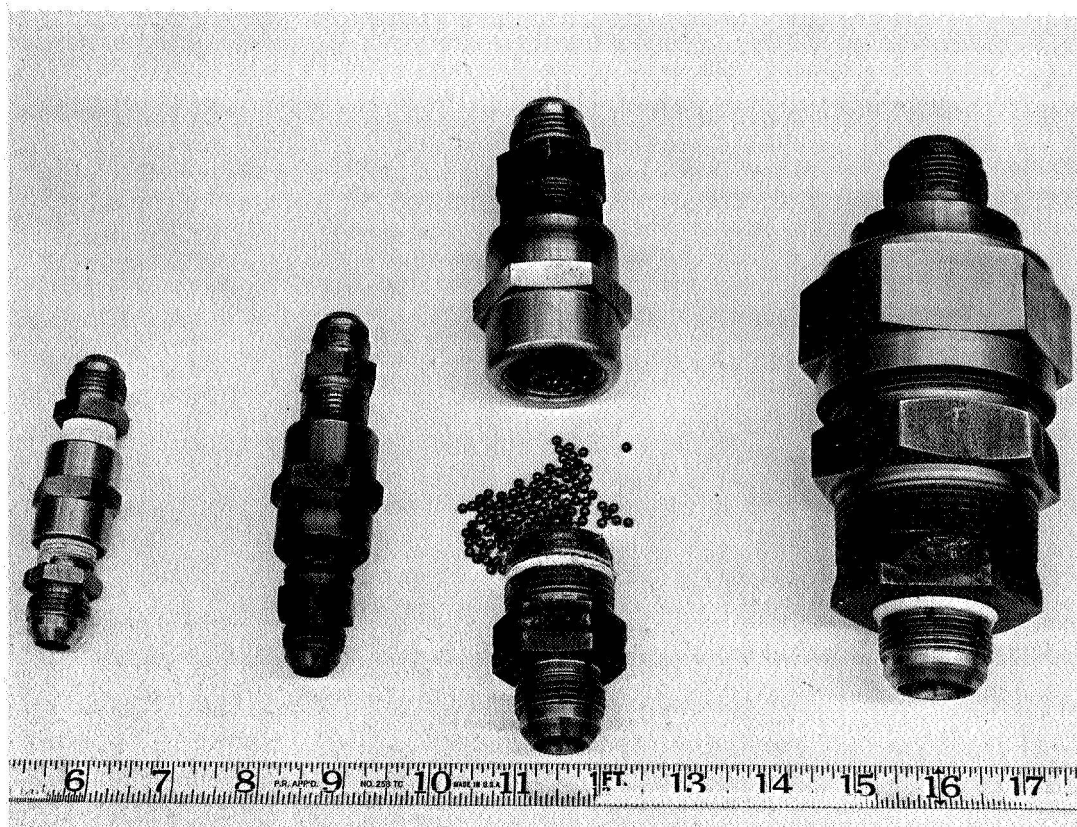
Figure 25.   Close-Up of Packed Beds
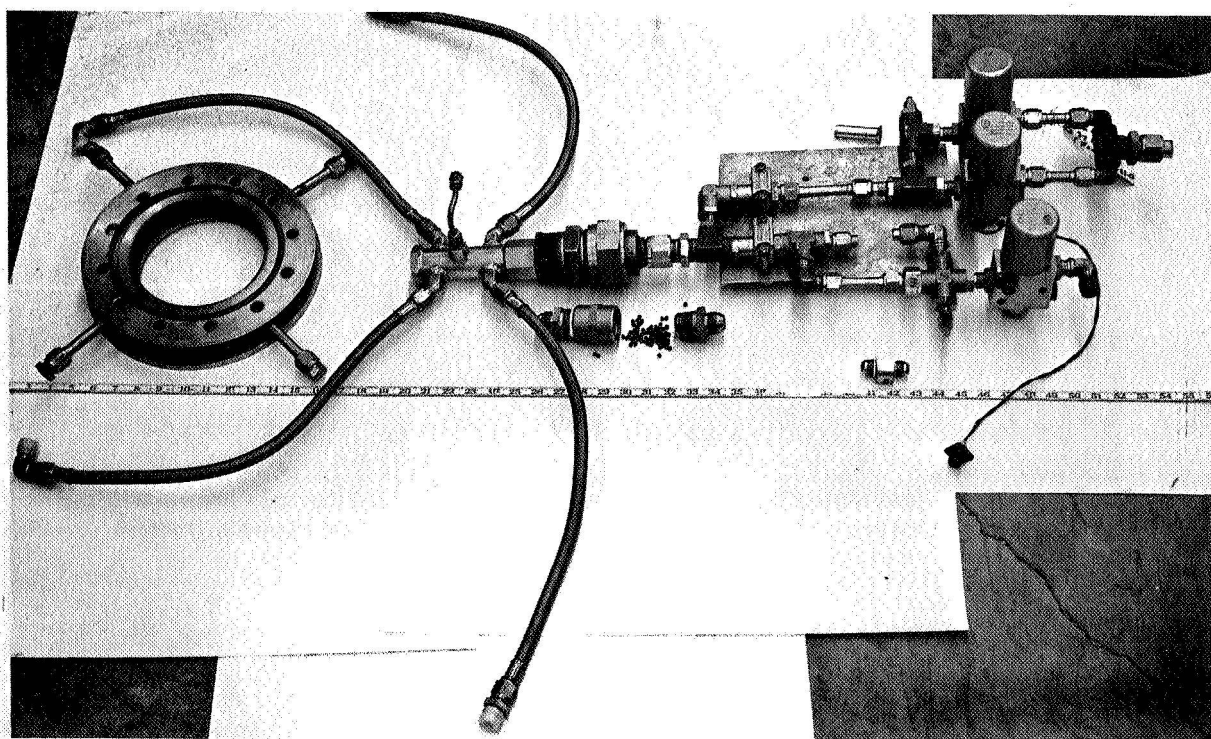
Figure 26.   Close-Coupled Foam Generator

35
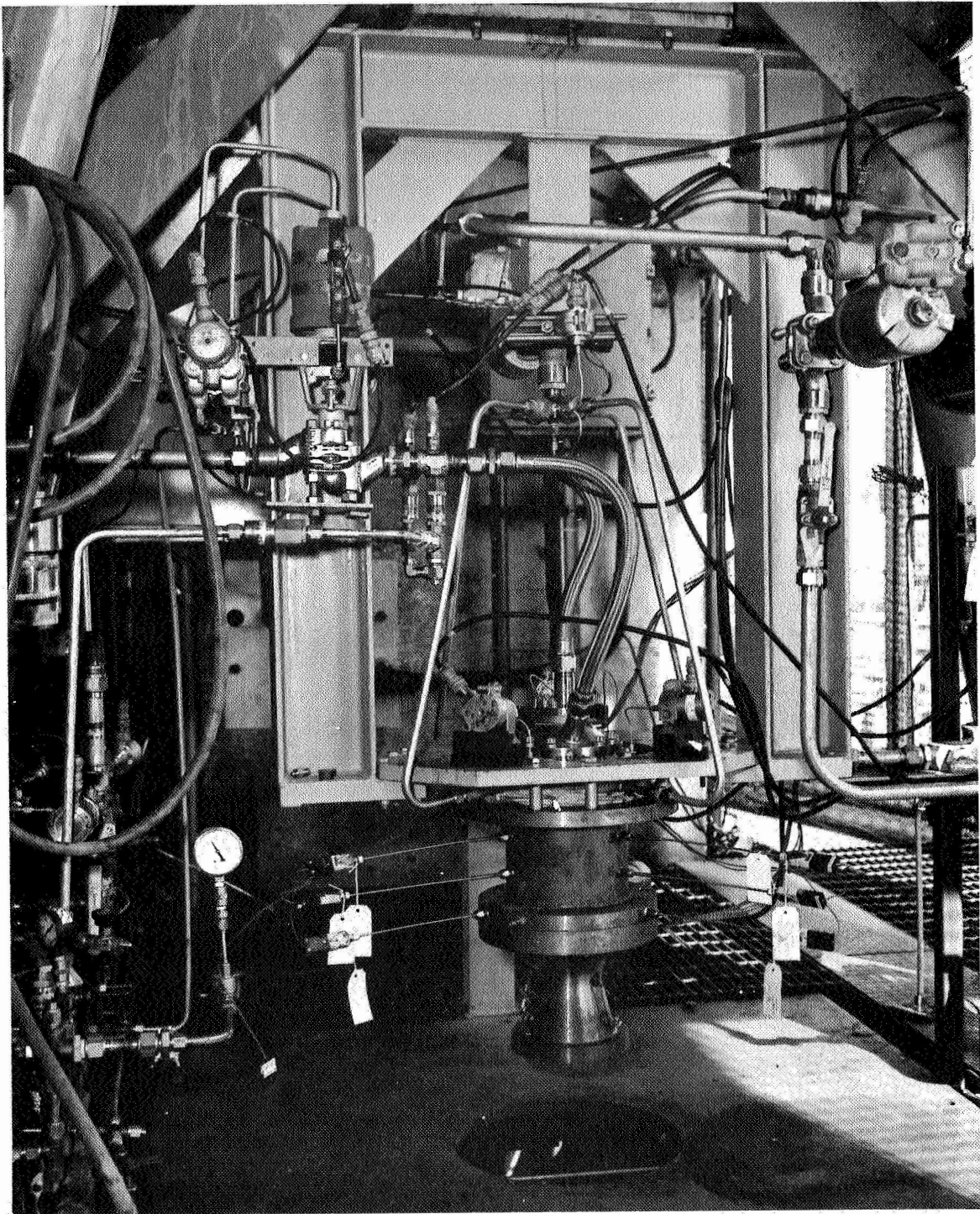
Figure 27.   Thruster and Foam Generator Test Stand Setup
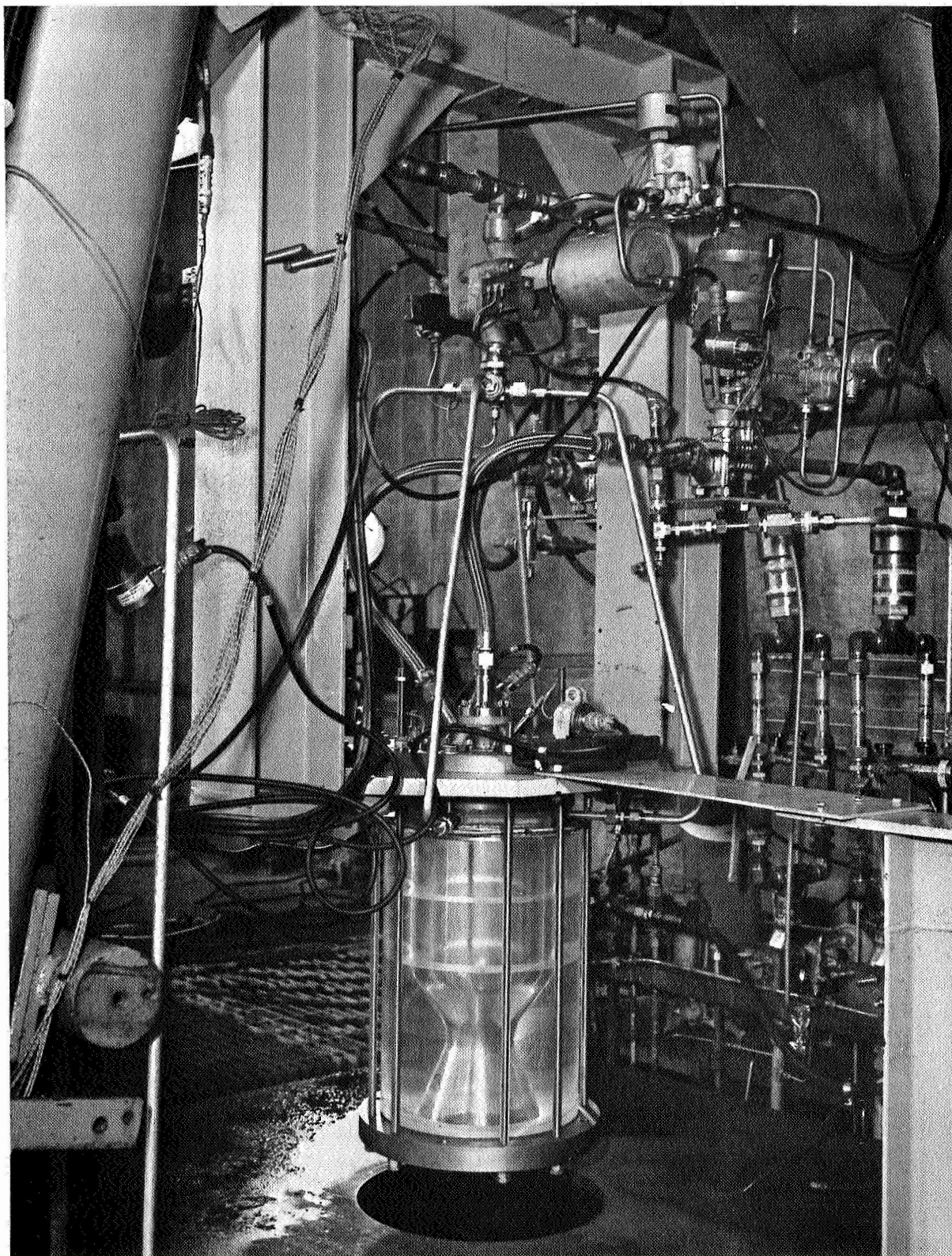
Figure 28.   Acrylic Engine Setup for Test
of TRW Injector
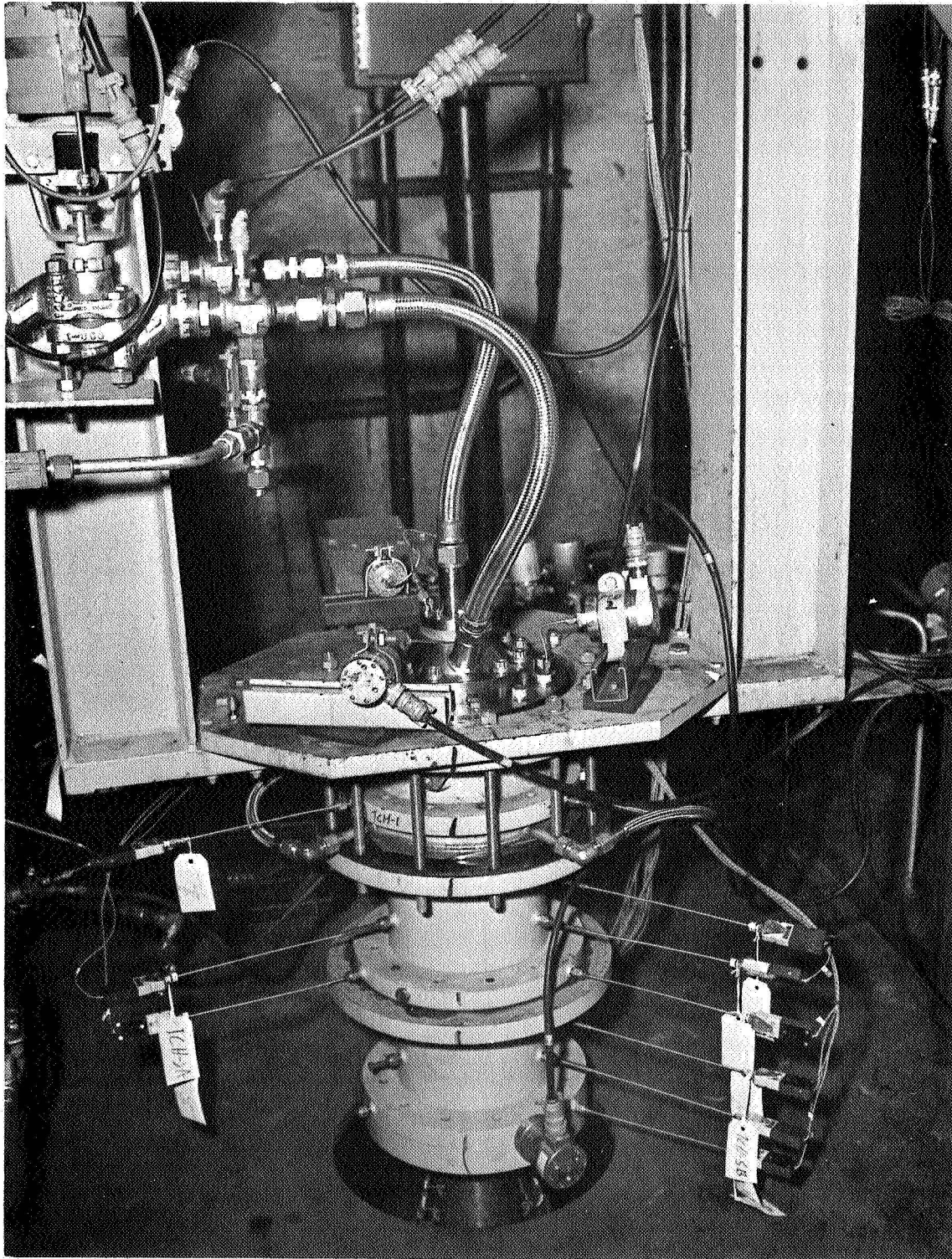
Figure 29. Heat Sink Hardware Setup for Runs 446 through 459 and Runs 469 through 471
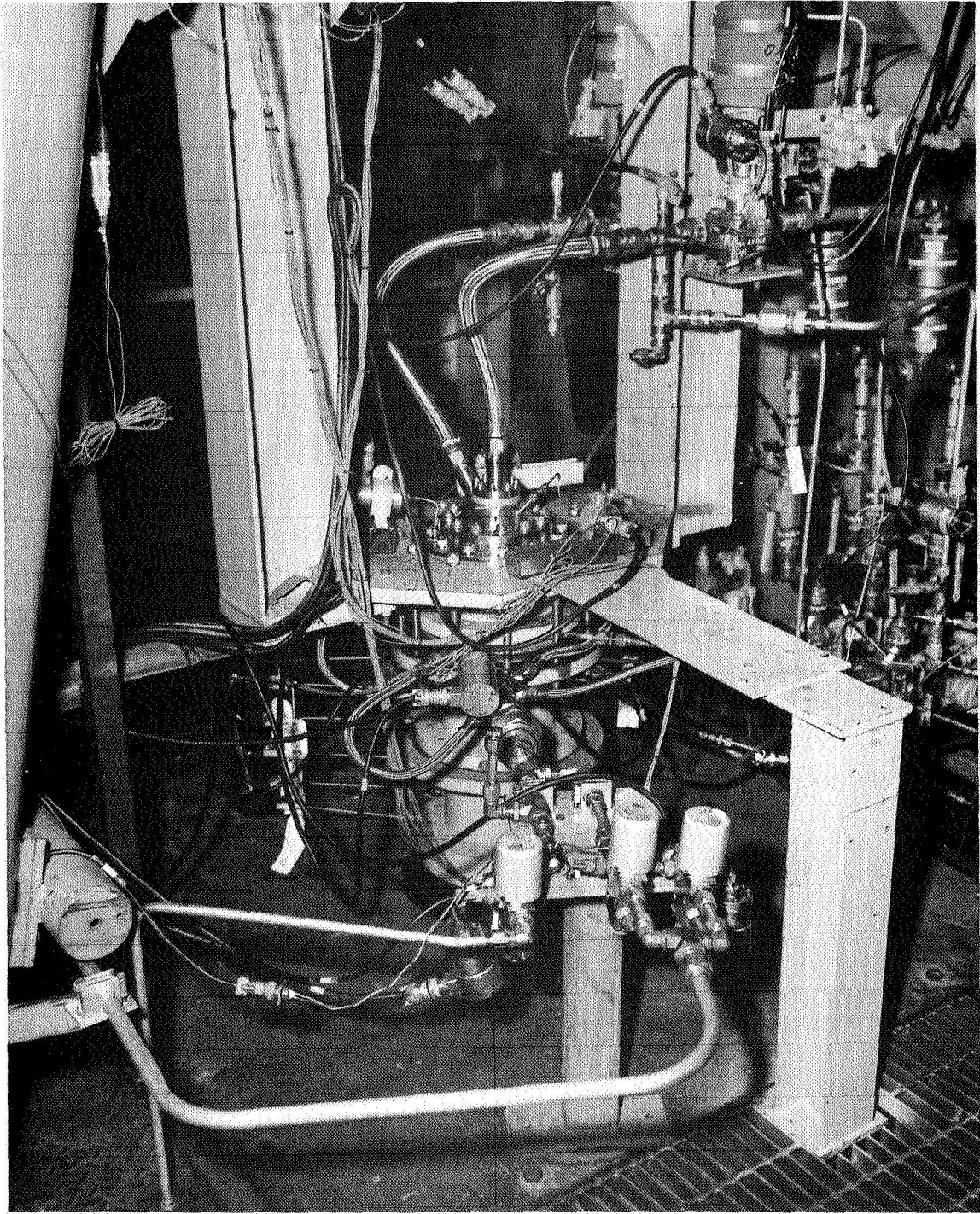
Figure 30. Photograph of Close-Coupled Foam Generator
Used for all Runs After 431
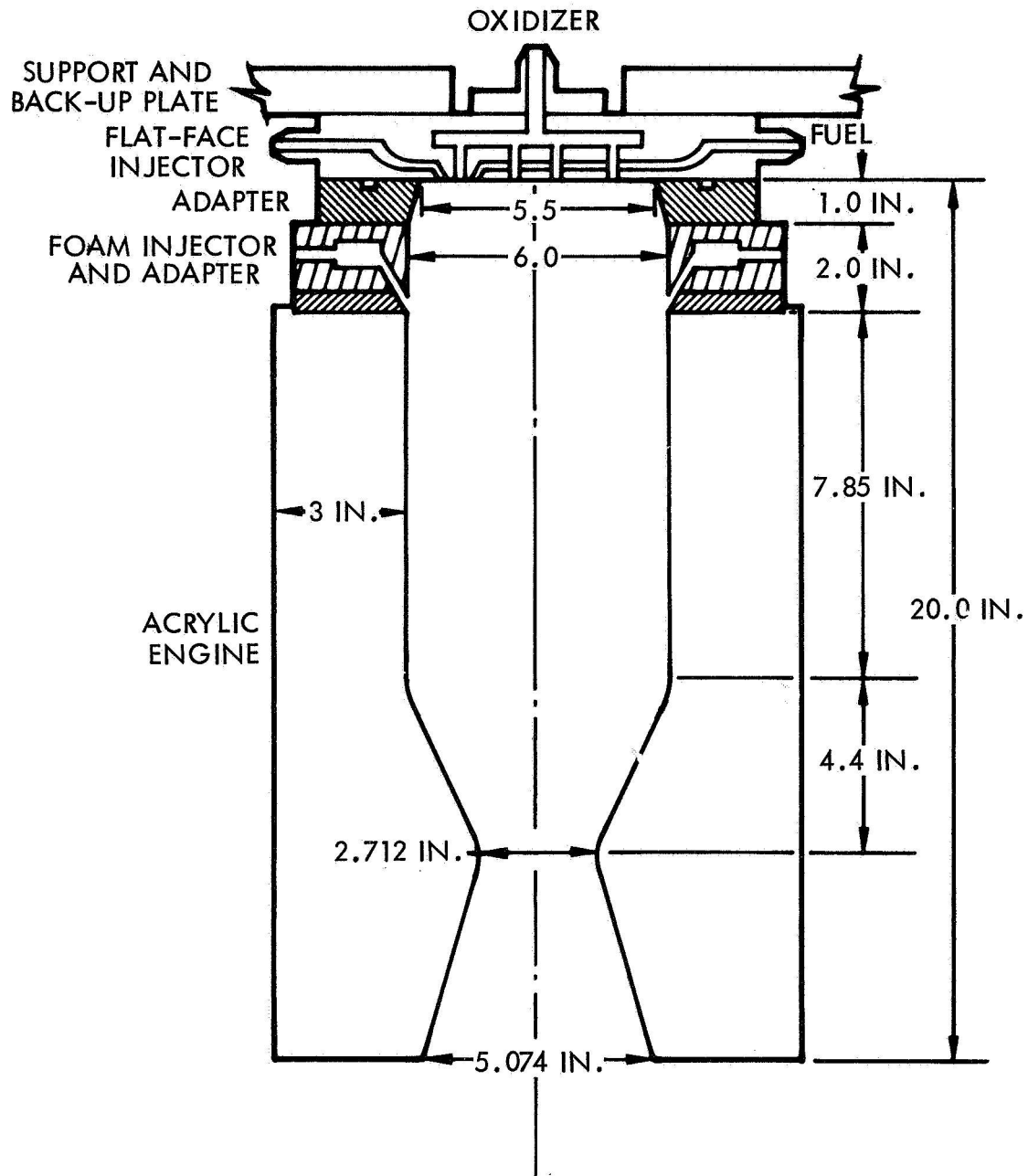
Figure 31.   Schematic of Acrylic Engine Setup
with Flat-Face Injector, Run 460
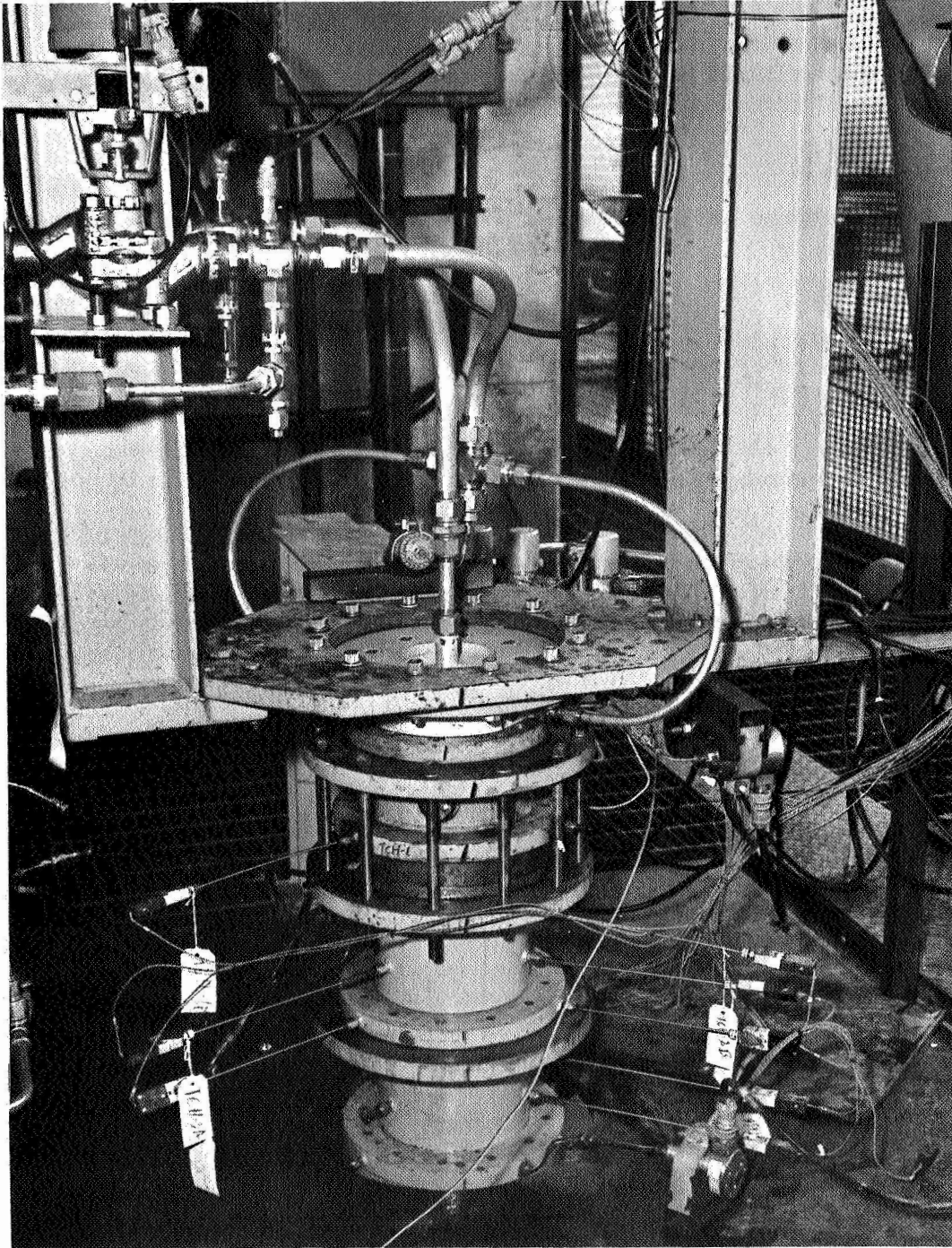
Figure 32.   Heat Sink Hardware Setup
for Runs 461 Through 468

The propellant flow schemes were developed in the Air Force Program and utilized independently pressurized propellant tanks, cavitating venturis, and redundant turbine meters for flow measurements.

Instrumentation

Preliminary analysis of the thermal instrumentation and means of data reduction were made of the methods employed in the Air Force program (Contract C-0054) to insure satisfactory documentation of coolant performance. Important aspects of this study were considered to be documentation of length of chamber cooled, radial temperature variations (susceptability of coolant to streaking), and heat load on the engine at the coolant saturatin temperature.

In the Air Force program a combination steel chamber-copper throat arrangement was selected on the basis that both chamber and throat would have nearly identical thermal responses to 1000° to $1500^\circ F$ ranging from 4 to 7 seconds. Fast responding, chromel-alumel surface thermocouples made by the Nanmac Corporation of Indian Head, Maryland, were used to measure the inner wall temperature of the chamber, as a function of time. Throat temperature-time traces were documented by the conventional copper plug technique. Temperature measurements were made in three longitudal rows spaced 120 degrees apart.

The Nanmac surface thermocouple and copper plug give typical temperature-time traces as sketched below. As would be expected the response of the surface thermocouples is very fast and eventually approaches the gas recovery temperature. The response of the copper plugs is, of course, much slower but is a function of plug thickness.
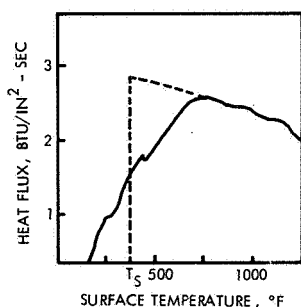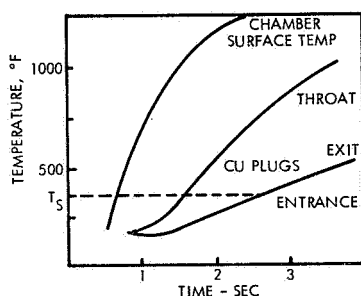
A method for the determination of local heat flux from transient temperature measurements of surface thermocouples, discussed in Reference 22, forms the bases of an in-house computer program used to reduce these data. The data output takes the form sketched below. Useful heat flux data are not obtained until after the engine startup transient (usually 0.5 sec or 600° to $800^\circ F$ into the run) is passed. The most meaningful data for the heat transfer study is the heat flux at the coolant saturation temperature, $\sim375^\circ F$. To arrive at this it is necessary to back-extrapolate the data to $375^\circ F$ according to the formula:

$$Q/A = (T_r - T_w) = hT_r - hT_w$$

which is in the form of the classical equation of a straight line:

$$y = mx + b$$

42

where

$$m = -h$$

$$b = hT_r$$

Unfortunately, some uncertainty is introduced into the extrapolation if the data do not form a straight line. Throat heat fluxes were compiled according to

$$\frac{dQ}{dA} = Cp\,t\rho\,\frac{dT}{d\theta}$$

from response data near the beginning of the run to minimize corrections due to the conductivity. (A complete discussion on the use of copper plugs with their convection factors is given in Reference 23.) A sketch of the dimensions of the copper plug and externally contoured throat is given below.
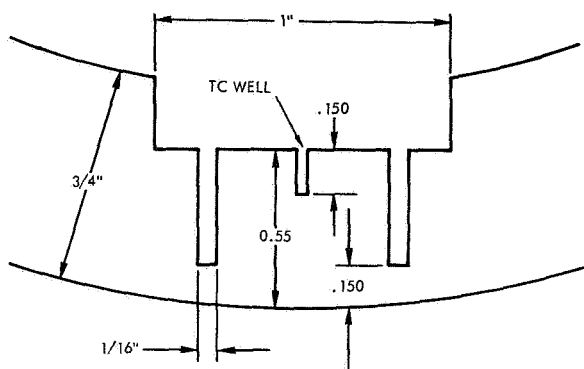
A comparison of these two methods of measuring no coolant heat flux data leads to the conclusion that the copper plug technique probably gives the best estimate of heat fluxes at the coolant saturation temperature. However, it is evident that fast, precise measurement of localized wall temperatures during runs with coolant is best accomplished by the Nanmac thermocouples since the copper plugs have an approximate order-of-magnitude slower response. The high thermal conductivity of copper also makes localized variation hard to detect. Thus, a difficult tradeoff exists for the selection of engine material and measurement techniques because of type of data desired and coolant flow rate.

A steel chamber with a copper throat was selected for the investigation, Nanmac thermocouples were spaced ~2 1/2-inches longitudinally and 120 degrees radially. Similarily, two rows of three copper plugs and one row of seven copper plugs were selected for the throat. Long durations were planned for runs at high coolant flow rates to give the copper plug temperature sufficient time to stabilize.

The instrumentation locations used in this program for the engine configuration used in the actual test effort are shown in Figures 33 through 35.
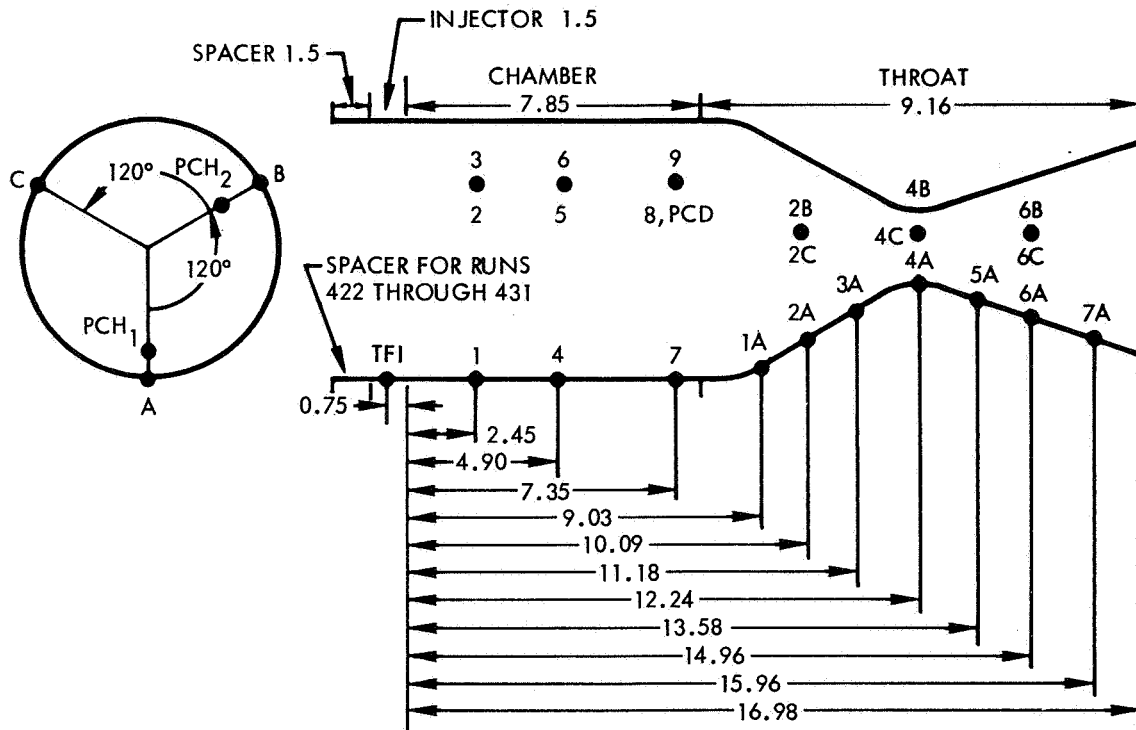
Figure 33. Instrumentation Schematic for Runs 417 through 430
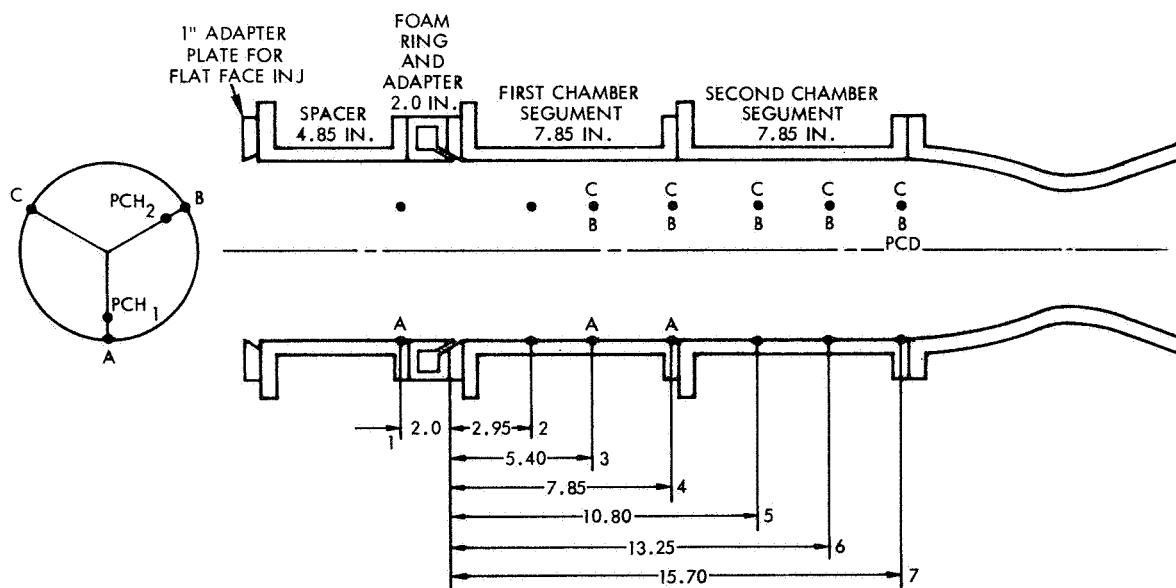
Figure 34. Instrumentation Schematic for Runs 447 through 471, Excluding Run 460

Figure 35. Insturmentation Schematic for Run 446
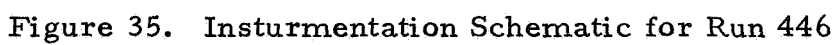
4. RESULTS OF COLD FLOW TESTING

The objectives of the cold flow tasks were:

(1)   To extend the pressure evaluation of foams to at least 300 psia

(2)   To investigate the foam flow pattern of the injector

(3)   Construct and test the high pressure foam generator prior to hot firing.

4.1 PRESSURE EVALUATION OF FOAMS

In these evaluations cold flow studies were carried out in glass hardware to investigate the resistance to shear stripping, potential bubble collapse, and overall stability of the foam under dynamic flow conditions.

Foam film attachment studies were conducted in a 1/2-inch OD, 3/8-inch ID glass venturi having dimensions simulating a typical engine setup (15-inch chamber, 5-inch converging section, and 5-inch diverging section) shown in Figure 36. Foam was injected onto the far side of the glass venturi through a tiny slot in a masking tape gasket surrounding the straightening tube admitting the high pressure core gas flow.

The chamber was designed so that the Reynolds number varied linearly from 1×10^6 to 5×10^6 through the pressure range from 100 to 500 psia. (The Reynold's number through the contraction section of the throat increases with contraction section diameter and reaches a maximum at the throat approximately 3.2 times greater than in the chamber.)

A parametric study involving pressure level, foam flow rate, foaming agent, expansion, and ultimate shear stress was made for the three types of water fire-fighting foams, water, and aerated water. In general there appeared to be no large qualitative differences between the three types of foam as the pressure was varied from 30 to 300 psia, although there appeared to be an increase in the ability of the foam to persist through the converging and diverging section. The most positive result from these tests appeared to be that foam will persist tenaciously and evenly for flow paths up to at least 20 inches, Figures 36 and 37. In addition, the unequivocal existence of foam at pressures of at least 300 psia was confirmed.

An effort was made to check foam stability at increasing film thickness by increasing the foam flow rate to the cell. However, the shearing action of the high speed gas caused the foam to spread quickly over the entire 360-degree circumference, and, thus, precluded visual observation, Figure 36. It did appear, though, that the film thickness remained fairly constant, regardless of foam flow rate. This can be interpreted to mean that film velocity increases with foam flow rate. Visual observations appear to confirm this point.

46
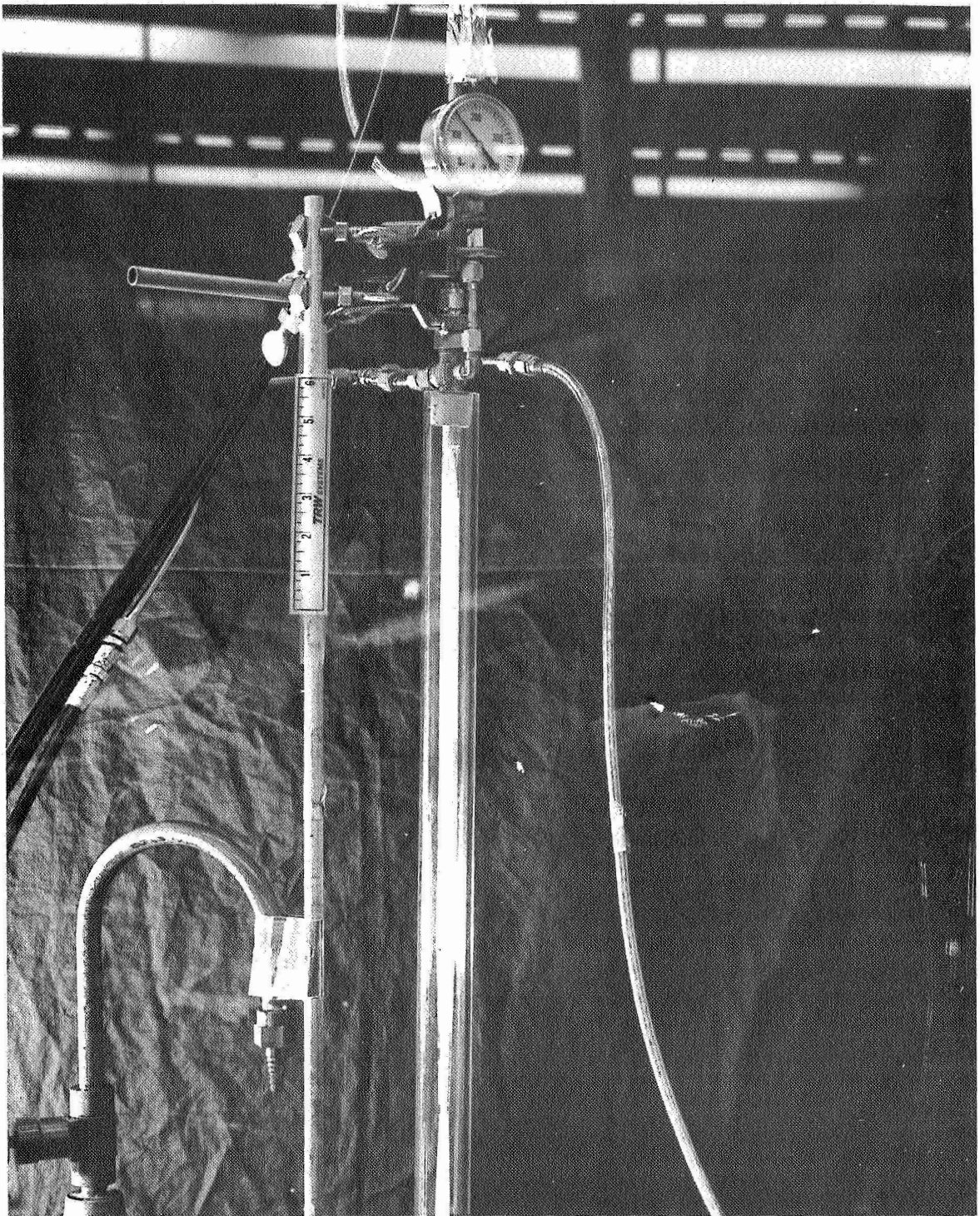
Figure 36. Foam Film Attachment at 100 psig
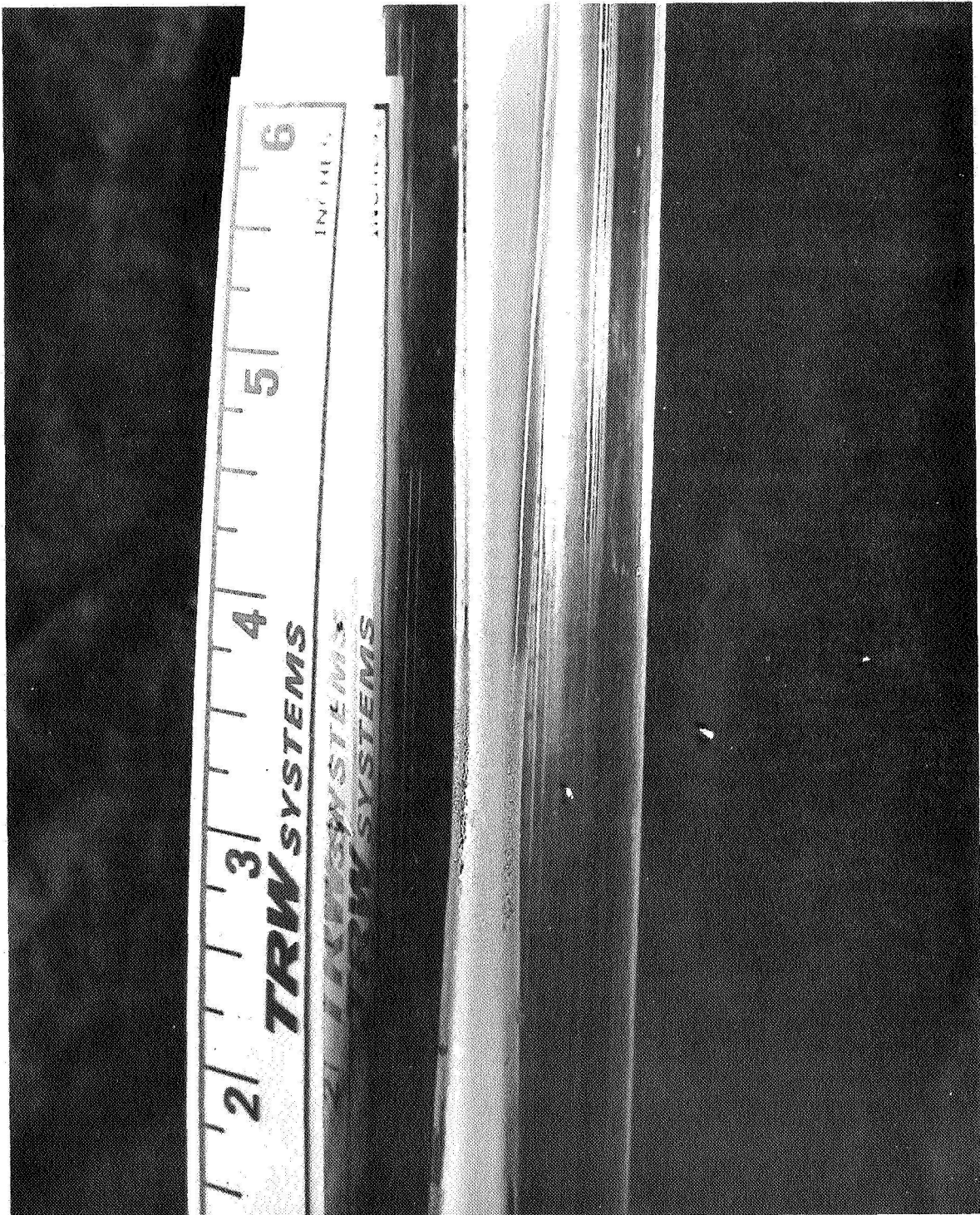
Figure 37. Foam Film Attachment in the Sonic, Transonic and Supersonic Flow Regimes at 100 psig

The foam film attachment studies were extended to a solution of hydrazine containing 5% polymeric foaming agent. The testing was done remotely, primarily to avoid the atomized hydrazine fumes and nitrogen gas issuing from the venturi exit (see Figure 38). In general there appeared to be no qualitative difference between the hydrazine and water foam, confirming previous TRW studies. The results were documented by motion pictures.

4.2 COLD FLOW FROM INJECTOR TESTS

Cold flow tests of the method of injecting foam were conducted to prove and optimize the concept and to find optimum gap settings.

Cold flow testing of the foam injector at 300 psia was simulated by equivalent atmospheric foam as shown in Figures 39 through 41. In this particular series of tests the film coolant thickness was maintained at 0.052-inch while the expansion was varied from 1.0 (liquid) to 10.0. The open places in the foam blanket were found to be caused by some metal clips lodged near the gap outlet. The most even tubular foam blanket seemed to be formed at injection velocities ranging from 5 to 10 ft/sec. The injector gave similar results at 0.3 lb/sec when the gap was correspondingly reduced. The generally tenacious quality of the foam was again demonstrated.

During these tests, the injector pressure drop was also characterized as a function of gap setting and expansion ratio. The results of a typical test are summarized in Table 8 and show that to a first approximation, the conventional ΔP formula is followed:

$$\Delta P_f = \frac{C\left(\frac{\dot{w}}{A}\right)^2}{\rho_{foam}} = \frac{C\left(\frac{\dot{w}}{A}\right)^2}{\rho_L}EXP$$

4.3 HIGH PRESSURE FOAM GENERATOR

Construction and testing of the high pressure foam generator revolved around selection of percent coolant ranges, allocation of pressure drop, experimental sizing of packed bed improvers, and calibration of venturis.

Table 9 lists the coolant foam generators sizes which were selected for construction. Thus the percent coolant flow could be varied from 2 to 30 percent of the total propellant flow in the actual engine tests.

Pressure allocation criteria were that a "stiff" system would be best from the point of view of minimizing engine perturbations. Therefore, the venturis were sized for a minimum upstream pressure of 600 psia. Experimental testing showed that venturi flow rates were independent of back stream pressure up to 80 percent of the upstream pressure. Therefore the packed bed improvers were sized for a pressure drop of 50 to 150 psia (sufficient pressure drop to provide a good quality foam) and a maximum ΔP of 50 psi was allowed for the foam injector.
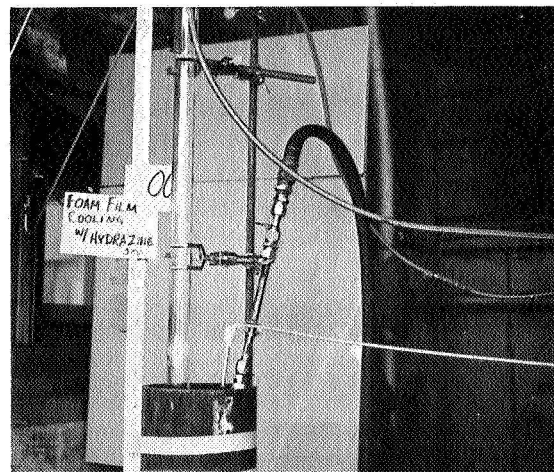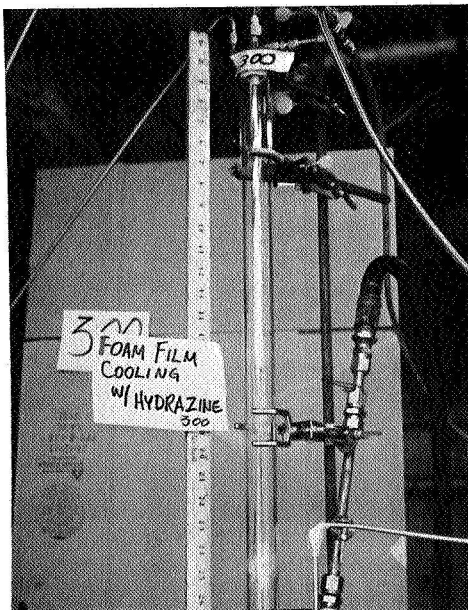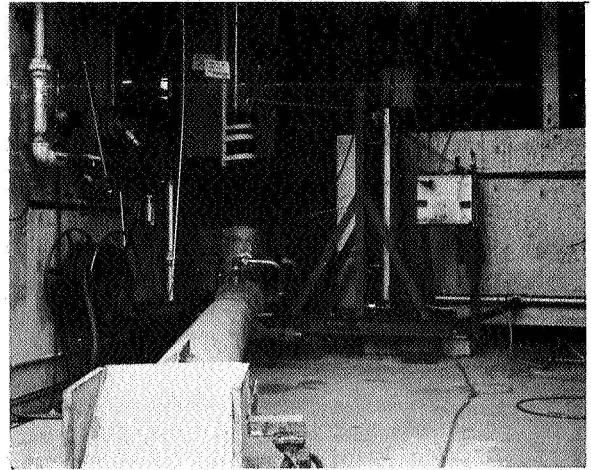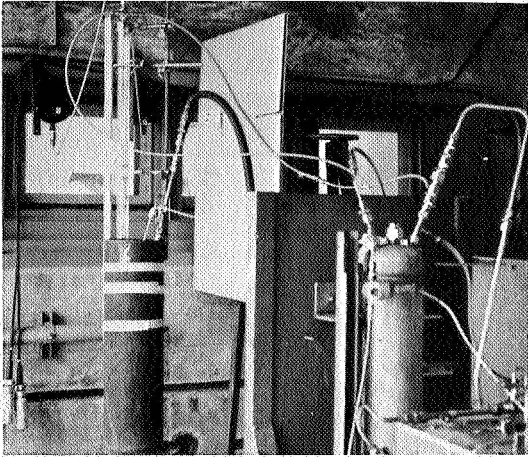
Figure 38. Hydrazine Foam Film Attachment Studies
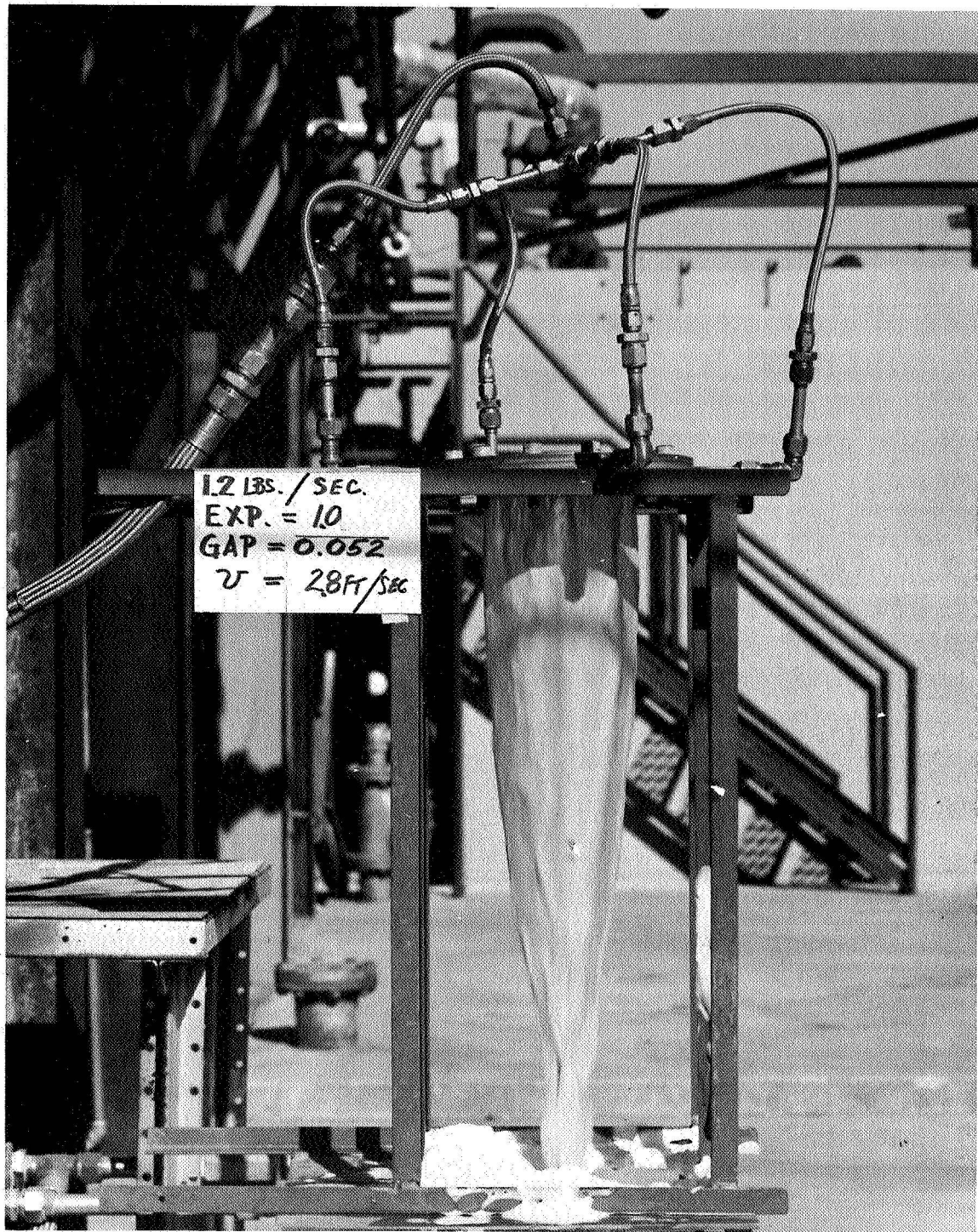
Figure 39. Cold Flow Testing of Foam Injector

Figure 40. Cold Flow Testing of Foam Injector
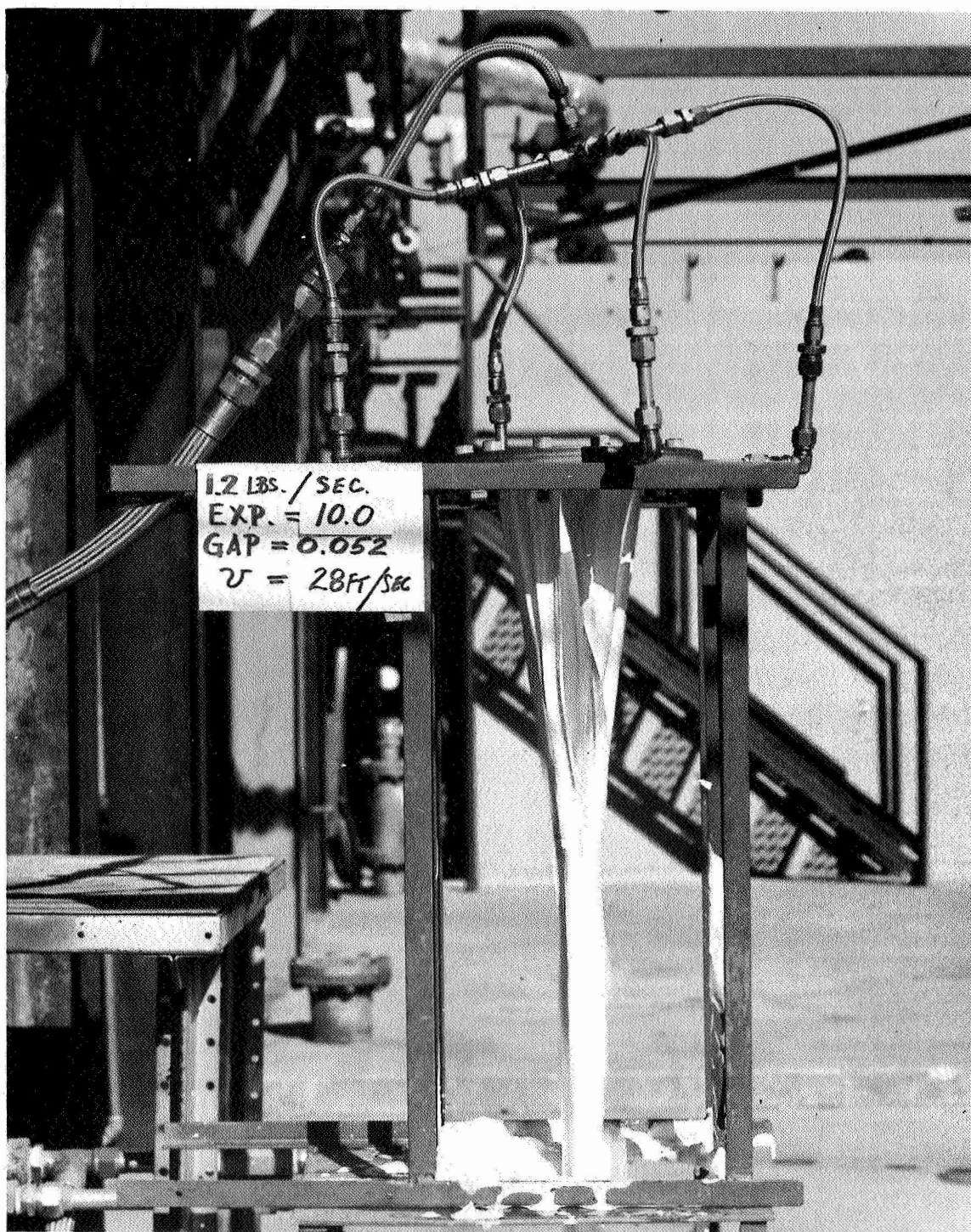
Figure 41.   Cold Flow Testing of Foam Injector

Table 8. Foam Injector Pressure Drop Characterization

Injector Gap = 0.012 inches (0.024 shims)

Liquid $D_L = 0.052$ in		Gas $D_g = 0.028$ in			
PoL psia	$\dot{w}_1$ lb/sec	Pog psia	EXP	v INJ ft/sec	ΔP INJ psig
725	0.248	14.7 (off)	1.0	2.5	~0.1
725	0.248	100	5.5	14.0	2.9
725	0.248	195	9.7	24.0	6.5
725	0.248	595	28.0	70.0	14.0
		Injector Gap = 0.003			
697	0.242	14.7 (off)	1.0	9.9	6.0
697	0.242	81	5.0	49.0	18.0
697	0.242	188	9.6	94.0	25.6

Table 9. Coolant Foam Generators

Coolant lb/sec	Liquid Venturi		Gas Venturi		EXP
	D, in	P_o, psia	D, in	P_o, psia	
0.23 to 0.37	0.052	600 — 1200	0.043		
0.52 to 0.74	0.076	600 — 1200	0.052, 0.11 0.11 + 0.052 0.1405	1000 — 2000	5 — 30
1.2 to 1.66	0.11	600 — 1200	0.076	1000 — 2000	5, 10
2.15 to 3.0	0.152	600 — 1200	0.11 + 0.076 0.076 + 0.052	1000 — 2000	5, 10

54

The packed beds were sized experimentally by varying bed length, ball size, and bed diameter until a satisfactory pressure drop was obtained. The beds were built in such a manner that the end fittings provided anti-channeling rings (see Table 10).

Liquid venturi flow rates were calibrated by the conventional catch and weight techniques as a function of pressure and type of liquid. There is little difference between water, water with 3% protein agent, or water with 23% polymer agent and all points seem to fall in a straight line on a $\dot{w}$ versus log P plot, Figure 43, which is to be predicted from the flow equation:

$$\frac{\dot{w}}{A} = C\sqrt{P_o - P_{VP}} = C\sqrt{P}$$

It was found, however, that care must be taken not to aerate the liquid foam while mixing or reduced flow rates would result.

Gas venturis were calibrated against standard rotometers, Figures 44 and 45.

Table 10. Packed Bed Dimensions

Capacity Foam (lb/sec)	Ball Size	Depth (in.)	Bed Diameter (in.)	Flow Diameter (in.)
2.5	0.170	7/8	1.76	0.825
1.2	1/8	1.0	1.140	0.605
0.5	1/8	7/8	0.675	0.39
0.3	1/8	11/16	0.55	0.376
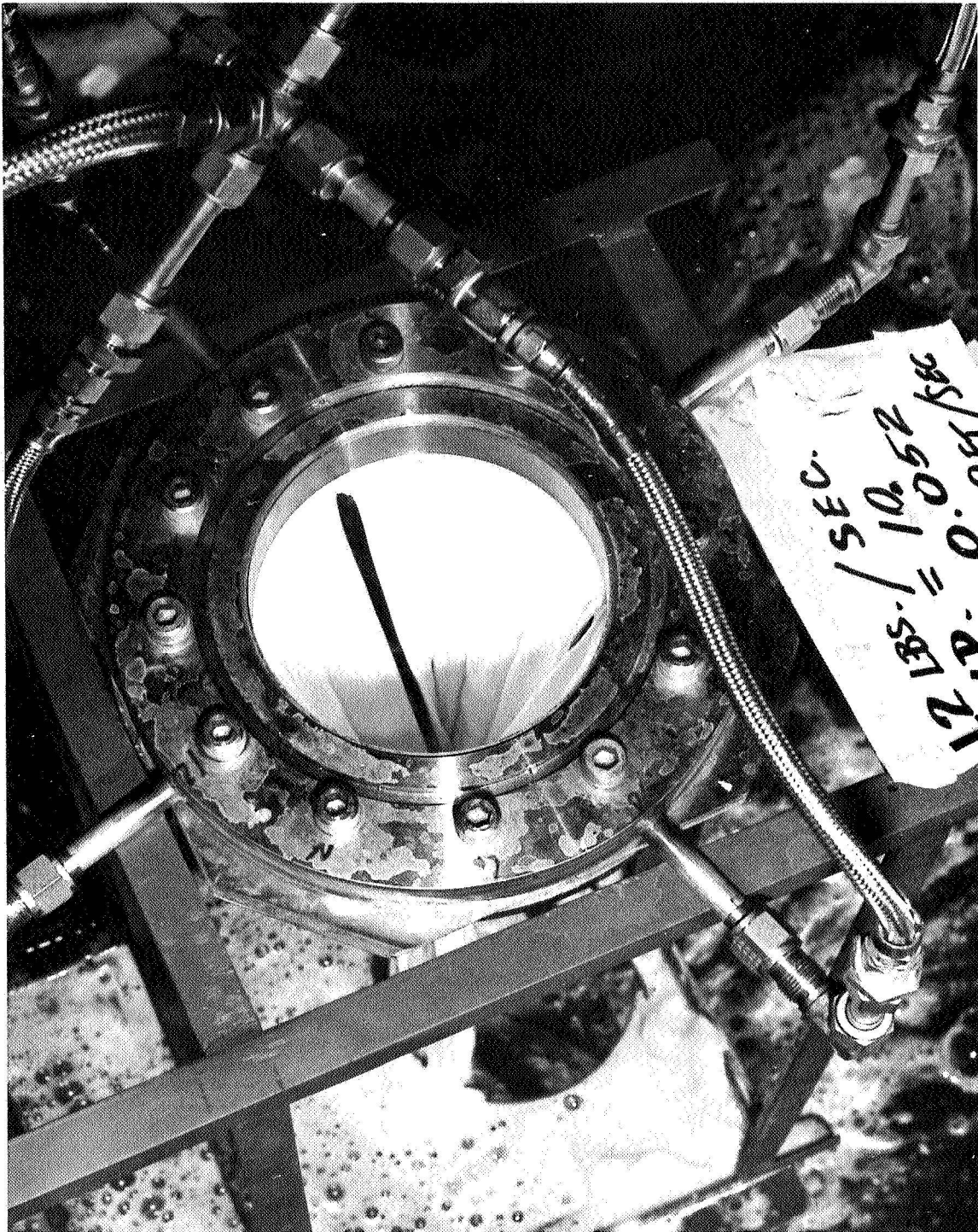
Figure 42. Cold Flow Testing of Foam Injector
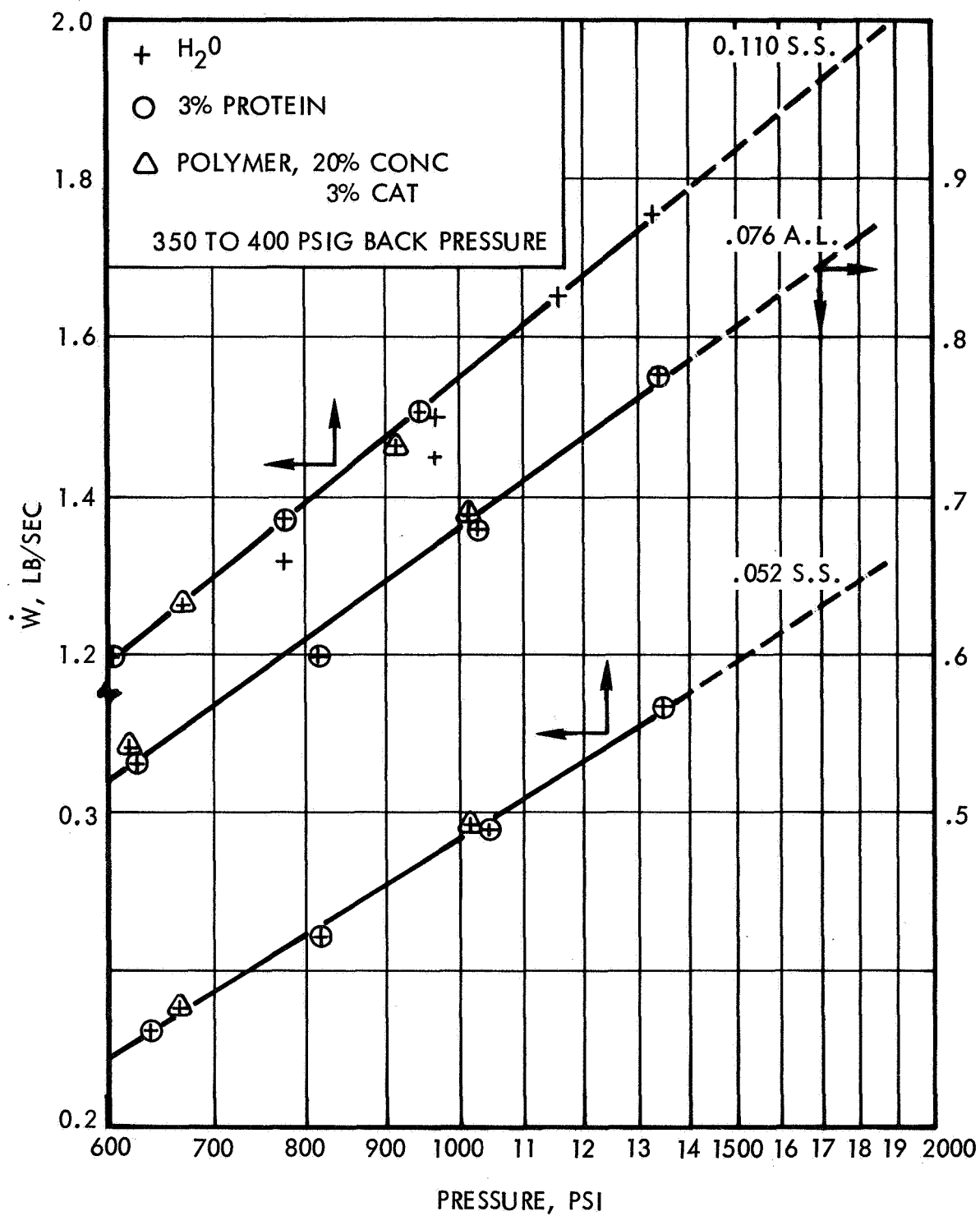
Figure 43. Liquid Calibration Curves for
Venturis

57
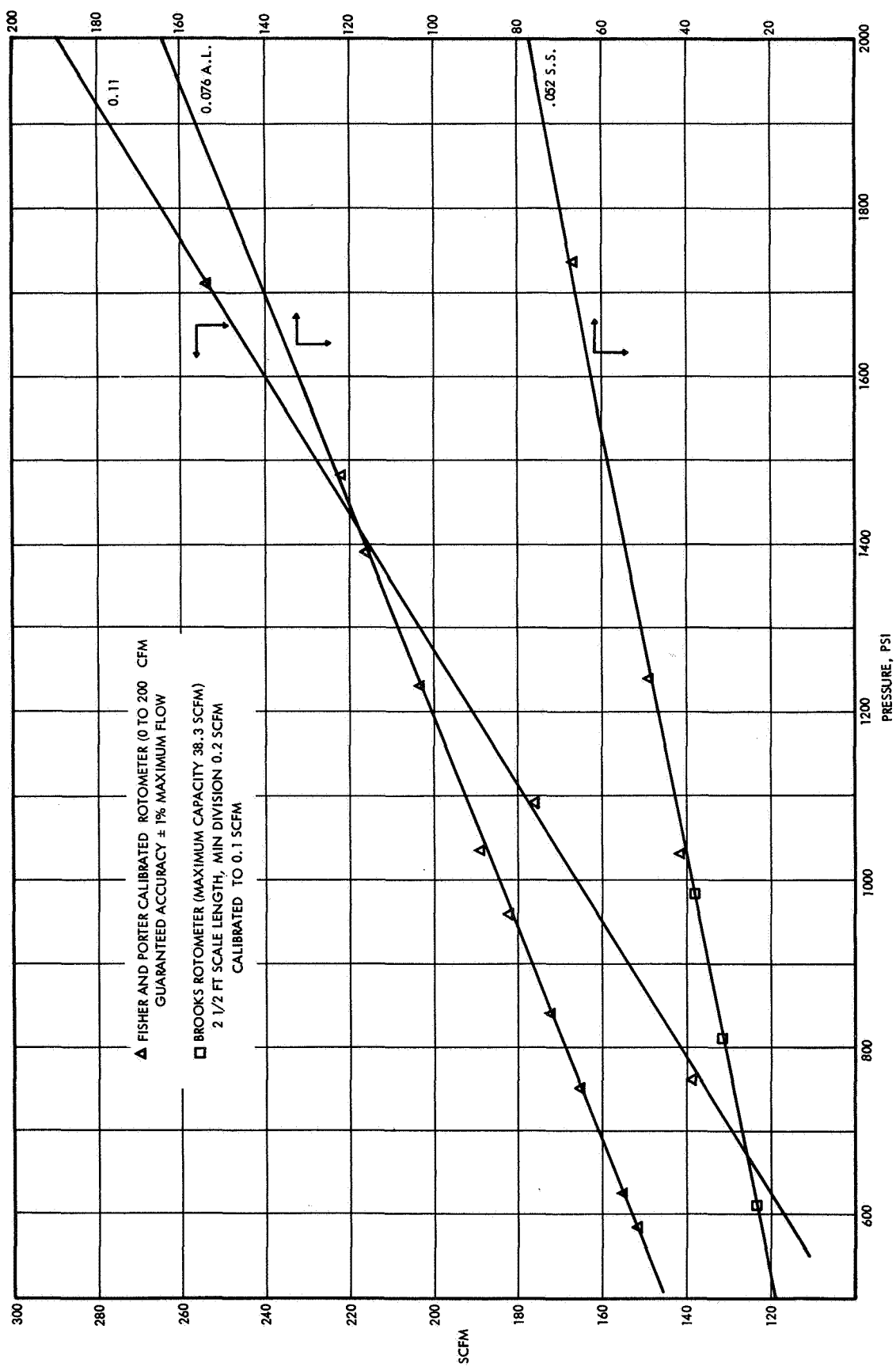
Figure 44. Gas Calibration Curves for Choked Venturis, High Range

58
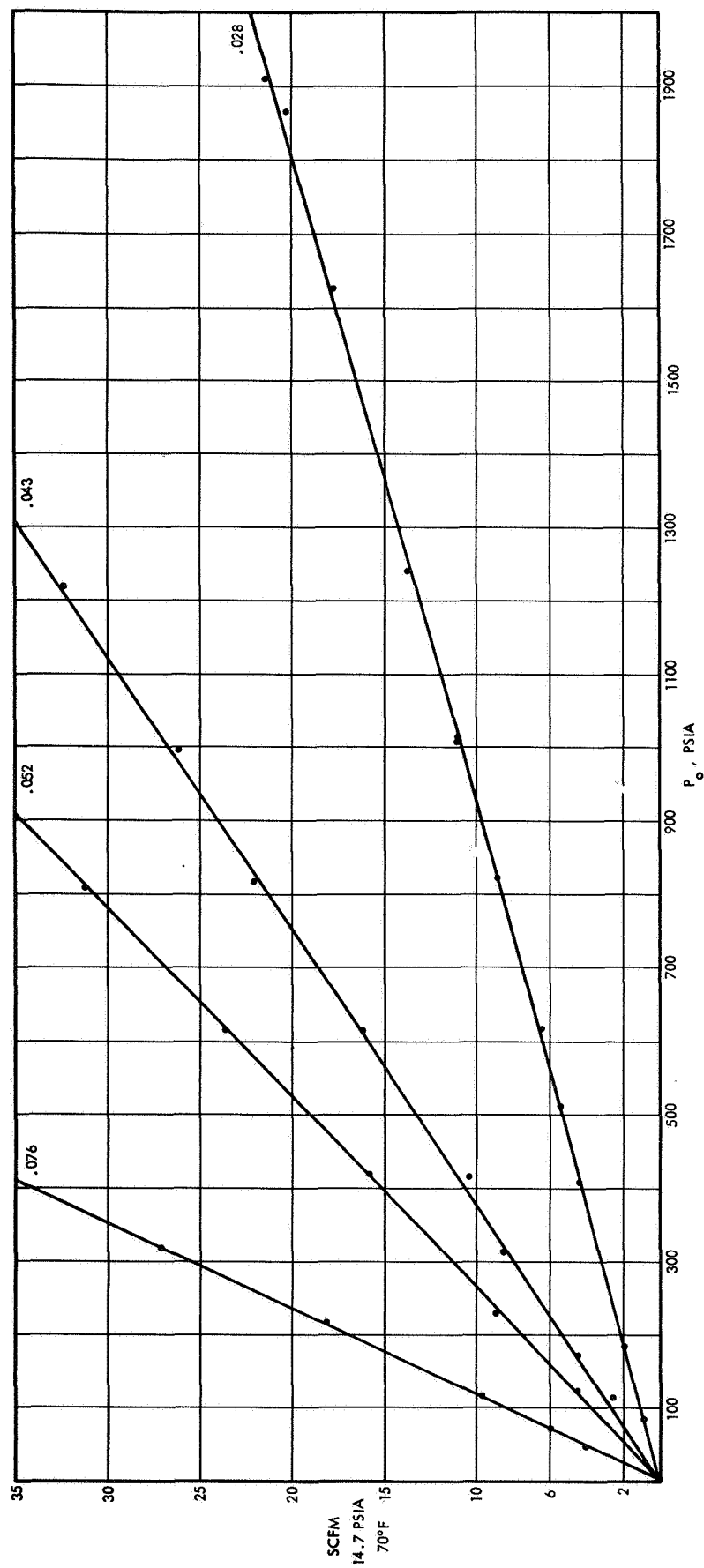
Figure 45. Gas Calibration Curves for Choked Venturis, Low Range

5. HEAT TRANSFER TESTS AND RESULTS

The original program planning called for conducting 30 tests with N_2O_4/N_2H_4 main engine propellants at a nominal chamber pressure of 300 psia. The three foaming agents, protein, Aer-O-Foam 100, and aerated water, in water and N_2H_4, were to be evaluated at various percentages of agent and foam expansion ratio. The overall thermal effectiveness of the foam, for single points of injection, was to be determined along with obtaining data on the expected distance a foam could be pushed in a chamber without streaking.

5. 1 ENGINE TEST SUMMARY

A total of 41 tests were conducted. Engine, coolant, and performance data for the 41 heat transfer runs are summarized in Table 11.

Three tests — 417, 418, and 419 — were made to check out the main injector with a blank ring inserted for the foam injector to establish no-coolant heat transfer data at a nominal pressure of 300 psia and at conditions of 10% higher and lower than nominal. Based on the results of a related Air Force program, a nominal MR of 1.2 was selected as the optimum for these tests. The results of the checkout runs were encouraging since high performance was achieved with no hardware damage.

The successful checkout runs were followed by a series of runs (420 to 423) in which the coolant flow rate (H_2O) was increased from 1.2 to 2.5 lb/sec in an effort to cool the entire engine to the saturation temperature. During these runs, the expansion ratio was set at 5.0 and the protein foaming agent was used. The runs indicated low cooling efficiencies comparable to those expected with straight liquid injection. Since the TRW injector provides cool head-end regions due to fuel film cooling, there was some suspicion that the low efficiencies may have been due to liquid fuel lifting the foam at the point of injection, or that the foam momentum vector, ρv, was resulting in main stream penetration by the foam. The point of foam injection was moved 1.5 inches downstream by inserting a dummy foam ring between the main injector and the foam injector and the run was repeated (Run 422). No qualitative differences were noted.

In Runs 424 through 429, the foaming agent type and expansion ratio was varied at a nominal 2.5 lb/sec in an effort to see if any of these parameters would markedly influence cooling efficiency. There appeared to be no qualitative improvements in cooling efficiencies.

Run 430 was made as a baseline run for an acrylic engine test at maximum foam generator flow.

The acrylic engine test, Run 431, was conducted so that the area adjacent to the point of foam injection could be observed for possible free stream stripping and its cause. Figure 46 shows the acrylic engine

60

Table 11. Summary of Engine Performance Data for Foam Coolant Runs

	ENGINE				COOLANT						
TEST	PC	$\dot{\omega}_P$	MR	CORR THRUST	TYPE	FOAM AGENT	$\dot{\omega}_L$	EXP	ΔP	GAP	VEL
417	304	10.21	1.21	2650	None						
418	334	11.12	1.195	2940	None						
419	263	9.03	1.153	2305	None						
420	304	9.74	1.21	2690	H_2O	3% Protein	1.19	4.92	34	0.056	12.8
421	311	9.66	1.205	2725	H_2O	↓	1.63	4.91	49	0.056	17.6
422	313	9.76	1.215	2775	H_2O		1.63	5.04	47	0.056	18
423	283	8.67	1.09	2470	H_2O		2.35	5.4	74	0.056	27.8
424	287	8.79	1.12	?	H_2O	23% Polymer	2.21	6.0	72	0.056	29.7
425	283.6	8.86	1.125	2460	H_2O	3% Protein	2.42	1.0	2.9	0.030	9.9
426	282.8	8.91	1.135	2480	H_2O	3% Protein	2.38	1.0	.9	0.030	9.7
427	283.5	?	?	2490	H_2O	None	2.43	1.0	?	0.030	9.95
428	292	8.68	1.13	2540	H_2O	3% Protein	2.46	9.42	52	0.1075	27.4
429	293	8.78	1.12	2590	H_2O	23% Polymer	2.40	10.6	49	0.1075	29.0
430	292	8.69	1.115	2590	H_2O	3% Protein	3.0	5.39	63	0.1075	11.0
431	275	8.95	1.14	2545	H_2O	3% Protein	2.92	5.6	66.1	0.1075	18.6
446	315	9.73	1.19	2780	H_2O	3% Protein	1.53	4.08	?	0.020	38.3

Table 11.   Summary of Engine Performance Data for Foam Coolant Runs (Continued)

ENGINE					COOLANT						
TEST	PC	$\dot{\omega}_P$	MR	CORR THRUST	TYPE	FOAM AGENT	$\dot{\omega}_L$	EXP	ΔP	GAP	VEL
447	314	9.49	1.15	2760	H_2O	3% Protein	1.22	4.85	25.5	.130	5.6
448	316	9.84	1.22	2760	H_2O	3% Protein	1.23	10.2	31.4	.130	11.8
449	300	9.82	1.22	2650	None	Liquid	0	α	0.20	.130	10.5
450	315.5	9.82	1.21	2780	H_2O	23% Polymer	1.19	10.0	32.6	.130	11.2
451	315.5	9.80	1.21	2780	H_2O	1.5% Deter-gents	1.17	10.1	41.1	.130	11.1
452	320.2	9.84	1.22	2800	H_2O	1.5% Deter-gents	1.21	9.4	39.8	.070 (?)	19.9
453	309	9.74	1.195	2720	H_2O	None	1.20	1.0	1.9	.070	2.1
454	304	9.795	1.24	2670	H_2O	3% Protein	0.52	5.13	8.93	.070	4.7
455	311.5	9.83	1.235	2745	H_2O	3% Protein	0.528	26.6	24.3	.070	24.6
456	323	10.10	1.285	2850	H_2O	1.5% Deter-gent	0.511	32.6	19.2	.070	29.3
457	283	8.62	1.32	2490	H_2O	6% Protein	1.18	22.0 EST	40.9	.070	46.0 EST
458	281	8.60	1.08	2460	H_2O	6% Protein	1.2	22.0 EST	41.3	.070	46.0 EST

Table 11. Summary of Engine Performance Data for Foam Coolant Runs (Continued)

	ENGINE				COOLANT						
TEST	PC	$\dot\omega_P$	MR	CORR THRUST	TYPE	FOAM AGENT	$\dot\omega_L$	EXP	ΔP	GAP	VEL
459	300	9.13	1.22	2620	H_2O	6% Protein	1.16	22.0 EST	37.6	.070	46.0 EST
460	300.7	9.09	1.20	2571	H_2O	3% Protein	1.68	5.34	49.4	.070	15.7
461	267	9.06	2.10	2345	None						
462	266	8.95	2.05	2305	None						
463	270.9	8.66	2.07	2350	H_2O	3% Protein	1.08	6.1	32.9	.070	11.6
464	269	8.83	2.07	2340	H_2O	3% Protein	0.525	5.55	11.6	.070	5.1
465	268.8	8.63	2.08	2340	H_2O	3% Protein	0.52	31.3	31.3?	.070	28.5?
466	272.5	9.02	2.08	2375	H_2O	None	0.522	1.0	?	.070	0.915
467	261.5	8.84	2.07	2280	None	None	0	α	(.108 ft^3/sec)	.070	11.8
468	268	8.42	2.04	2330	H_2O	3% Protein	1.63	5.8	53.5?	.070	16.5
469	277.5	8.44	2.055		H_2O	3% Protein	1.63	5.93	43.6	.070	16.9
470	273.5	8.44	2.055	2420	H_2O	None	1.635	1.0	?	.070	2.86
471	274.5	8.65	2.07	2398	H_2O	3% Protein	0.52	30.1	36.9	.070	27.4

Table 11. Summary of Engine Performance Data for
Foam Coolant Runs (Continued)

Run	Main Injector Type	Chamber Length Upstream of Foam Injection Point	Downstream of Foam Injection Point	Fuel Propellant
417	TRW	---	---	N_2H_4
418		---	---	
419		---	---	
420		1.5	7.85	
421		1.5		
422		3.0		
423				
424				
425				
426				
427				
428				
429				
430				
431			acrylic engine	
446		6.35	15.70	
447				
448				
449				
450				
451				
452				
453				
454				
455				
456				
457				
458				
459				
460	Flat Face	2.5	7.85 acrylic engine	
461	Flat Face	7.35	16.2	UDMH
462	TRW	6.35		
463	Flat Face	7.35		
464	Flat Face			
465	Flat Face			
466	Flat Face			
467	Flat Face			
468	Flat Face			
469	TRW	6.35		
470	TRW			
471	TRW			

64
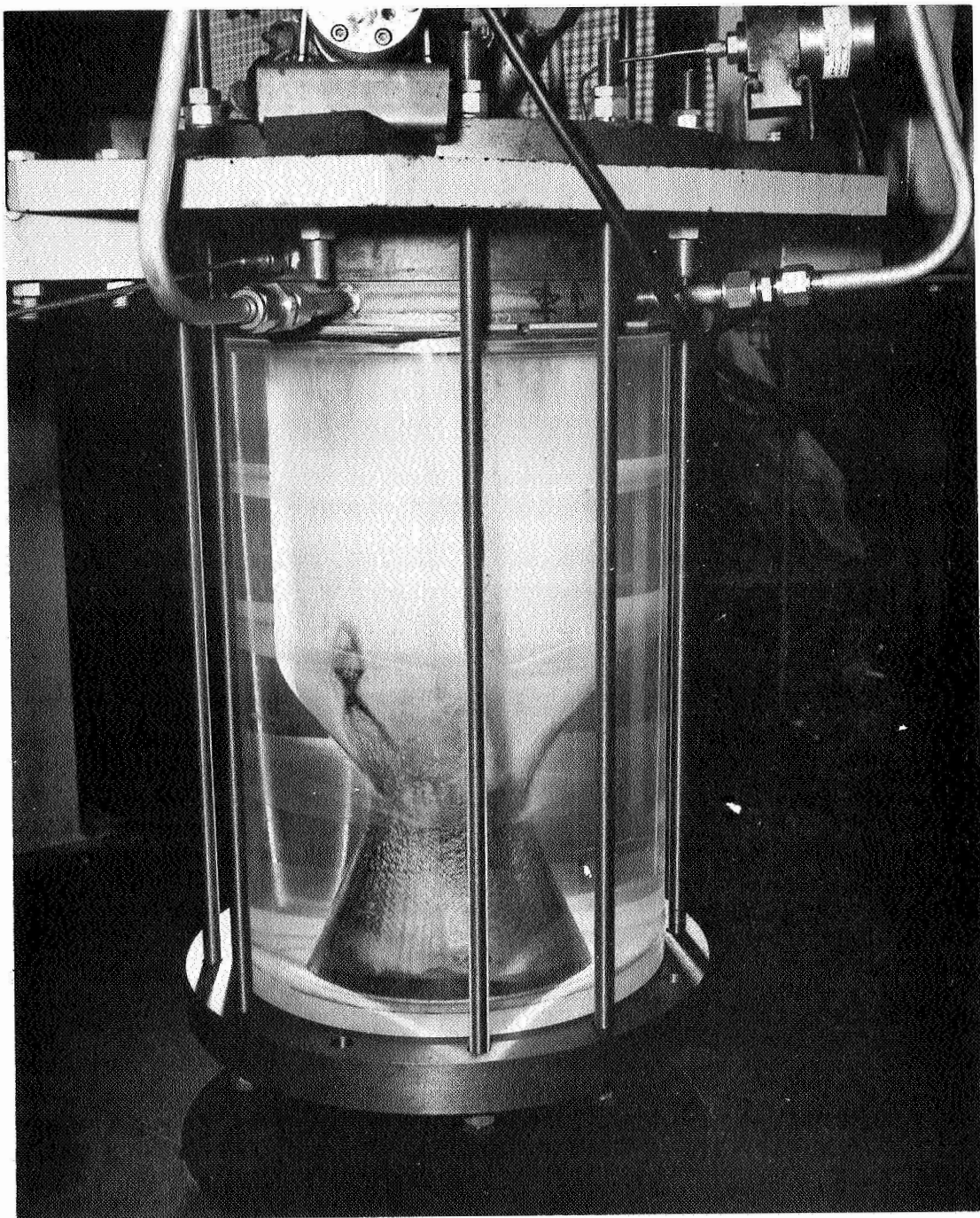
Figure 46. Photograph of Acrylic Engine
after 4 Seconds of Firing

after 4 seconds of firing. It is readily obvious that some erosion occurred in the region of the throat, but the foam persisted for a distance of 12 inches (see Figure 47) with only minor streaking in the combustion chamber. During the course of the run the chamber pressure declined from 290 to 262 psia.

Detailed examination of high speed movies and the chamber revealed a probable cause of low cooling efficiency.

Other close-ups of the acrylic engine are shown in Figures 48 through 51. Of the close-up pictures, Figure 49 is the most significant since it reveals minor but perceptible discolorations, indicating the probable presence of fuel propellant penetrating beneath the foam blanket. These streaks extend 2 to 4 inches below the point of foam injection.

Although these streaks represent a form of propellant film cooling, they are very detrimental to film attachment as the movie pictures showed. The films also:

- Confirmed the existence of foam at 300 psia under hot firing

- Showed an area of extremely turbulent combustion extending 2 to 4 inches below the point of foam injection

- Showed the existence of a myriad of small streaks extending 2 to 4 inches below the point of foam injection

- Showed that the small streaks closed up rapidly, indicating the antistreaking capability of foam

- Confirmed the existence of foam in the trans- and super-sonic flow regions

After the completion of the acrylic engine testing and analysis, the heat sink hardware was reassembled for Run 446 with the following changes to improve the results:

- The point of foam injection was moved 3.35 inches further downstream.

- The foam injection angle was redirected from 30 degrees to parallel to the wall by tack welding a thin walled deflector ring on the inside of the foam ring.

- The injection velocity of the foam was increased to minimize shearing action of the combustion gas

- An additional chamber section was added, bringing the total combustion length to 15.70 inches.

During the first part of the run all Nanmac thermocouples (including those located 15.20 inches from the foam injector) were

66
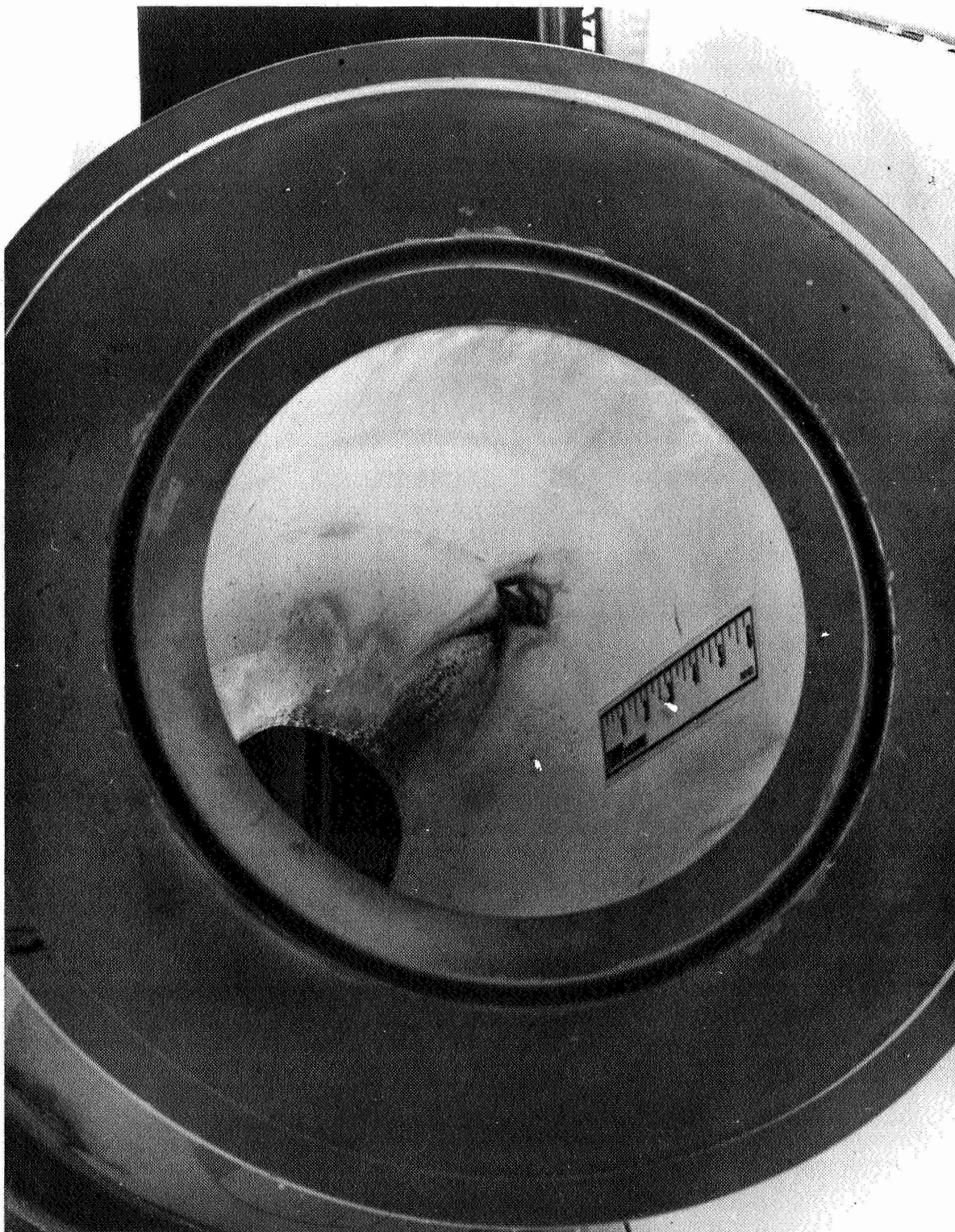
Figure 47. Close-up Photograph of the Chamber Wall of
the Acrylic Engine after Firing
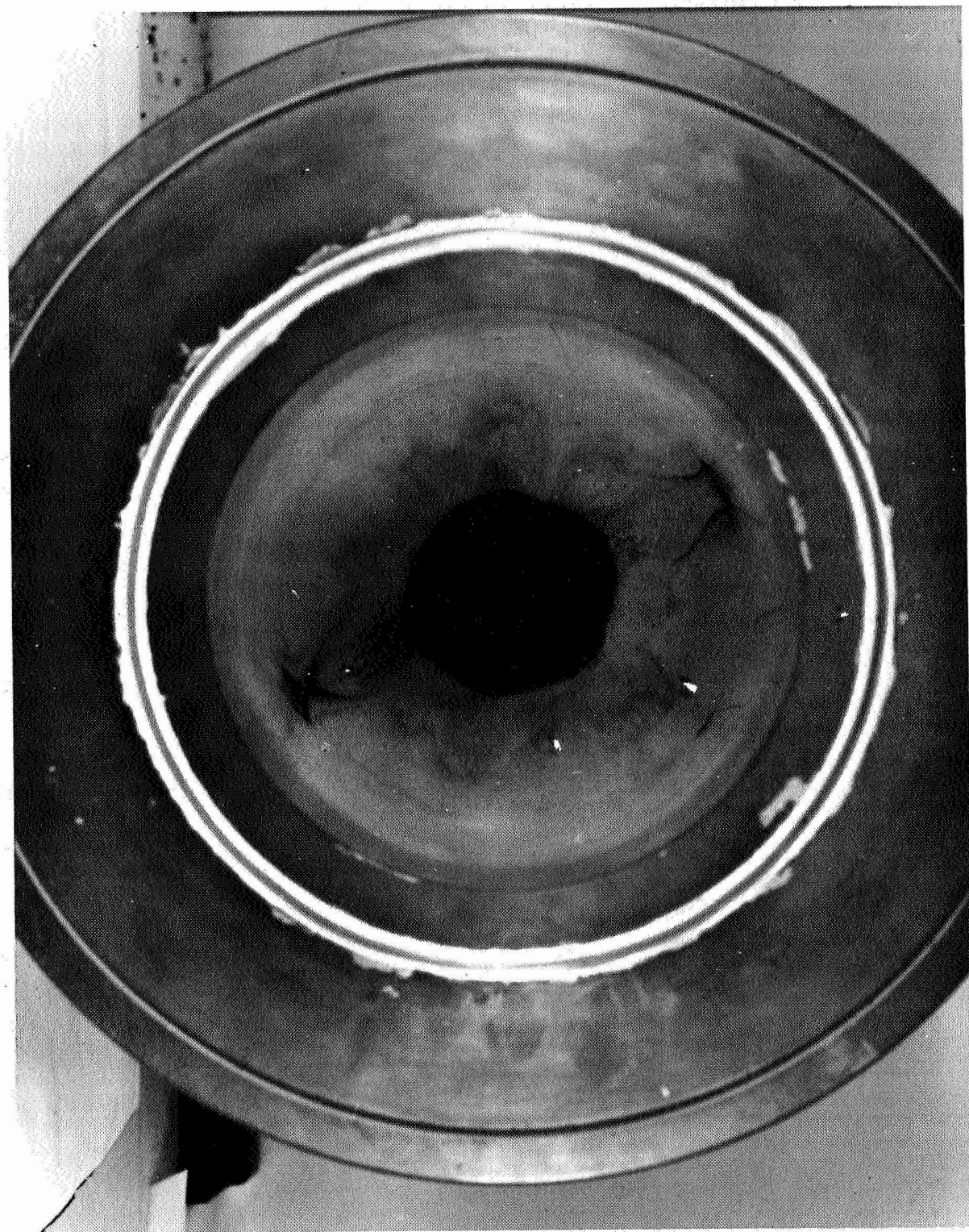
Figure 48.   Photograph of the Throat of the Acrylic
Engine after 4 Seconds of Firing

68
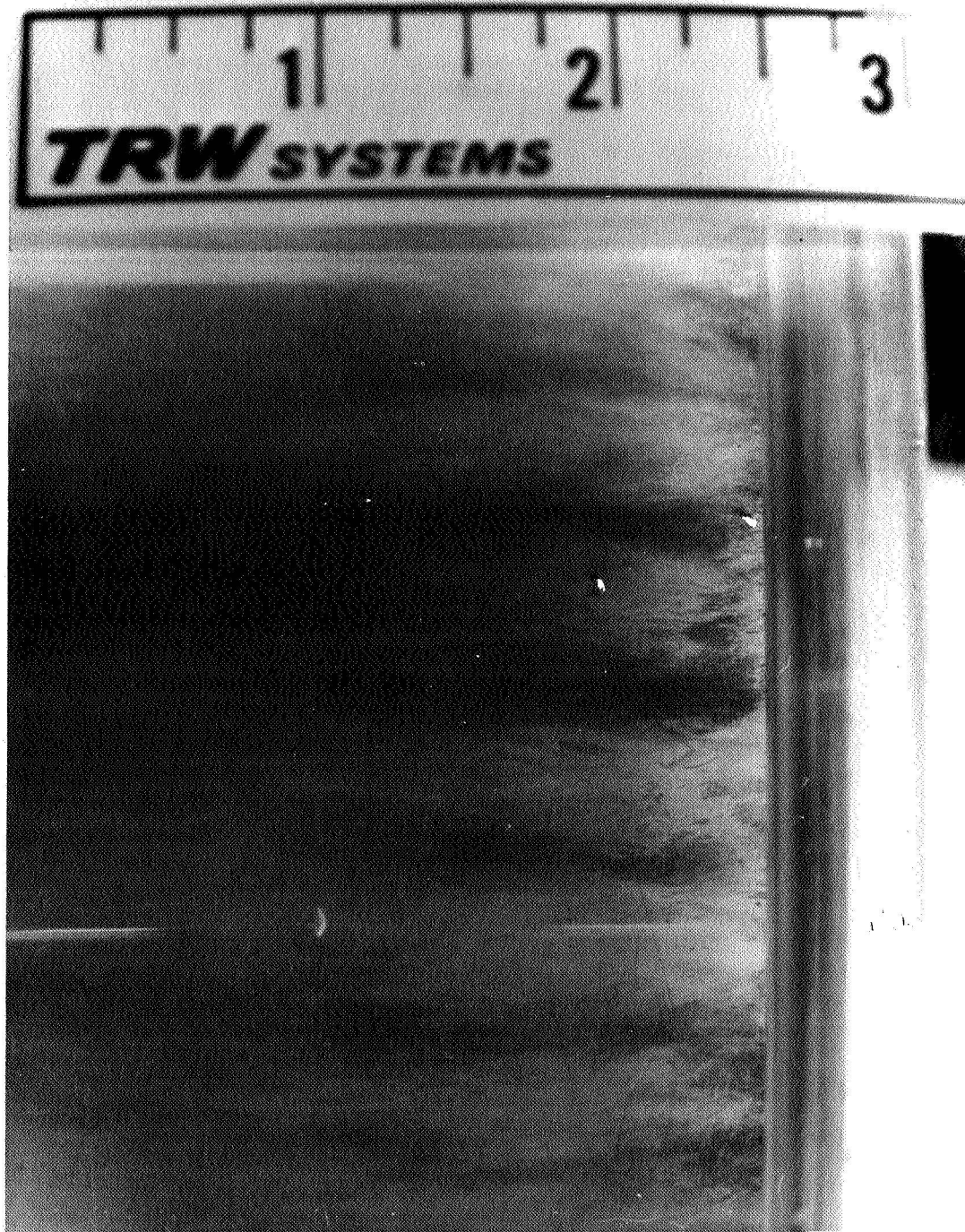
Figure 49. Close-up Photograph of the Area Immediately Adjacent to the Point of Foam Injection
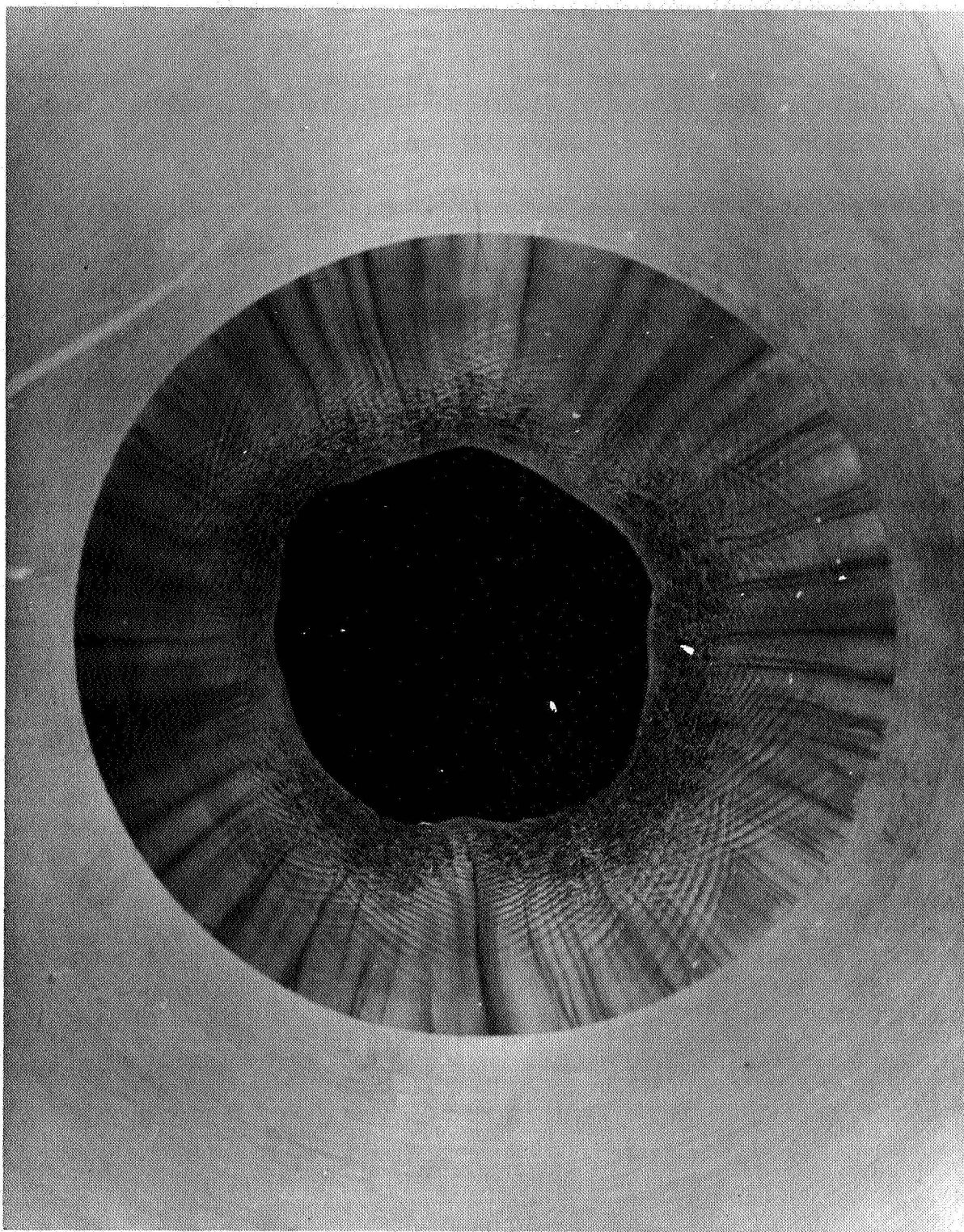
Figure 50.   Close-up Photograph of the Throat of the
Acrylic Rocket Engine from the Exit
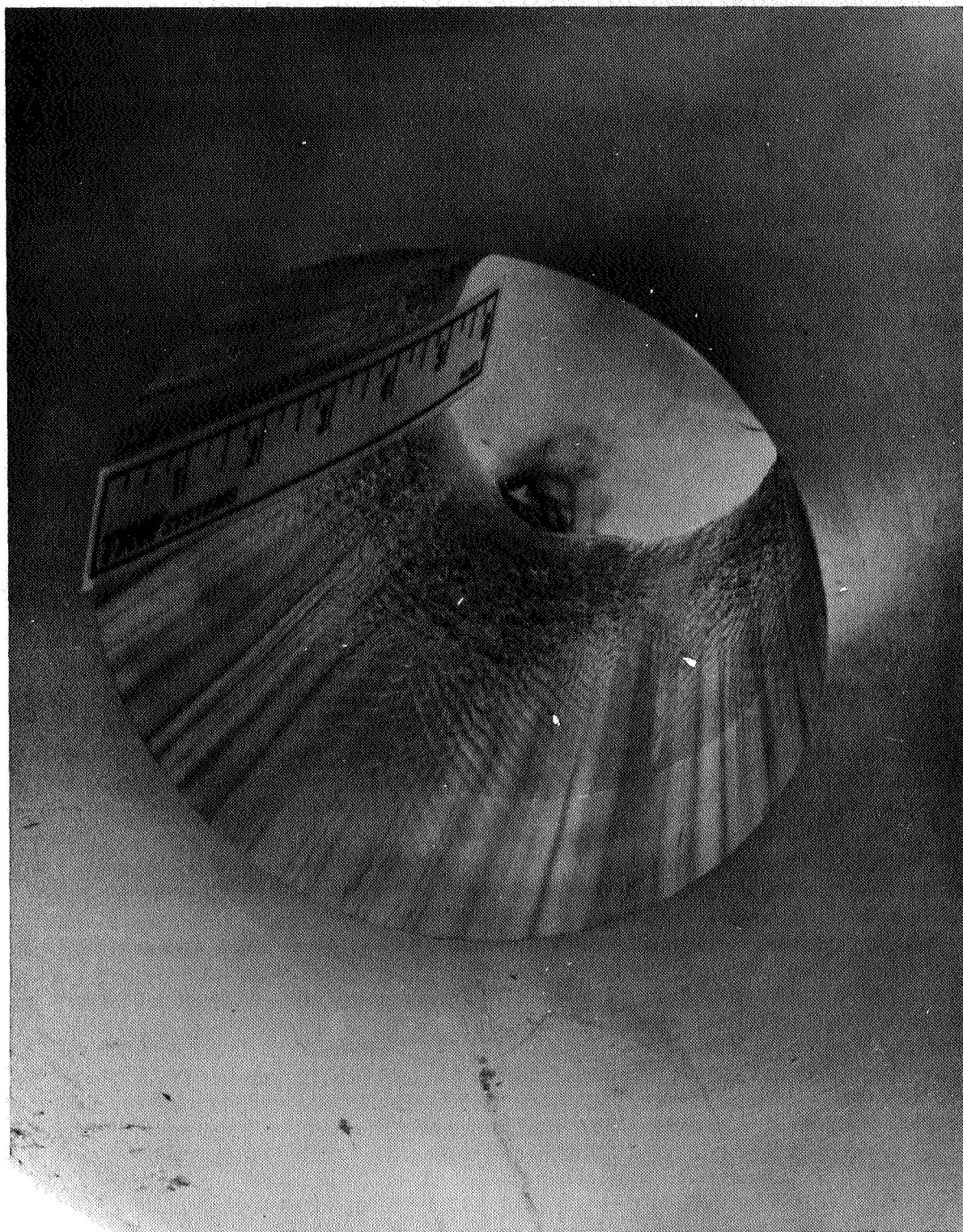
Figure 51. Close-up Photograph of the Skirt
of the Acrylic Engine

observed to stabilize at the coolant saturation temperature before heat caused the deflector to warp causing foam streaking and stoppage. However, cooling efficiencies in excess of 40 percent were observed during the stabilized part of the run. This result was considered quite encouraging. Although significantly increased cooling efficiencies were suspected, it was necessary to modify the foam injector because the deflector ring had expanded and warped, and as a result of foam ring modification changing the angle of injection from 30 to 12, chamber length was extended 0.5 inch as previously discussed. The results of test 447 verified that the cooling efficiency was approximately 20 to 30 percent higher than that of runs where foam injection was made at head end.

With cooling efficiency near 50 percent, a brief parametric study of foam parameters such as expansion ratio, agent type, and injection velocity was run to see if the cooling efficiency could be increased another 20 percent. Runs 448 through 453 were directed toward this objective. The results indicated no further significant increase in cooling. However, the earlier conclusions were confirmed:

- The protein foam was superior in cooling capacity.

- The polymeric foam gives antistreaking characteristics superior to pure water.

Runs 454, 455, and 456 were made with reduced coolant rates but this seemed to have little effect on overall cooling efficiency until the expansion ratio and injection velocity were drastically increased. This effect was not evident in Runs 457, 448, and 459 at the original flow rates.

At this point in the test program, the NASA injector became available and effort was directed toward evaluation if it.

A checkout test (Run 460) of the flat-faced injector supplied by NASA was made with the foam injector installed upon an acrylic engine. This approach was selected to minimize possible damage to expensive hardware and instrumentation in the event the injector went unstable. The previously demonstrated value of motion pictures in observing streaking, turbulence, and length of film cooling also influenced this decision.

Motion pictures of the test (Run 460, Table 11) showed:

- Smooth, even foam cooling over the entire engine until the combustion went unstable, with the engine coolant rate approximately halved (compare coolant data of Run 460 with Run 431 in Table 11) from previous runs. (See Figure 52 for still photos of firing.)

- Reduced wall turbulence effects resulting from main injector propellant impingement as compared to that for the coaxial injector.

72
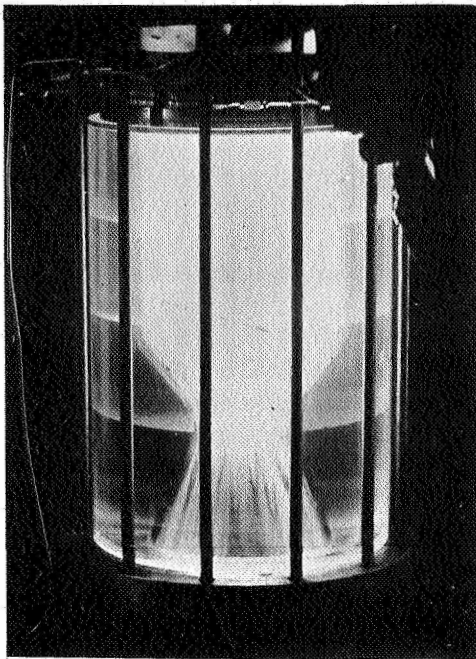
Nominal Stable Conditions
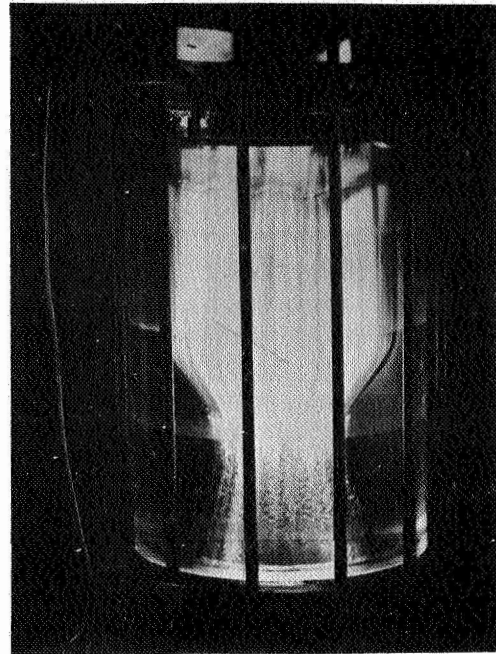
Shutdown
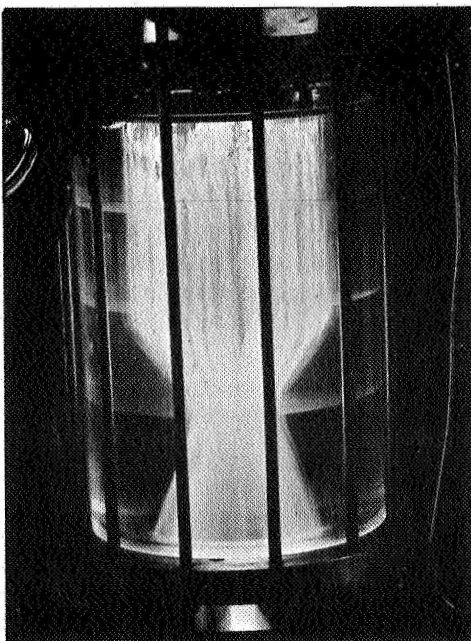
Startup
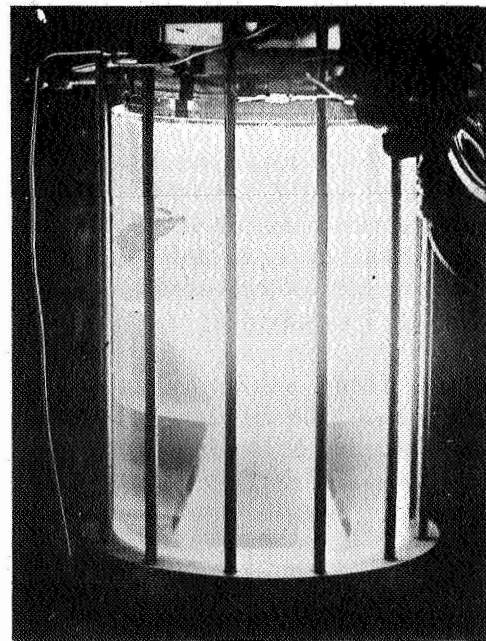
Unstable Conditions

Figure 52. Still Photos of Run 460

- Apparently reduced combustion noise effect for the flat face injector as compared to that for the coaxial injector until engine went unstable.

- Unstable combustion was triggered by several strong pops occurring near the nozzle.

- A swirling mode of combustion instability coupled with the longitudinal mode appeared which literally ate up the foam, slightly eroded out part of the wall (Figures 53 and 54), and strongly eroded the throat (Figure 55), and the skirt (Figure 56).

It was encouraging to note that the engine was totally cooled until it went unstable. Even after going unstable, the chamber was quite well protected and the run was allowed to go for its full duration.

Because of the generally rougher nature of N_2O_4/N_2H_4 combustion compared to most other propellants, and a desire to obtain valid comparison data between the coaxial type and flat face type injectors, it was concluded that the fuel UDMH should be substituted to provide smoother combustion.

At this juncture three series of tests were planned to evaluate foamed cooling with the propellant combination UDMH - N_2O_4 with the mixture ratio increased to 2.1 to approximate thermal conditions near those of N_2H_4 - N_2O_4 at a mixture ratio of 1.2 (see Appendix A). The first test series, Runs 461 and 462, consisted of baseline, no-coolant/ heat transfer testing for both injector types in combination with the long chamber. The results indicated a drop in local heat flux from that measured for N_2H_4, and a reduction of the combustion noise level to the insignificant level for both injectors. Heat fluxes were comparable.

The second series of tests, Runs 463 to 468, involved the evaluation of protein foam and water at flow rates and expansion ratios of 0.52 to 1.6 lb/sec, and 1.0 to 30 respectively, for the flat-face injector. The initial goal was exceeded in Run 468 when 1.63 lb/sec of protein foam was observed to cool the entire engine (16-inch combustion section and 9-inch throat). Conservatively estimated cooling efficiencies ranged from 50 to 70 percent.

The third series of tests, Runs 469 to 471, were conducted with the TRW injector in lieu of the flat-face injector. Cooling efficiencies were again remarkably high.

The program was terminated on a positive note when it was demonstrated that it was possible to cool an entire engine 25 inches long at a high cooling efficiency.
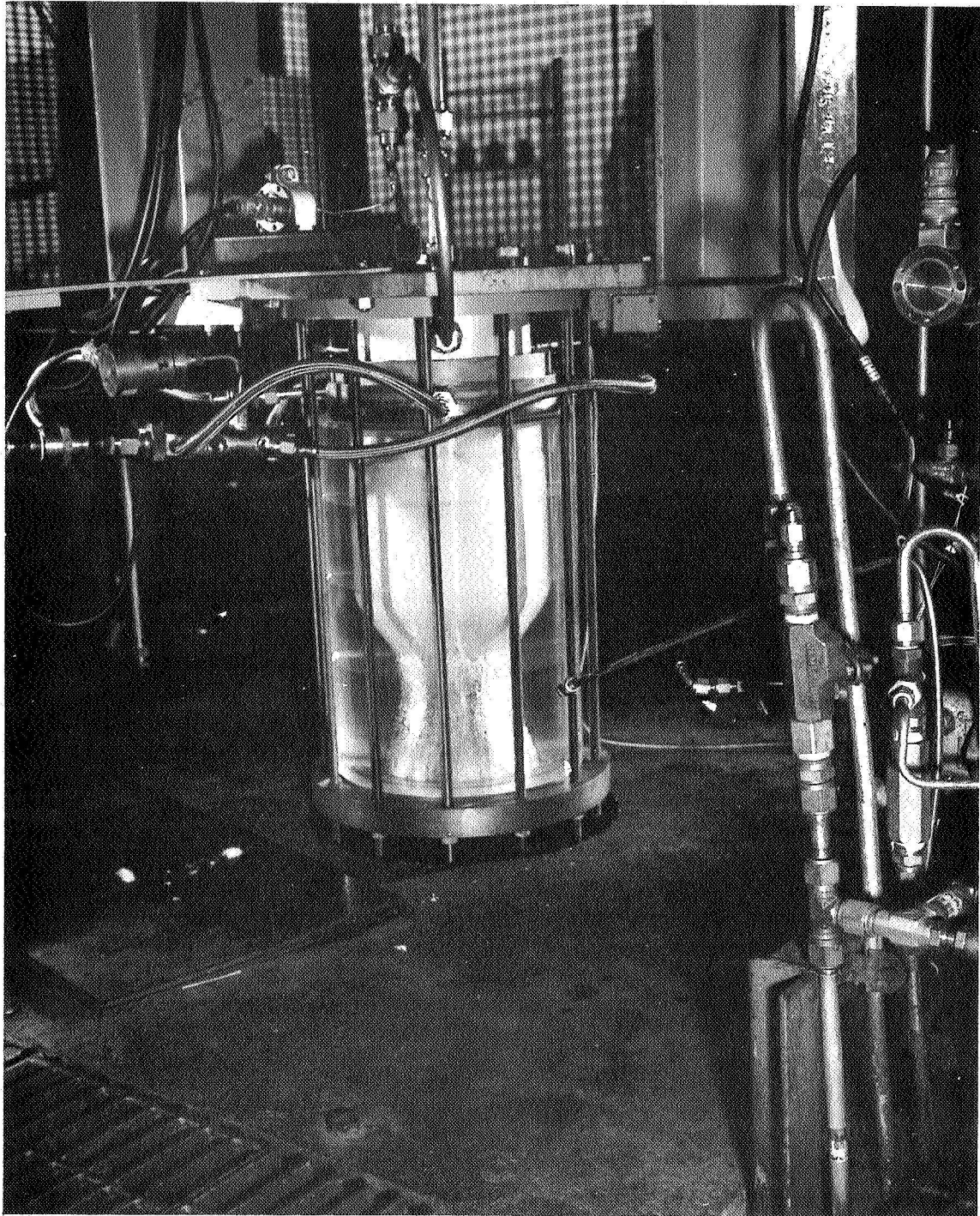
Figure 53. Photograph of Flat-Face Injector and Acrylic
Engine on Test Stand (Run 460)

Figure 54. Photograph of Chamber Wall of Acrylic Engine
after 4 Second Firing (Run 460)
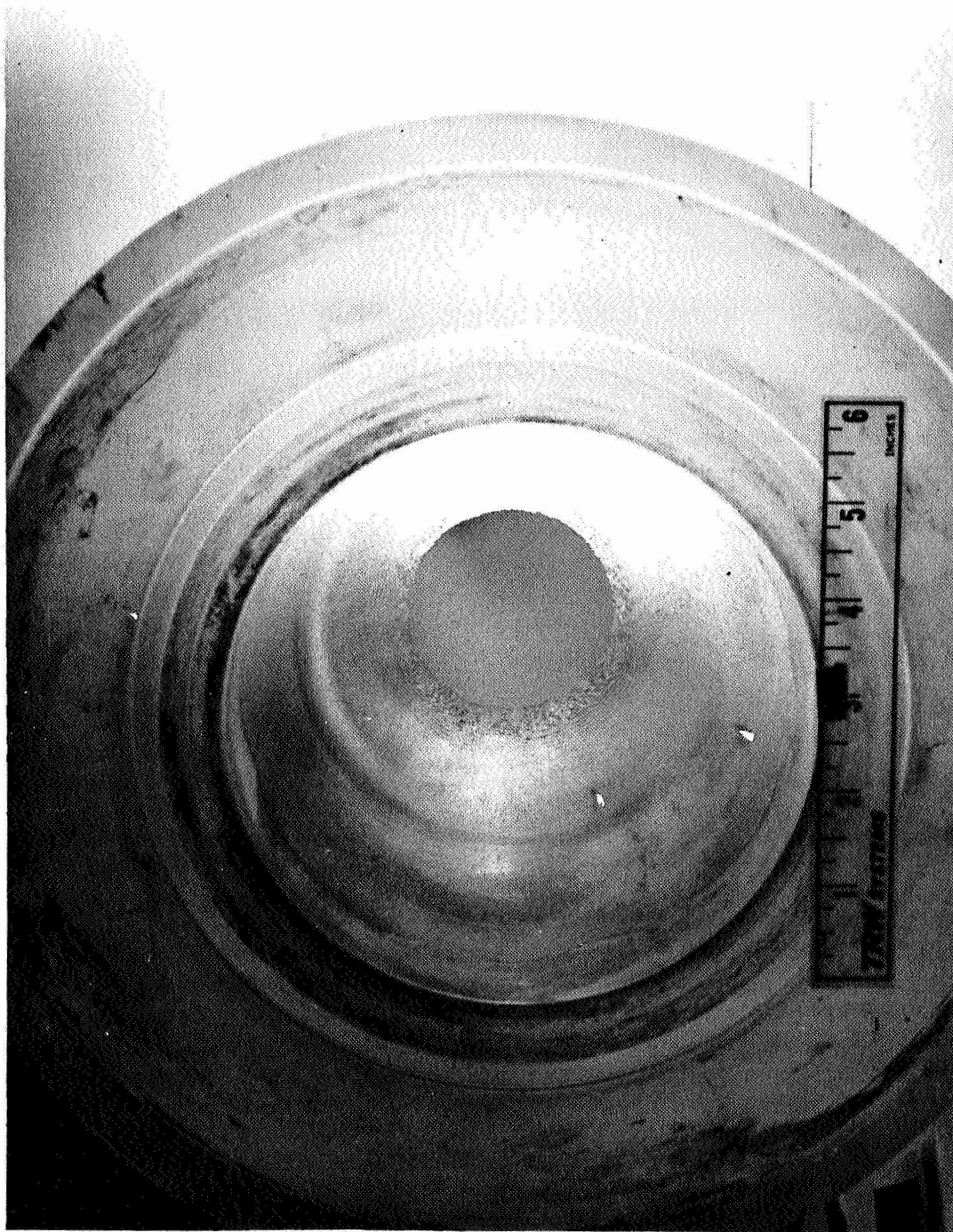
Figure 55. Photograph of Converging Section and Throat
of Acrylic Engine (Run 460)
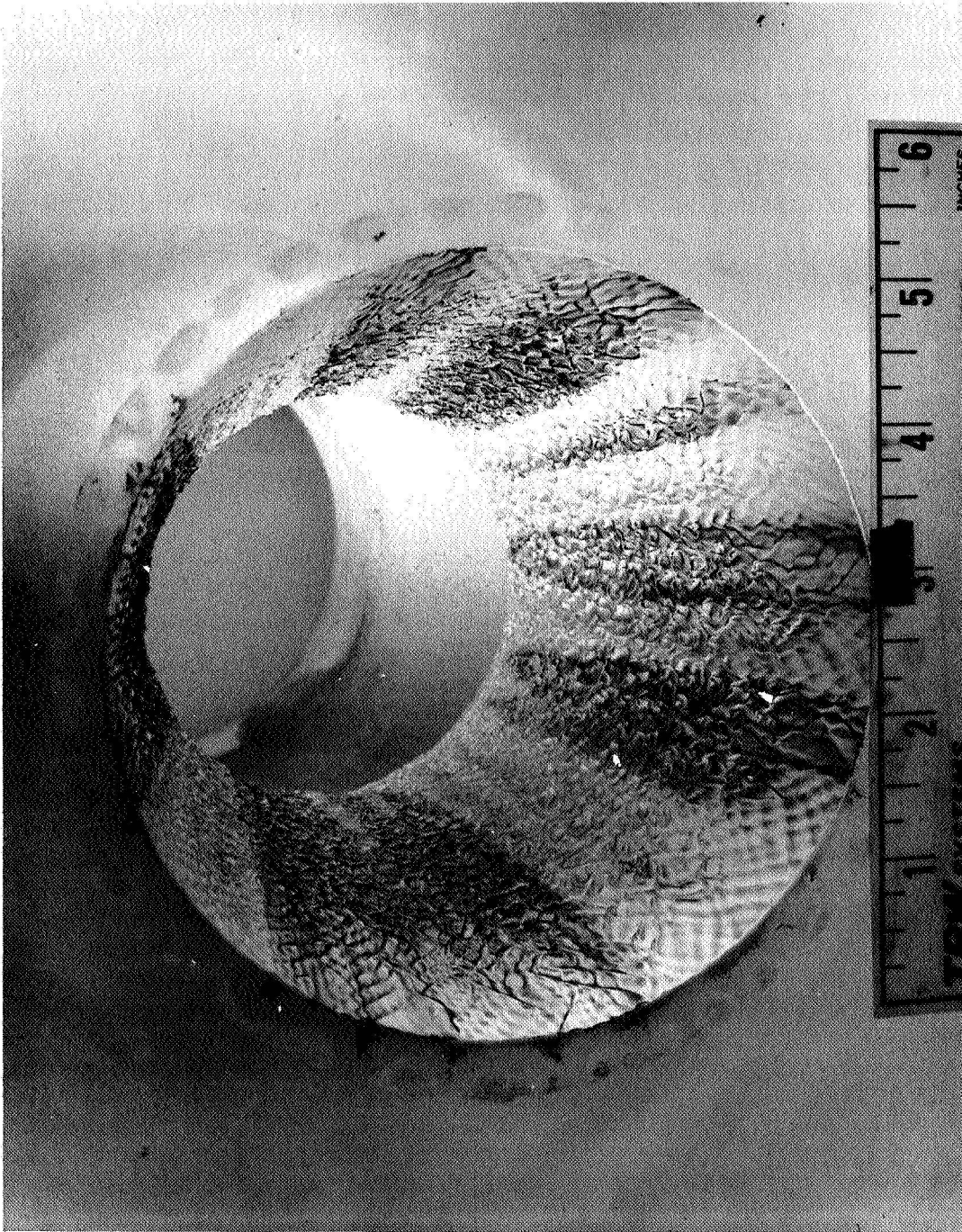
Figure 56. Photograph of Skirt of Acrylic
Engine (Run 460)

5.2 EXPERIMENTAL RESULTS AND ANALYSIS

The presentation and treatment of experimental results are given in the following manner:

Type of Run	Parameters
No Coolant	Type of Fuel
	Type of Injector
	Length of Chamber
Coolant	Type of Injector
	Coolant Properties
	Type of Fuel
Performance Analysis	

More importance will be placed upon the data from the last series of runs, because of significant coolant stripping occurring in Runs 420 to 431 when the foam was being injected near the head end. Coolant stripping makes data of questionable quantitive value.

5.2.1 No-Coolant Runs

Five no-coolant runs (417, 418, 419, 461, and 462) were made to establish baseline heat fluxes and performances for the engine configuration and parameters listed in Table 12. No-coolant baseline runs were not made for all engine configurations used in the coolant testing program, primarily because heat fluxes were found to be relatively constant, and because of low cooling efficiencies. A base-line test was not made with the flat face injector using N_2H_4 because of the possibility of combustion instability and the fear of hardware damage.

Table 12. Summary of Baseline No-coolant Runs

Run	Fuel Propellant	Injector Type	Chamber Length	Pressure	MR
417	N_2H_4	TRW	9.35 (see Figure 33)	304	1.21
418	N_2H_4	TRW	9.35 (see Figure 33)	334	1.20
419	N_2H_4	TRW	9.35 (see Figure 33)	263	1.15
461	UDMH	Flat Face	23.05 (see Figure 34)	275	2.12
462	UDMH	TRW	22.05 (see Figure 34)	266	2.05

Comparison of typical wall temperature-time traces as a function of propellant type and injector configuration is shown in Figure 57. It is readily apparent that an inner wall temperature of 1000°F is reached considerably faster with N_2H_4 as the fuel. Figure 58 translates these temperature-time traces into heat fluxes. On the average, Figure 61, heat fluxes with UDMH as the propellant were 30 to 40 percent lower than those with N_2H_4 as the fuel.

A secondary parameter related to heat flux appears to be injector type. According to Figure 61, local heat fluxes in the downstream portion of the chamber appear to be comparable with the flat face injector being slightly less.

Another factor of relative importance is the wall phenomenon occurring at the head end of the chamber. Curve A, Figure 61, shows higher local heat fluxes near the head end for the test with N_2H_4 as the fuel. The corresponding temperature time traces, Figure 59, confirm this point as the head end Nammac thermocouples show, on the average, faster temperature responses than those further downstream. The relative spacing of temperature-time traces at the same longitudinal plane is also indicative of nonuniform combustion.

When the fuel type was changed to UDMH, the head end of the engine became cooler than when N_2H_4 was used. And in particular when the TRW injector was used, Figure 62 shows that UDMH liquid fuel film cooling persisted along the wall for approximately 4.3 inches from the head end. Main propellant cooling such as this is considered quite beneficial to foam cooling since head heat fluxes are significantly reduced, Figure 61. In order to take advantage of this cooling, however, the design must account for it.

A typical comparison of no-coolant temperature-time traces for copper throat plugs is given in Figure 60. In general, the conclusions regarding the effects of propellant type and injector type are the same as those discussed in the preceding paragraphs.

The heat load on the chamber and throat for the baseline tests can be found by graphical integration of the area under the curves of Figure 61. The results are summarized in Table 13. Approximately one-half of the heat load is upon the throat.

5.3 COOLANT TESTS

Thirty-four coolant tests were conducted in which fuel type, engine configuration, coolant type, and coolant properties were varied over wide ranges. Initially 25 coolant tests were conducted with N_2H_4 as the fuel and with the TRW injector. In these tests the primary parameter relating to cooling efficiency appeared to be the point at which the coolant was injected into the chamber.

Nine coolant runs were conducted with UDMH substituted for N_2H_4 as the main propellant fuel. This change resulted in a remarkable
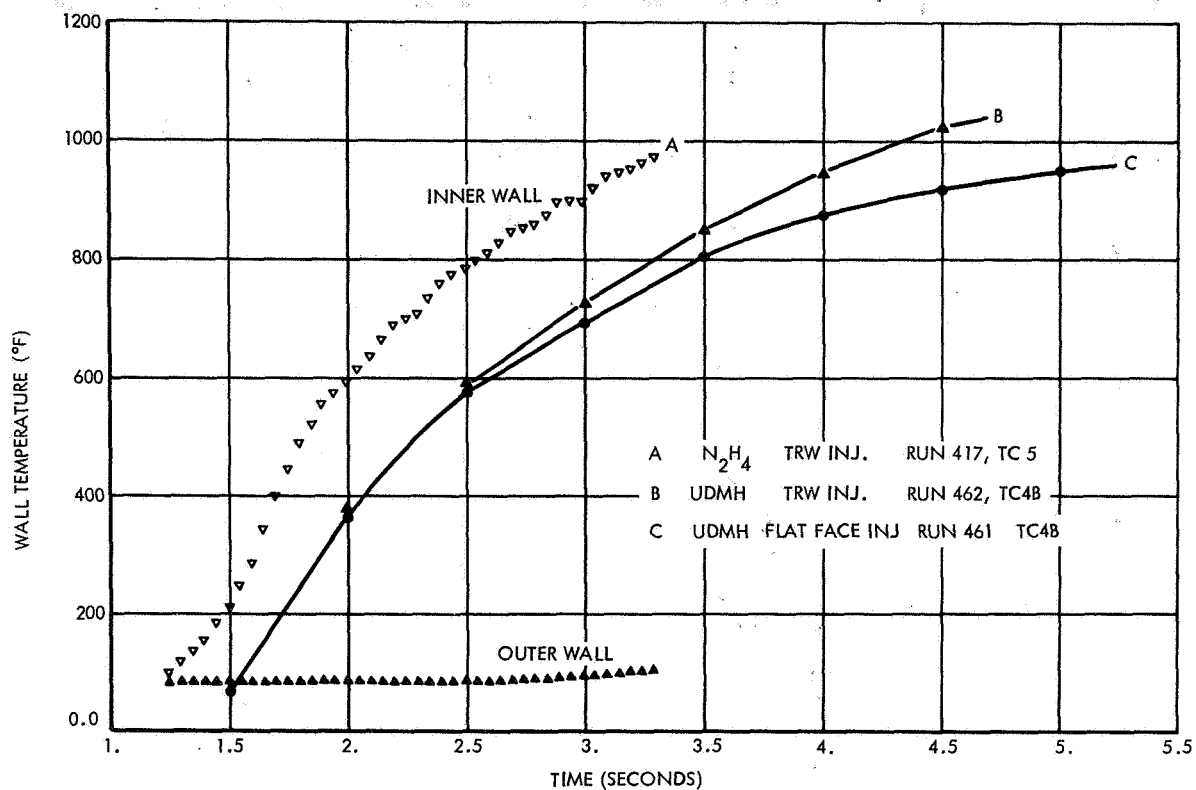
Figure 57. Wall Temperature versus Time, Comparison of Chamber
Thermocouples — Type of Injector and Type of Fuel
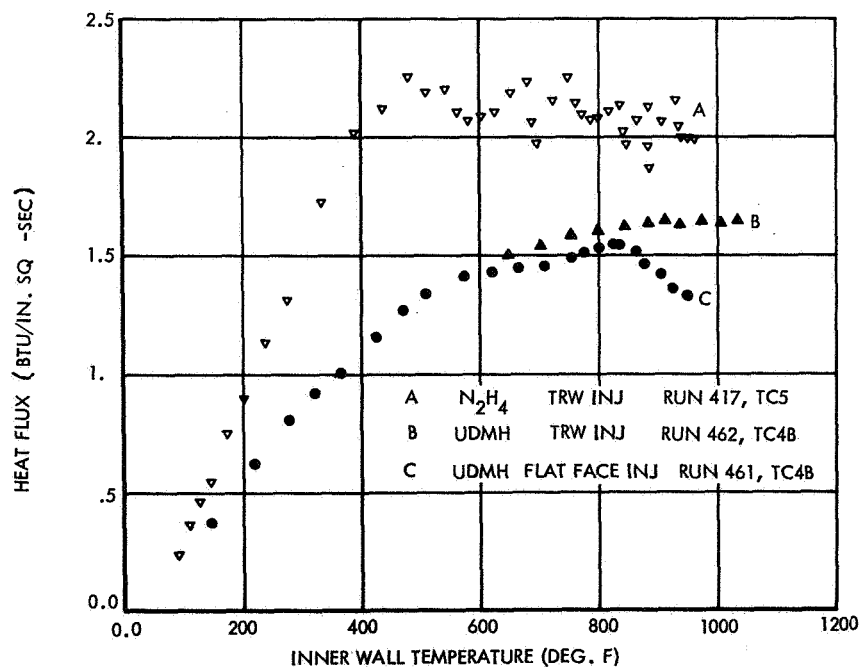
Figure 58. Heat Flux versus Inner Wall Temperature,
Comparison of Injector and Type of Fuel

81
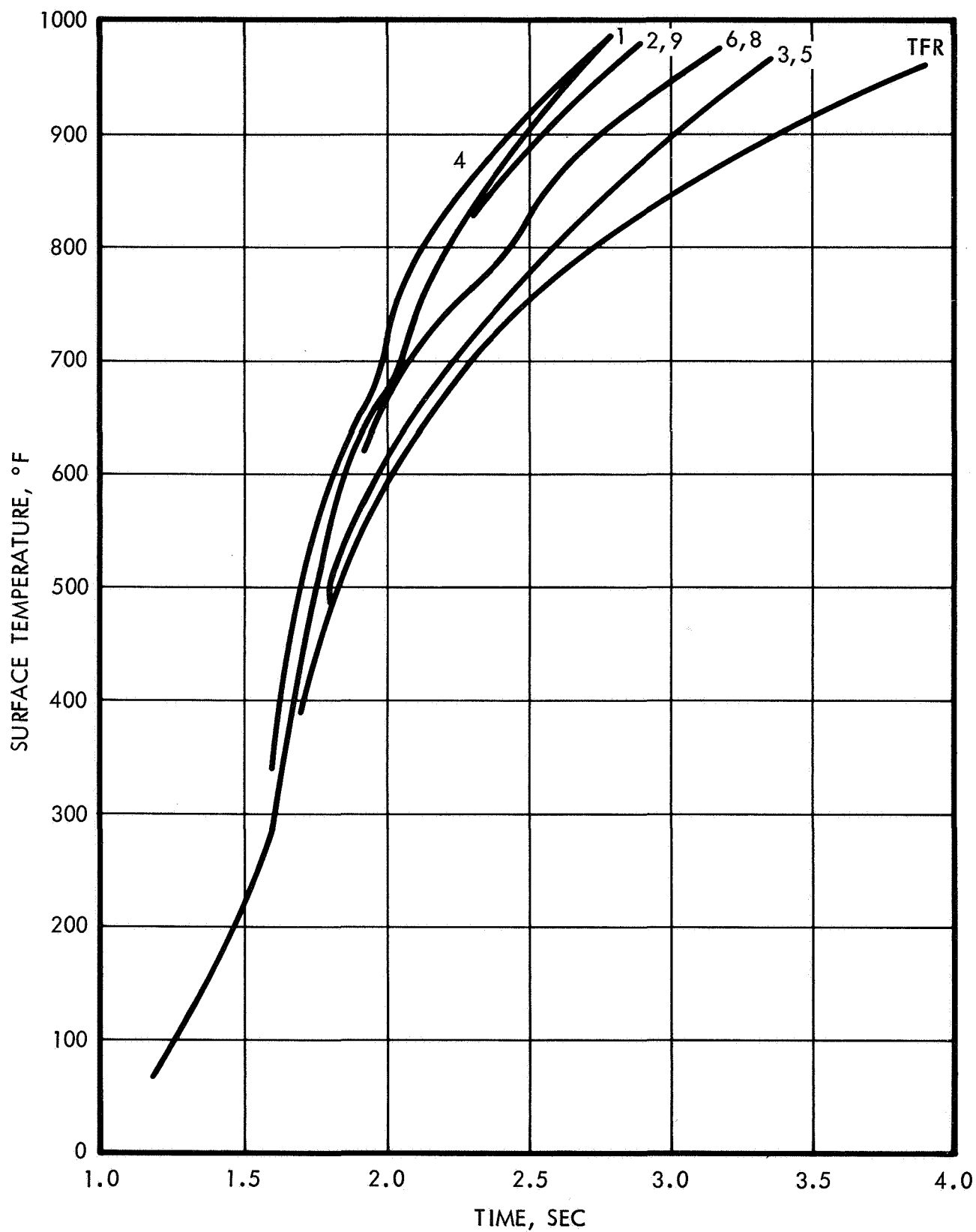
Figure 59. Wall Temperature versus Time for Run 417
at 300 psia, without Coolant
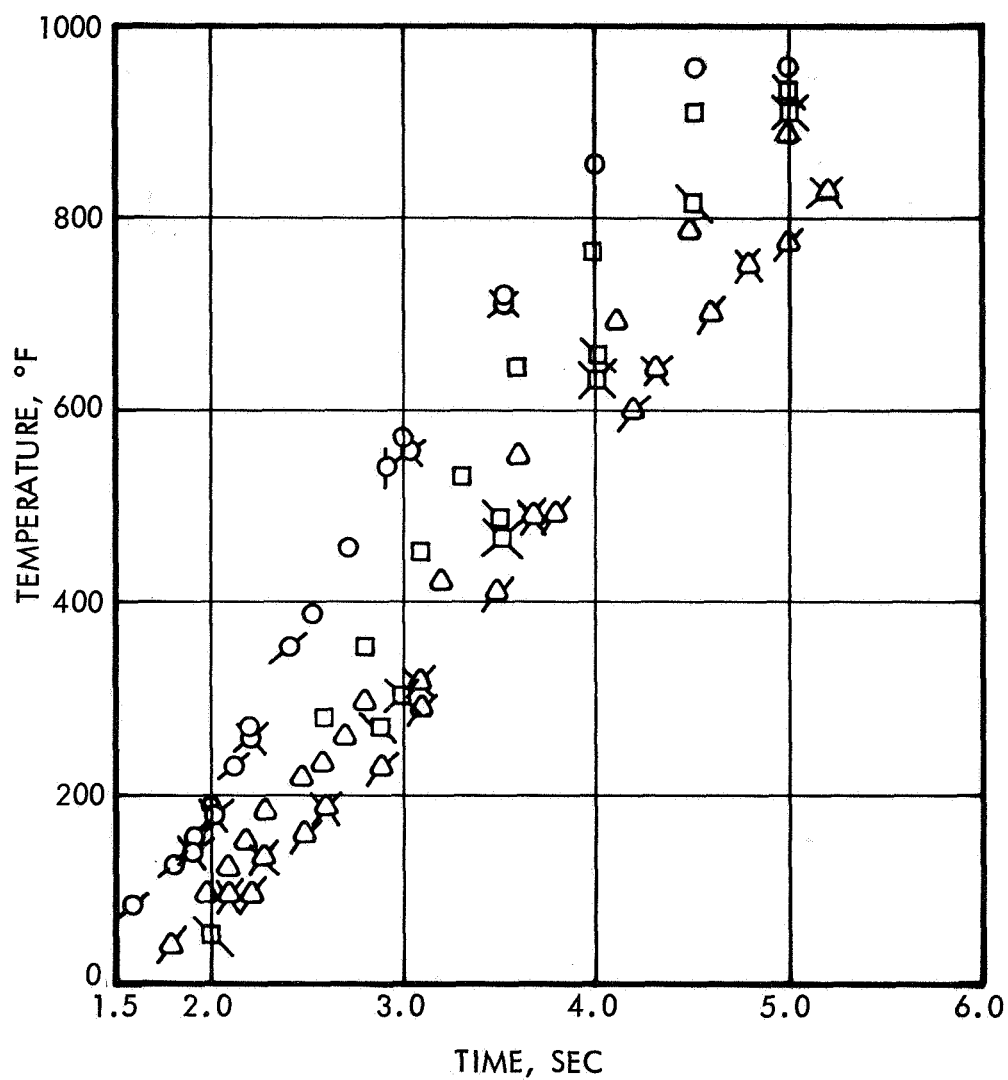
Figure 60. Comparison of No-Coolant Temperature-Time
Traces of Copper Plugs at Throat
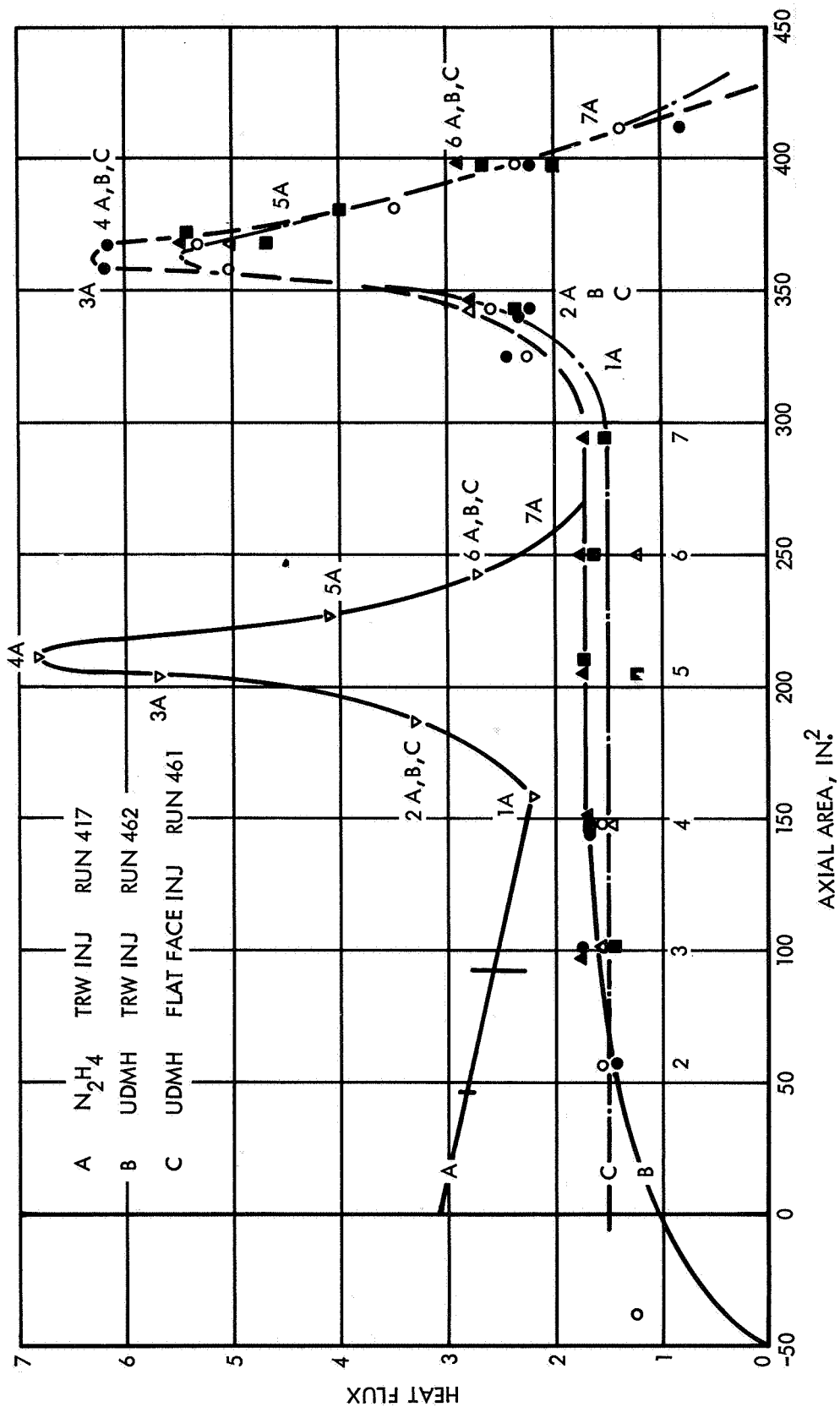
Figure 61. Comparison of No-Coolant Local Heat Flux Data, Type of Injector and Type of Fuel
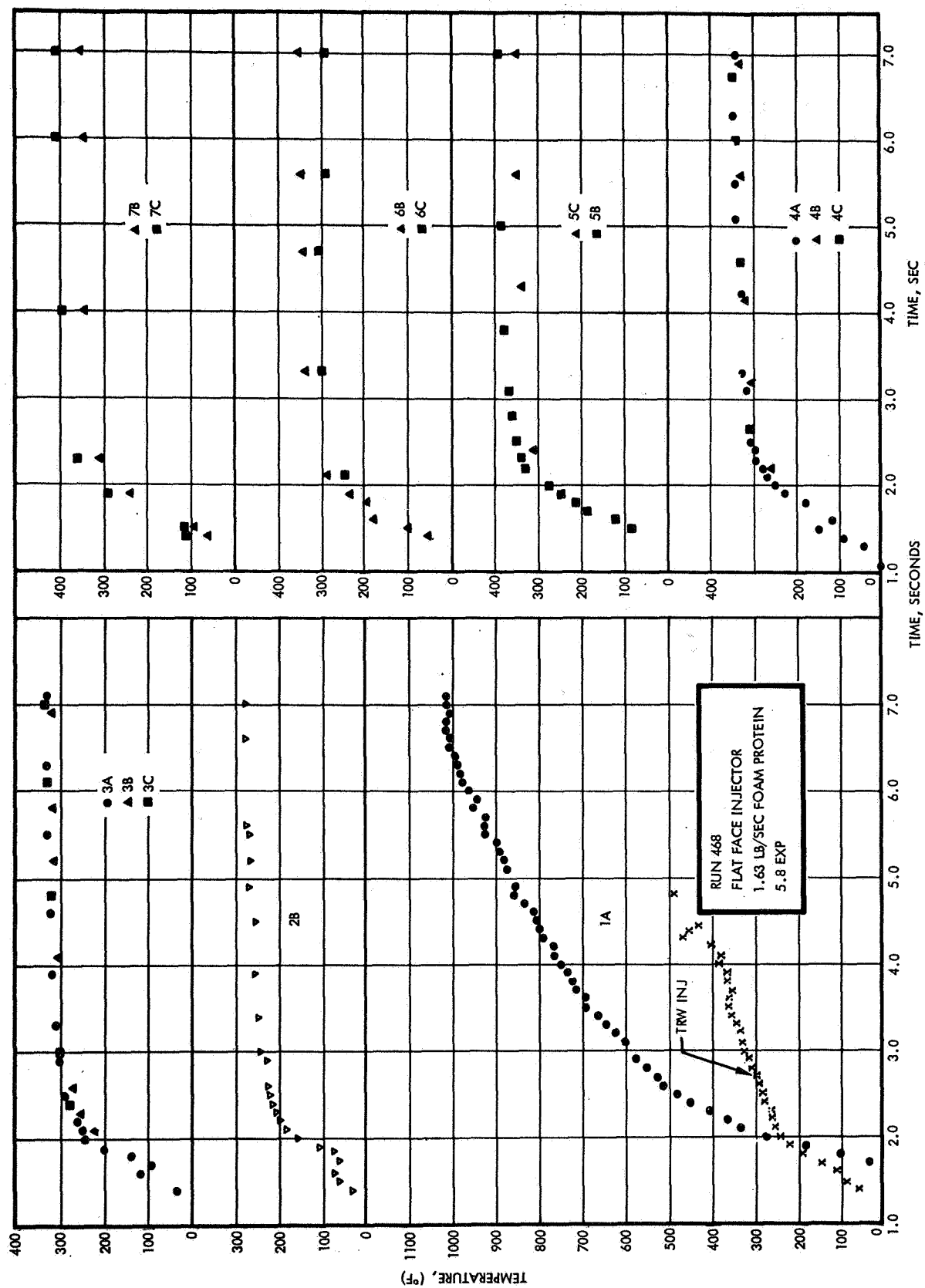
Figure 62.   Response of Namac Wall Thermocouples

85

Table 13. No-Coolant Baseline Heat Loads, Btu/sec

Run	Chamber	Throat	Total
417	400	390	789
461	458	321	779
462	535	337	872

improvement in cooling efficiency, and it was possible to demonstrate complete cooling of an entire engine. The improvement was attributed to the good combustion characteristics of UDMH which lead to significantly reduced heat fluxes and smooth combustion.

Because this is a feasibility study with a primary objective to demonstrate high cooling efficiencies and because of the much wider use of UDMH than N_2H_4 as a fuel, emphasis is placed on the last generation of testing. The initial tests are not viewed as a limitation upon the cooling technique, but that more detailed examination is required.

An example of typical temperature-time traces for chamber Nanmac and throat copper plug thermocuples is given in Figure 62 and 63. In this particular run 1.63 lb/sec of protein foam having an expansion ratio of 5.8 was being injected into a combustion chamber 16.20 inches long downstream of the point of foam injection (see Fugure 34). All Nanmac surface thermocouples, including the one 15.85 inches downstream of the point of foam injection and all throat temperatures are established at the saturation temperature of the coolant. The cooling efficiency has been estimated to be near 50 percent of the theoretical capability:

$$\frac{\int \left(\frac{Q}{A}\right)_{T_s} dA}{\dot{w}\Delta H} = \frac{776}{1.63(1000)} \cong 47\%$$

The efficiency may actually be somewhat higher, because the engine may actually be over-cooled.

The data from this are cross-plotted on Figure 64 along with the data from an equivalent run using the TRW coaxial injector.

Figure 65 shows the effect of coolant flow rate on wall temperatures at selected chamber and throat locations. As the coolant flow rate is decreased at constant expansion ratio, Runs 463, 464, and 468, a flow rate will be reached at which the coolant will not be able to cool the wall
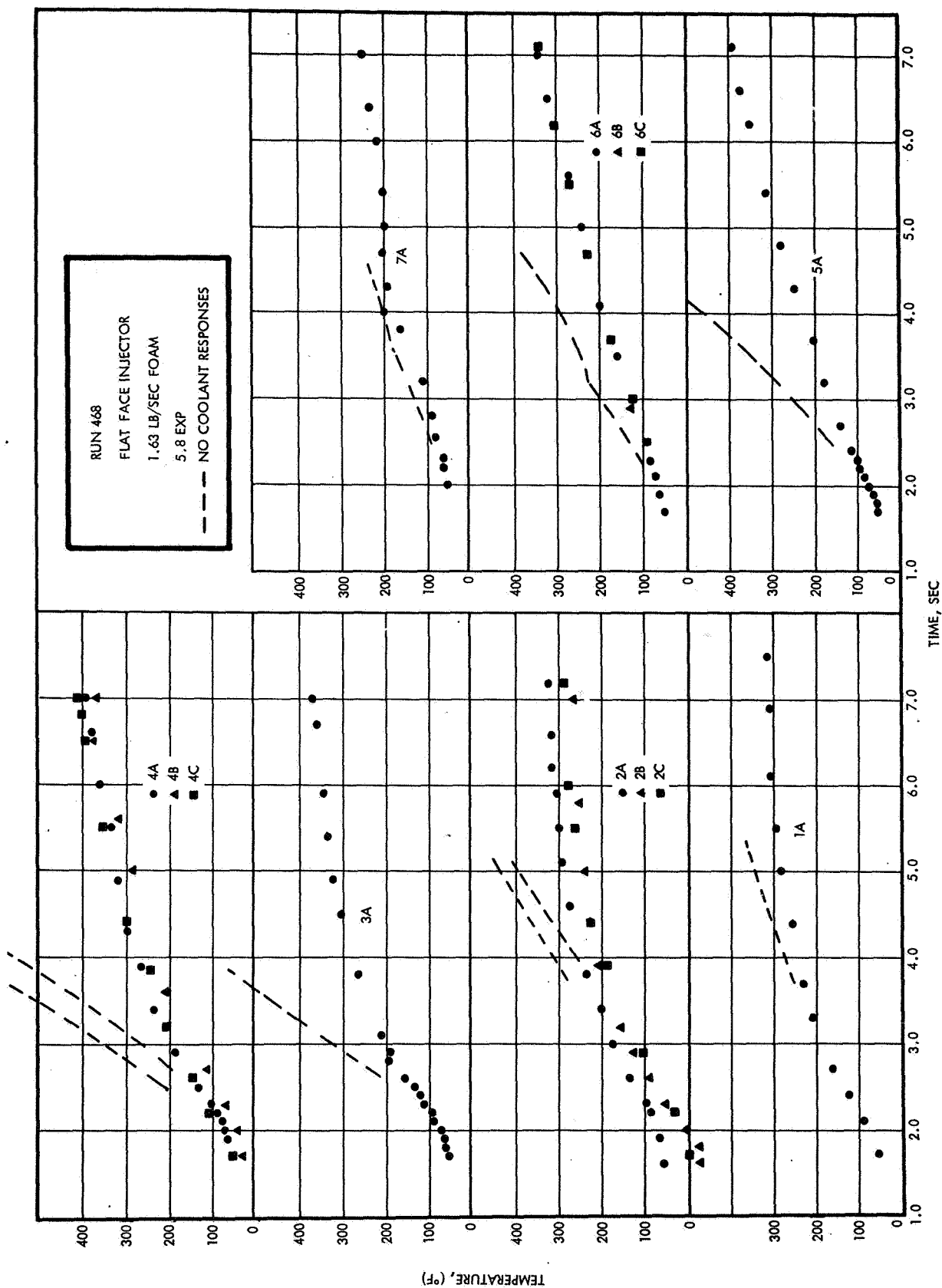
Figure 63. Temperature-Time Traces of Copper Plugs in Throat
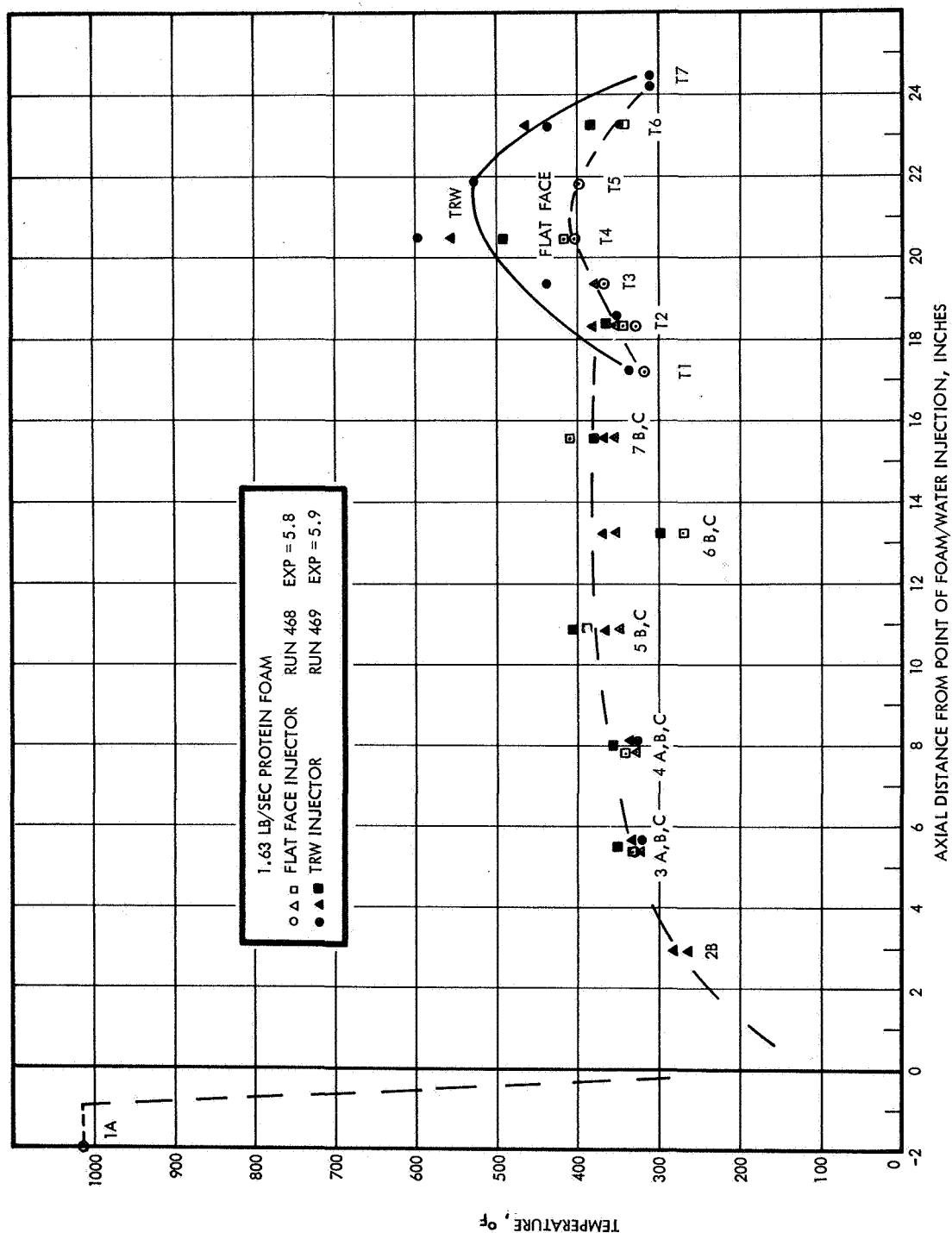
Figure 64. Comparison of Wall Temperature along Chamber — TRW Injector
and Flat Face Injector, High Coolant Flow

88
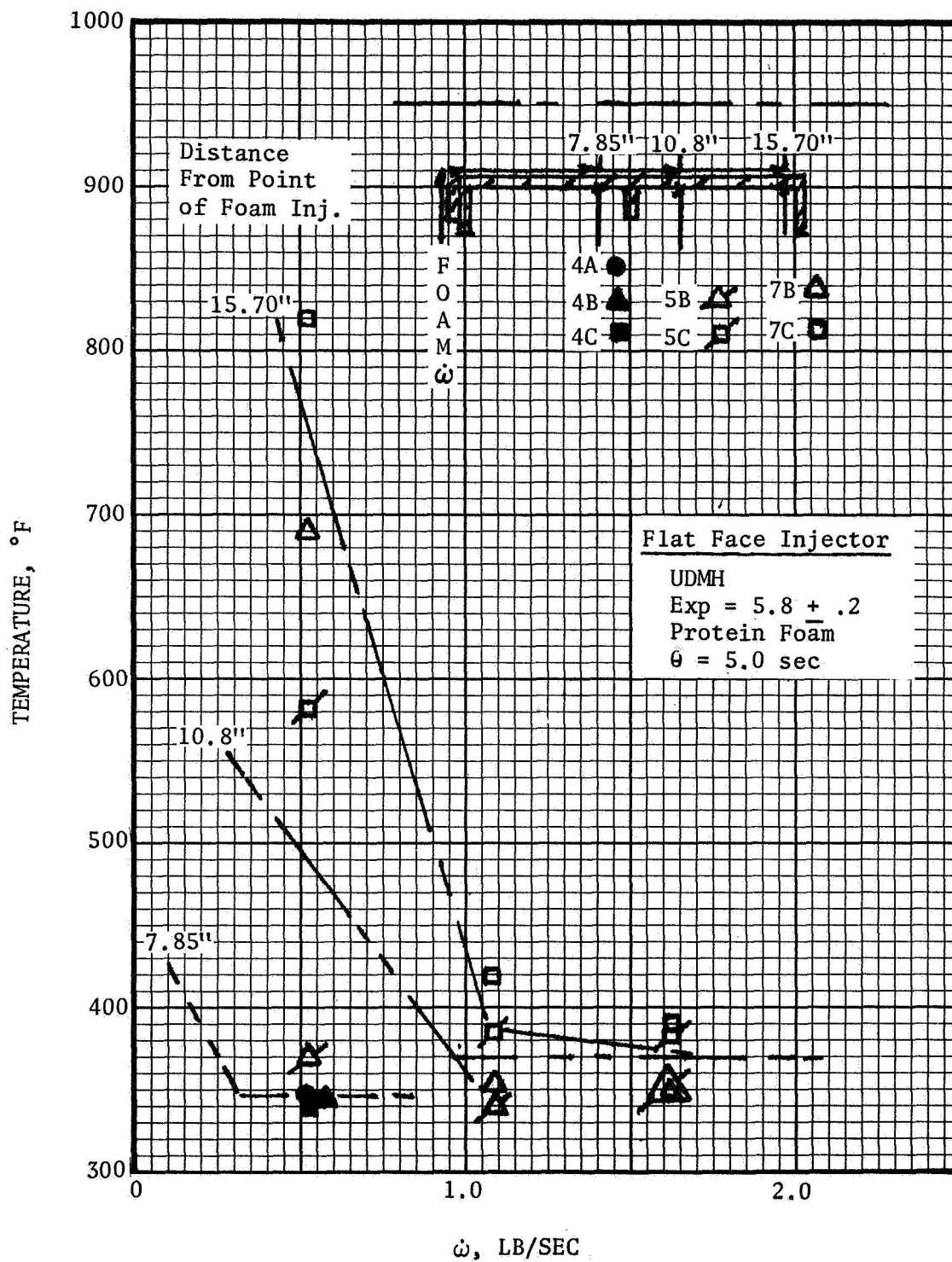
Figure 65a. Temperature-Flow Rate Profiles
At Selected Chamber Locations
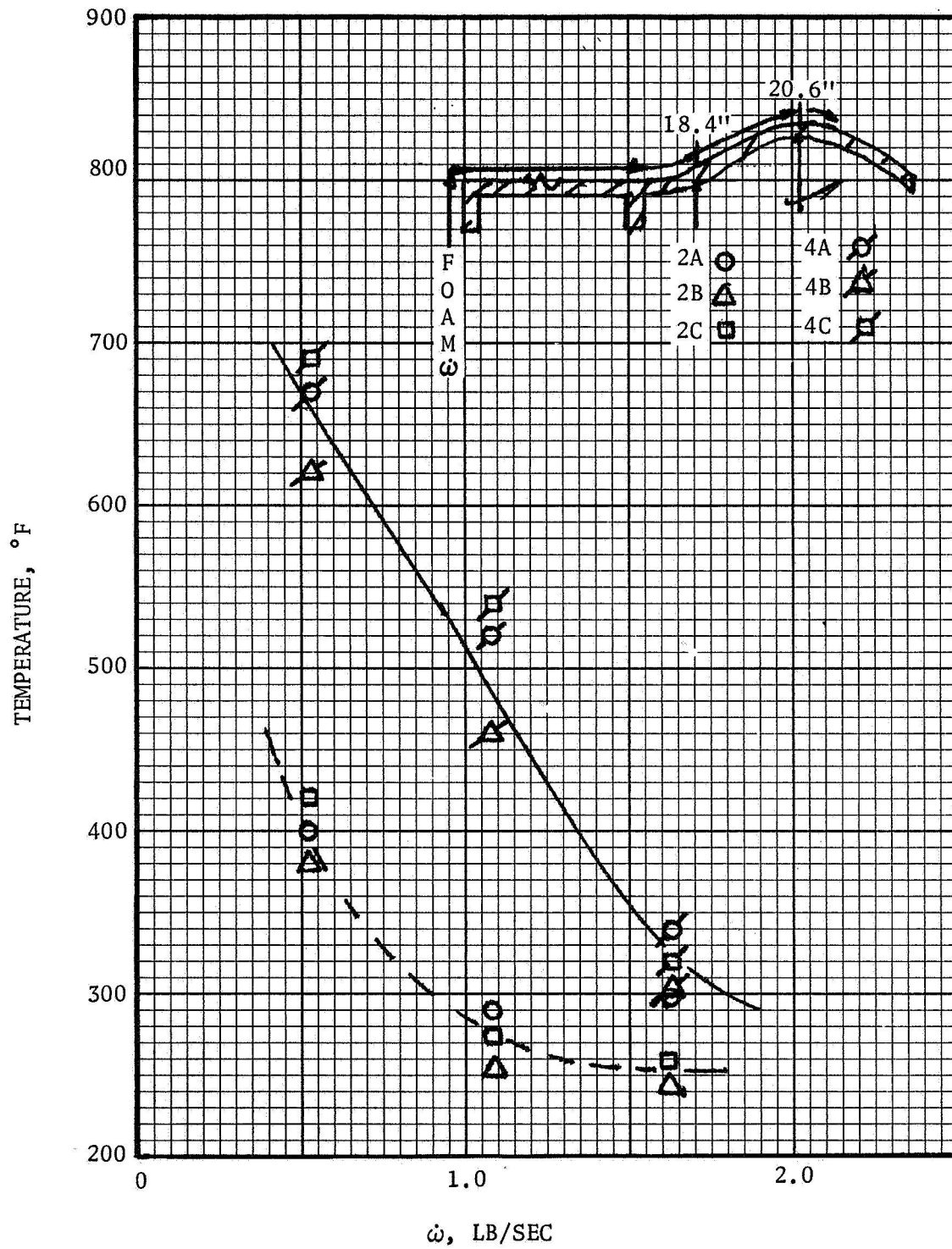
Figure 65b. Temperature-Flow Rate Profiles

to the saturation temperature. As the flow rate was reduced the cooling efficiency remained relatively constant at 45 to 55 percent. However, when the expansion ratio was increased to ~30, the efficiency was observed to increase to ~70 percent, independent of main injector used, Figure 66, thus strongly supporting a conclusion that the foam efficiency was nearly twice that of pure liquid by itself. There was not time at the close of the program to check the effect of expansion ratio on efficiency at the higher flow rates.

The predominate number of coolant tests were conducted with N_2H_4 fuel. As previously stated, one primary coolant variable appeared to be the distance from head end to point of foam injection. Figure 67 compares coolant data at two time slices for runs 447 and 420 when foam injection was 6.35 and 1.5 inches respectively, below main injector. During the early part of run 447, foam was observed to travel ~11 inches (~45% efficiency) or ~5 inches further than that for equivalent run 420, (cooling efficiency ~20%). As indicated the length of chamber cooled (and hence cooling efficiency) appeared to decrease with time to ~25%. Figure 68 shows the small effect of a wide expansion ratio change (cooling efficiency ~30 to 35%). The decrease in cooling efficiency with time may be due to low frequency combustion noise causing coolant film chugging. Comparison of these data with the coolant data when UDMH was used as a fuel shows that the coolant traveled ~3 times further with UDMH.

The effect of coolant parameters such as agent type and expansion ratio was investigated early in the program, Runs 423 to 430, and to a lesser extent in Runs 449 to 459. Most of these data are summarized in Figure 69a and 69b which present temperature-time traces for Cu plugs in the A radial position. The experimental procedure was to vary the $\dot{w}$ of the coolant as shown for a fixed foam type and expansion ratio until the threshold of complete cooling was reached for the short engine and then a parametric study of expansion ratio and foam type was conducted. A comparison of the results for the gel and protein agents indicate that:

- Protein foam exhibits the best cooling capacity

- Slightly better cooling is achieved at the higher expansions

- H_2O and the water foam with 23% polymeric agent exhibit nearly the same cooling capacity although the polymeric agent has a smaller but unknown heat of vaporization

- Once the coolant passes through the throat, any significant differences are minimized

The effect of foaming agent type and expansion ratio was again investigated with the point of foam injection lower in the long chamber configuration. These results are summarized in Table 14, and, in general, confirm the conclusions reached in the preceding paragraph.

91
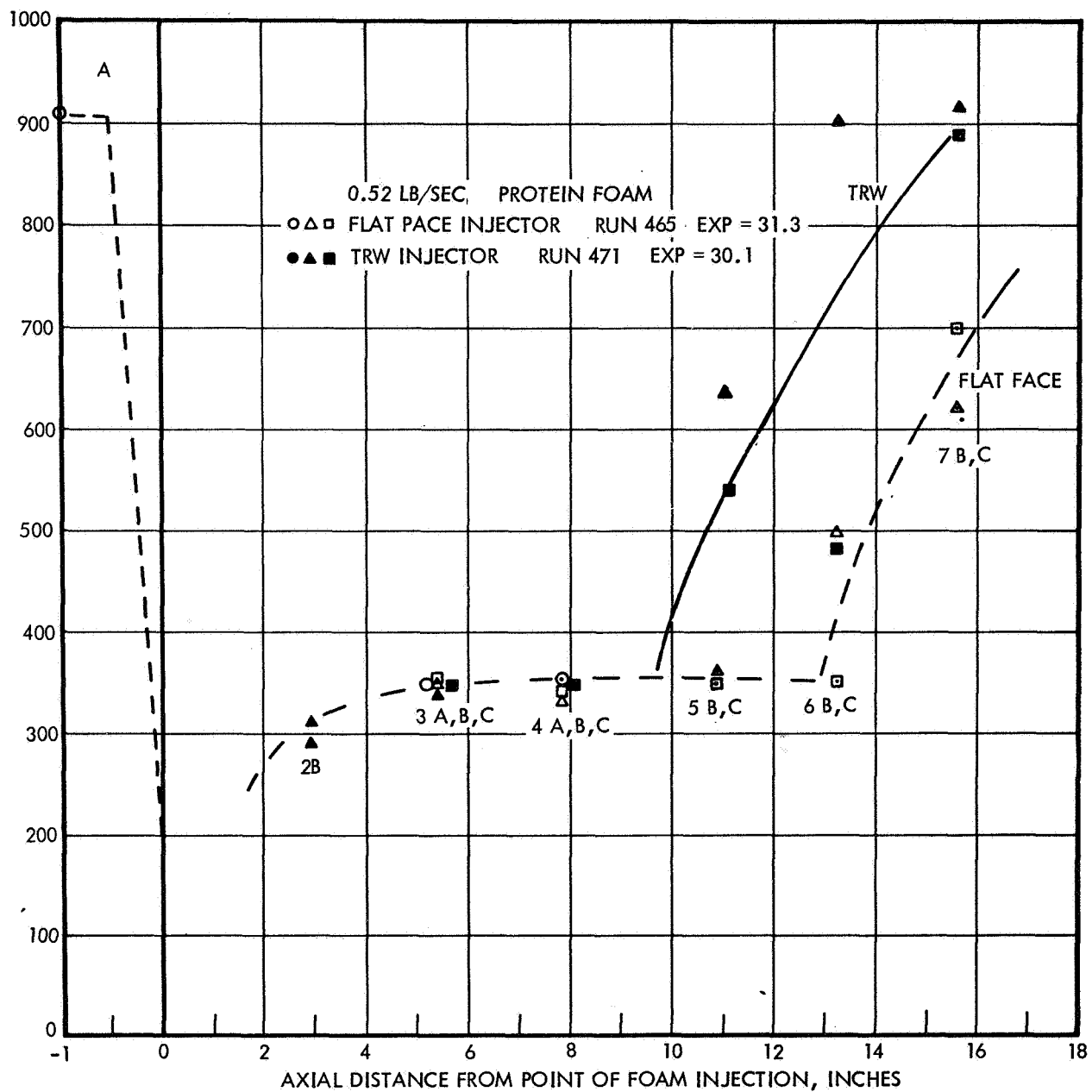
Figure 66. Comparison of Wall Temperature along Chamber, TRW
Injector and Flat Face Injector — Low Coolant Flow
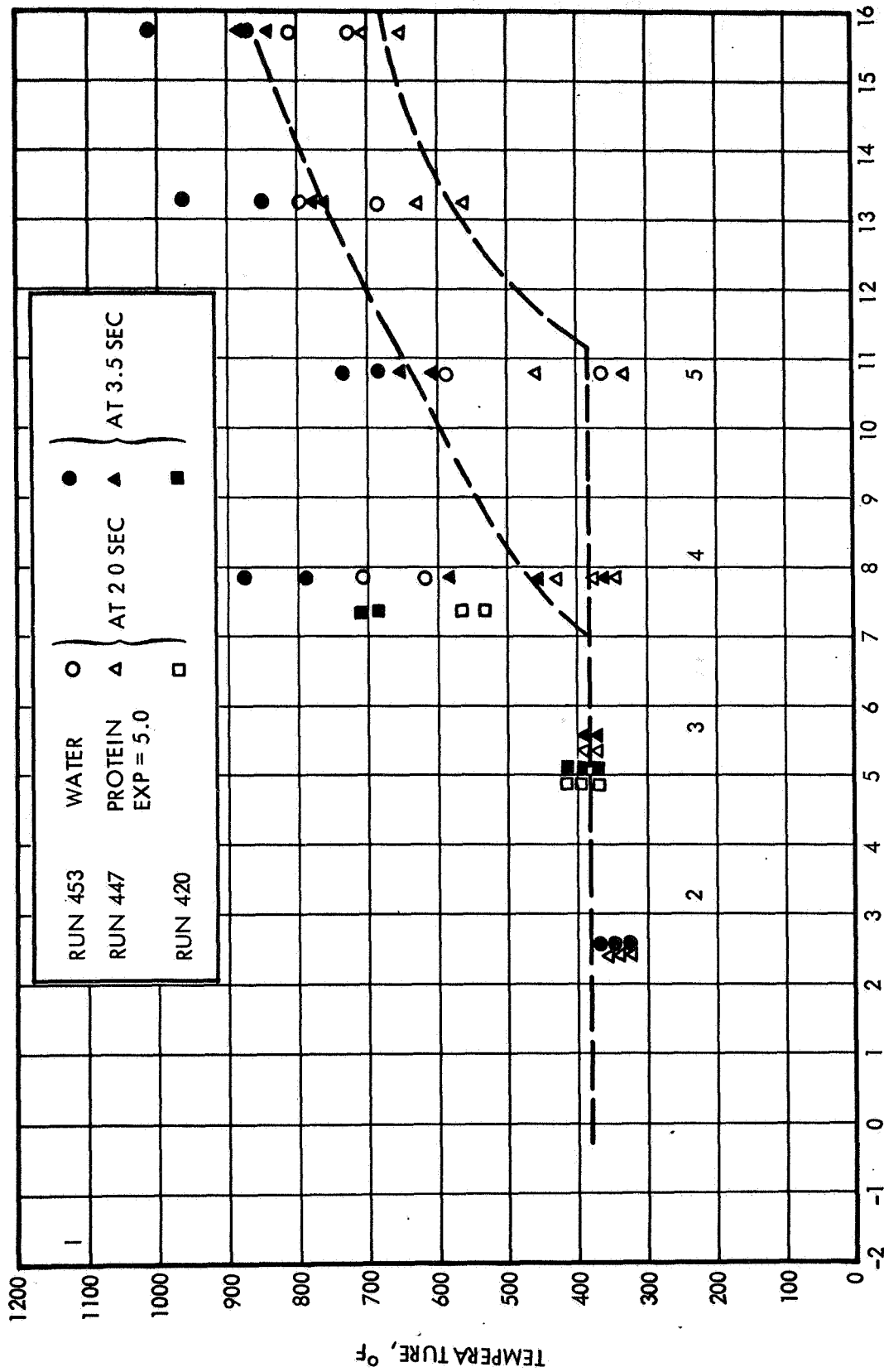
Figure 67. Comparison of Wall Temperature versus Distances
Traces for Water and Protein Foam

DISTANCE FROM POINT OF FOAM INJECTION
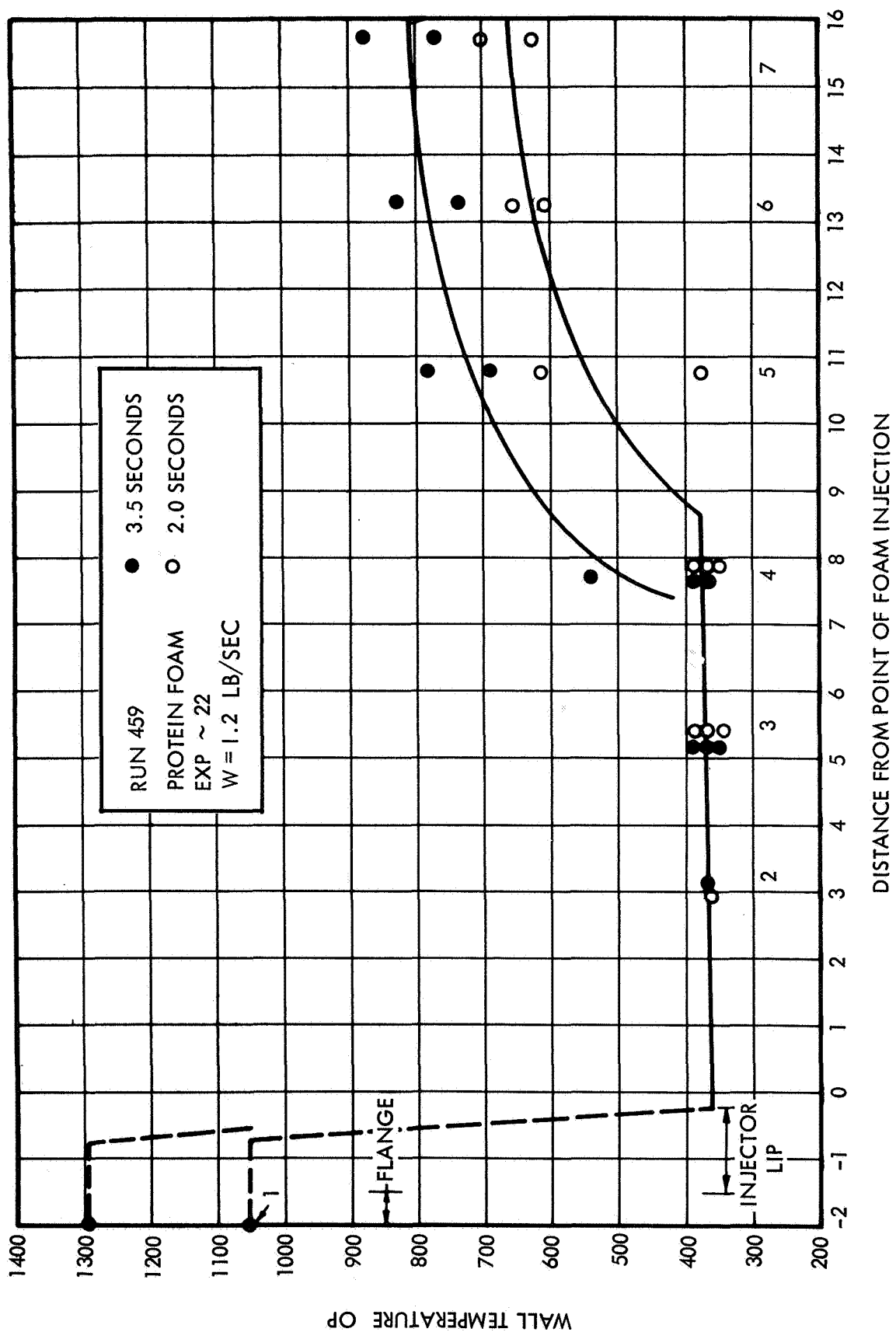
Figure 68. Wall Temperature versus Distance from Point of
Foam Injection at Selected Time Slices
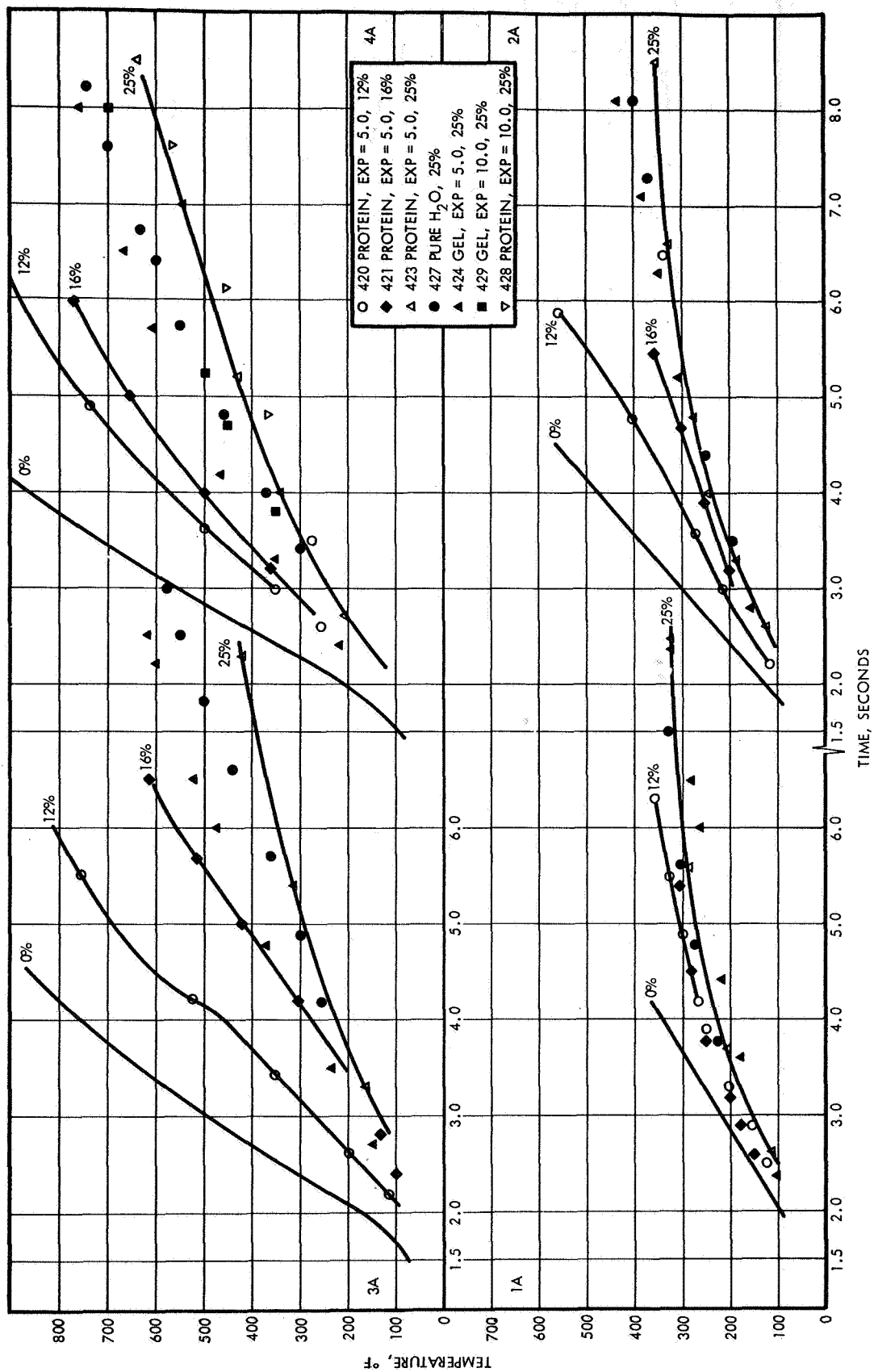
Figure 69a. Typical Cu Plug Temperature-Time Trace for Various Coolant Types

95
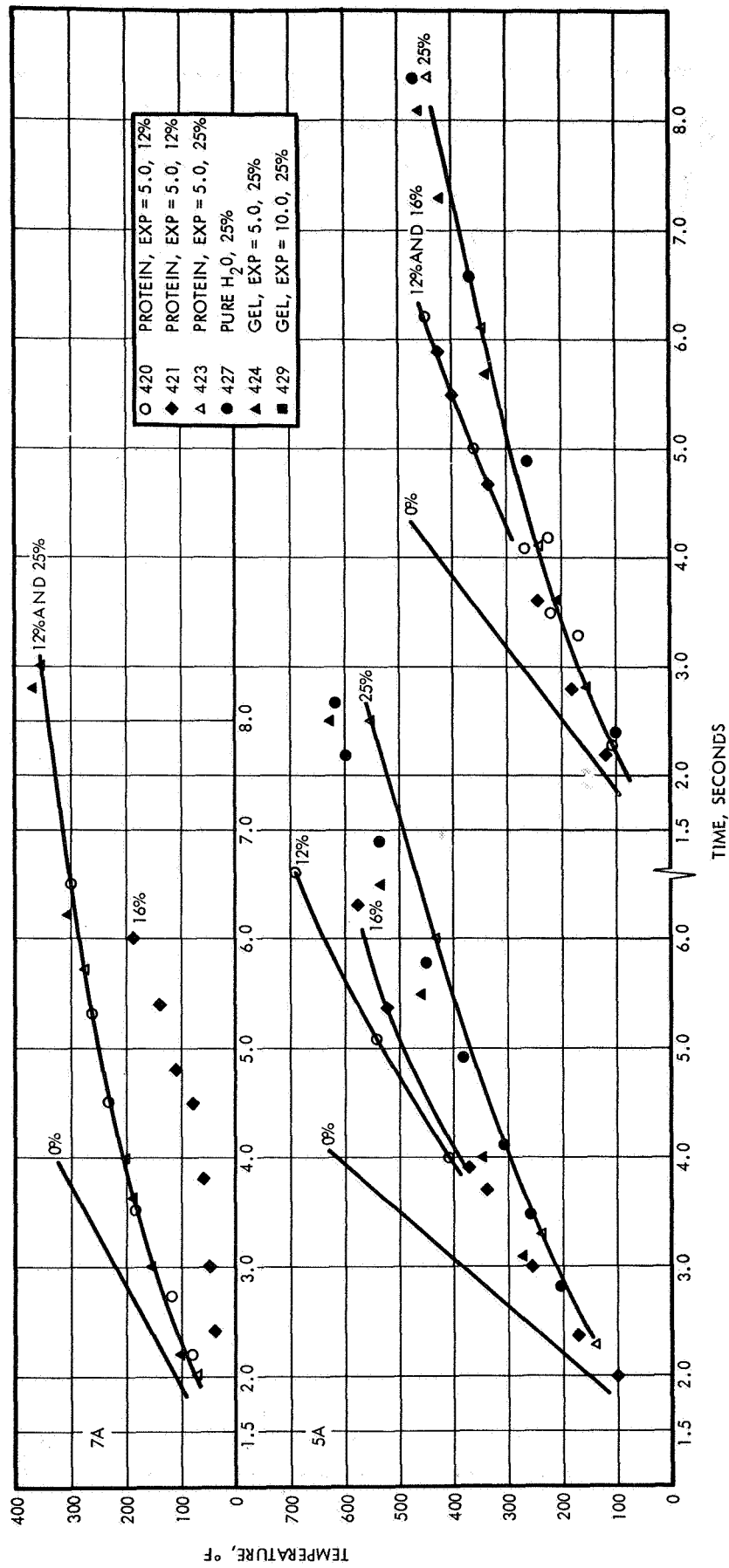
Figure 69b. Typical Cu Plug Temperature-Time Traces for Various Coolant Types

96

Table 14. Summary of Runs Conducted in Parametric Study of Agent Type, and Expansion Ratio with Long Chamber, TRW Injector, with Point of Foam Injection Lowered 6.35 inches

Run	Foaming Agent	Expansion	$\dot{W}$	Distance Cooled to Saturation Temperature
447	3% Protein	5	1.215	7.85
448	3% Protein	10	1.225	5.40 → 7.85
450	23% Polymer	10	1.19	5.40 → 7.85
451	1.5% Detergent	10	1.17	5.40 → 7.85
452	1.5% Detergent	10	1.21	5.40 · 7.85
454	3% Protein	5	0.52	2.95 → 5.40
455	3% Protein	27	0.528	5.40 → 7.85
456	1.5% Detergent	32	0.511	2.95 → 5.40
457	6% Protein	22	1.18	(?) 5.40 → 7.85
458	6% Protein	22	1.2	(?) 7.85 → 8.80
459	6% Protein	22	1.16	7.85

Six tests were conducted with unfoamed liquids, Table 15, to establish cooling capacities, stability, and susceptibility to streaking in relation to the foamed liquids. Foamed liquids can only be achieved through a certain degree of complexibility; therefore they must show some distinct advantages in relation to their parent liquids.

Figures 70 through 75 are comparsons of TC traces for copper plugs located in the same radial plane to illustrate the role of coolant type, agent, and expansion ratio on the undesirable phenomenon called streaking. Figures 70, 71, and 72 pertain to H_2O and illustrate how it streaked through the throat at station B. Little streaking was observed in the no coolant runs as indicated by the curves at the left.

Figures 73 and 74 give the effect of expansion ratio and foaming agent type on copper plug temperature traces at the throat. The polymeric agent unquestionably exhibits the best antistreaking capabilities, and the protein foam is far superior to water. Figure 75 gives the traces for the ungassed liquid with agents and shows that the polymeric liquid has intrinsic antistreaking qualities.

Table 15. Summary of Tests Conducted
with Unfoamed Liquids

Run	Foaming Agent	$\dot{W}$
425	23% Polymer	2.42
426	3% Protein	2.38
427	None (Water)	2.43
453	None (Water)	1.17
466	None (Water)	0.522
470	None (Water)	1.635

Three additional tests, Runs 453, 466, and 470, were conducted with pure water as a coolant. The results of test 453 when compared to the equivalent results of a foamed liquid, Figure 67, indicate that water has a smaller effective cooling capacity. Temperature-time traces of chamber thermocouples, Figure 76, for run 466 indicated that water channeled very badly to one side of the chamber. The streaking can probably be traced to an injector distribution problem, which becomes critical at low coolant flow.

Figure 77 shows that the cooling results obtained with water were not always consistent. In this particular instance, water was observed to cool a combustion section 16.2 inches long with only minor streaking through the throat. In general, though, water and unfoamed liquid containing surface active agents are susceptible to streaking, injector maldistribution, and, apparently, increased stripping.
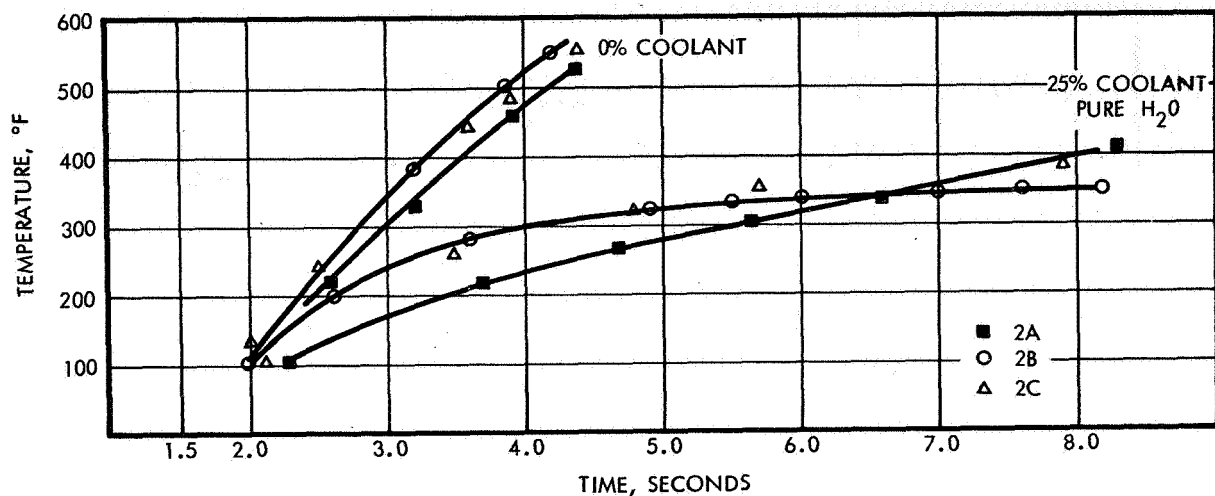
Figure 70. Radial Cu Plug Temperature-Time Traces for Water
Coolant Illustrating Streaking Characteristics
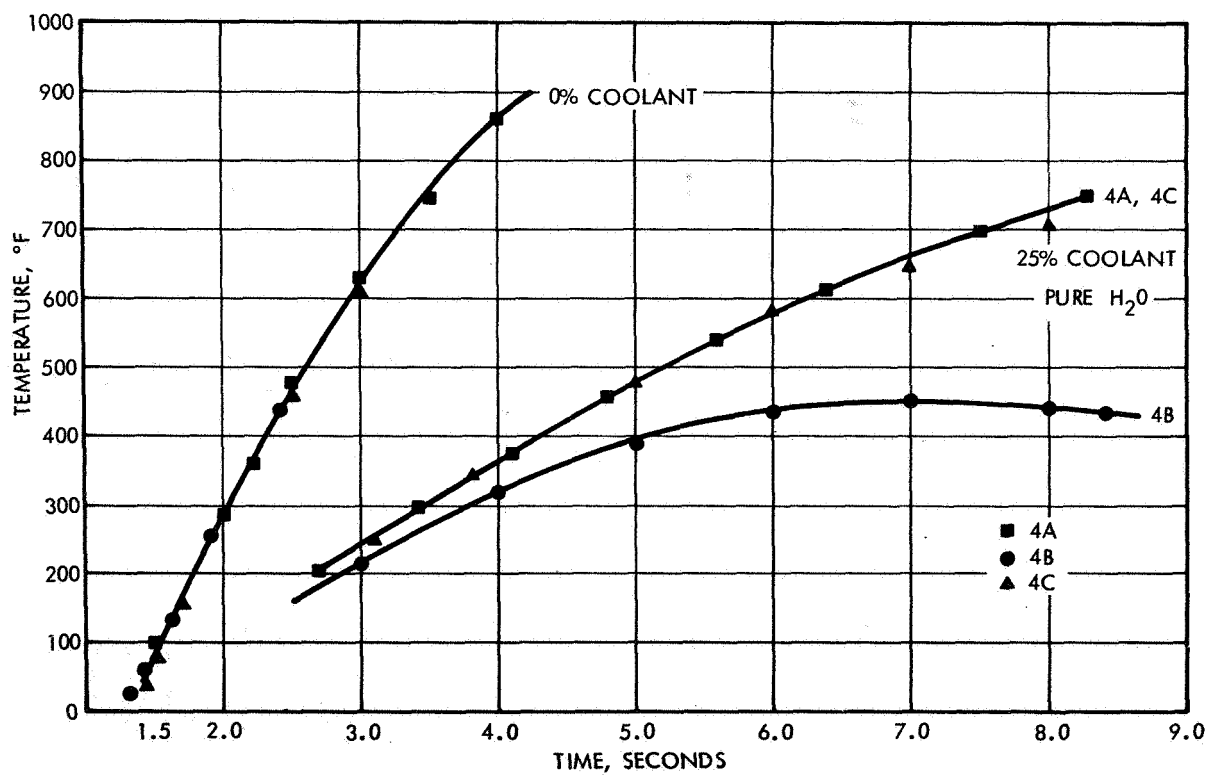
Figure 71. Radial Cu Plug Temperature-Time Traces for Water
Coolant Illustrating Streaking Characteristics

99
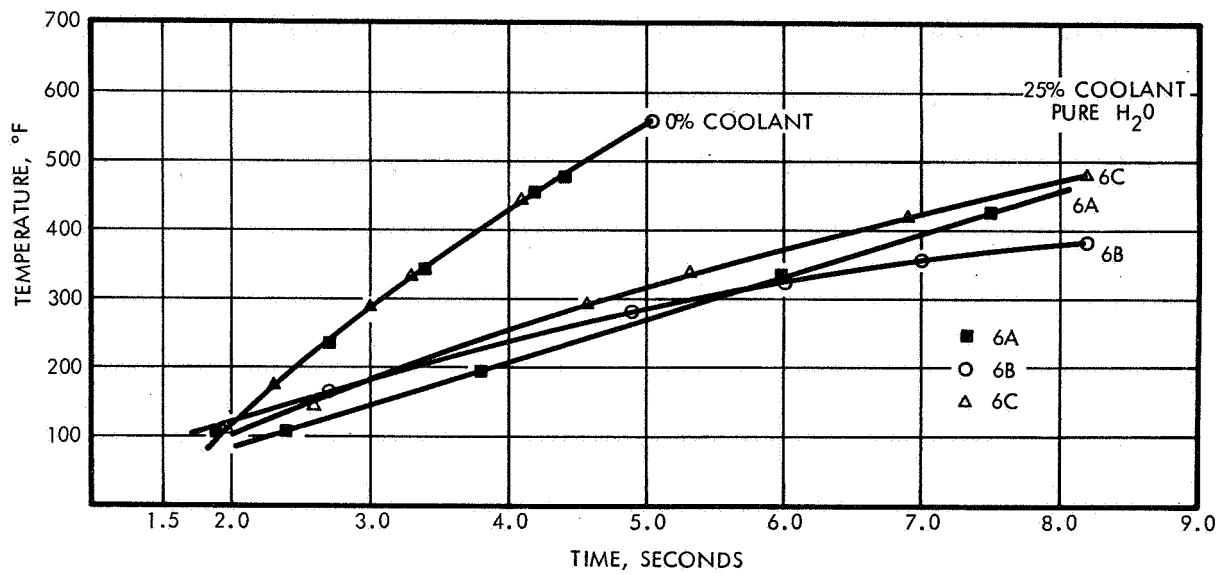
Figure 72. Radial Cu Plug Temperature-Time Traces for Water Coolant Illustrating Streaking Characteristics
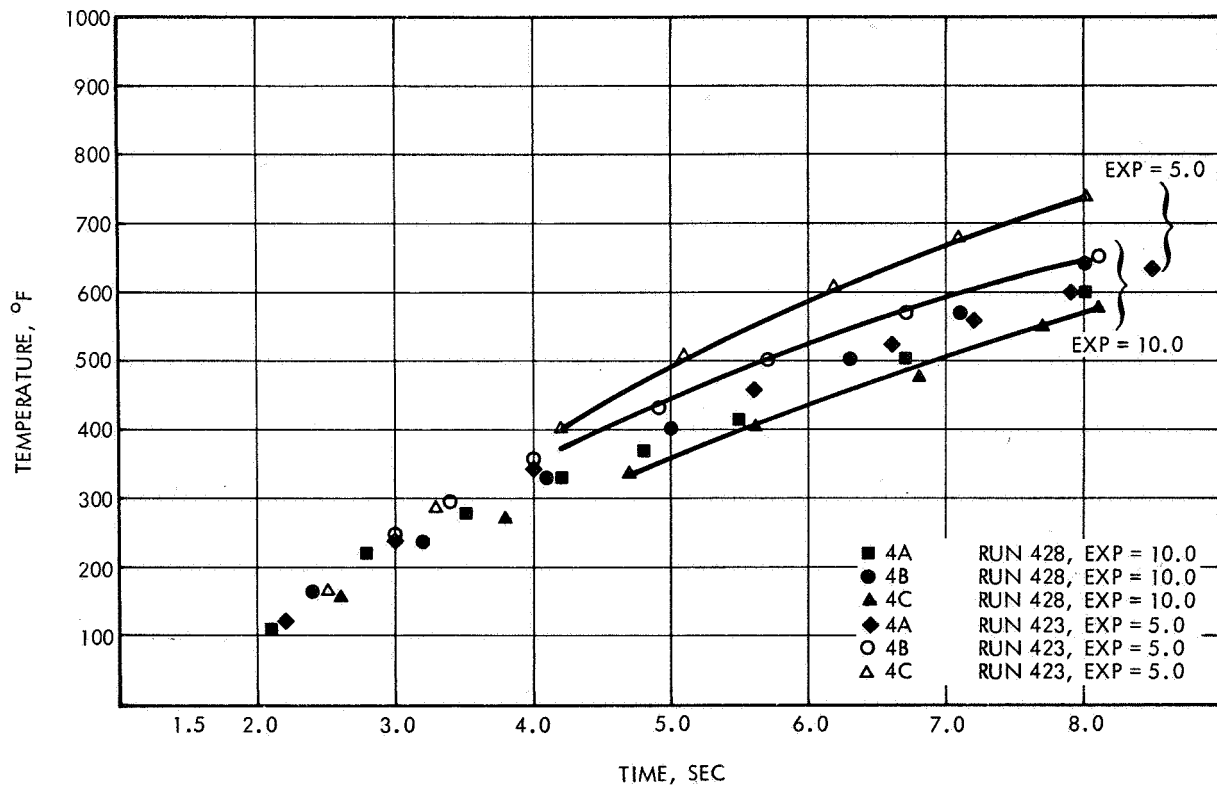
Figure 73. Radial Cu Plug Temperature-Time Traces for Protein Foam Illustrating Anti-Streaking Characteristics

100
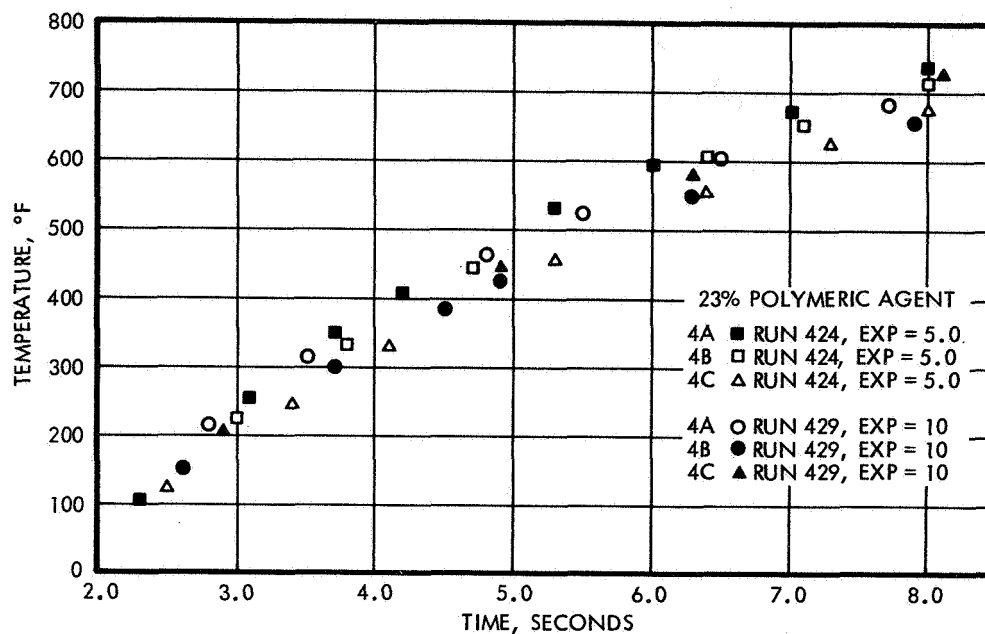
Figure 74. Radial Copper Plug Temperature-Time
Traces for Polymeric Foam Illustrating
Antistreaking Characteristics
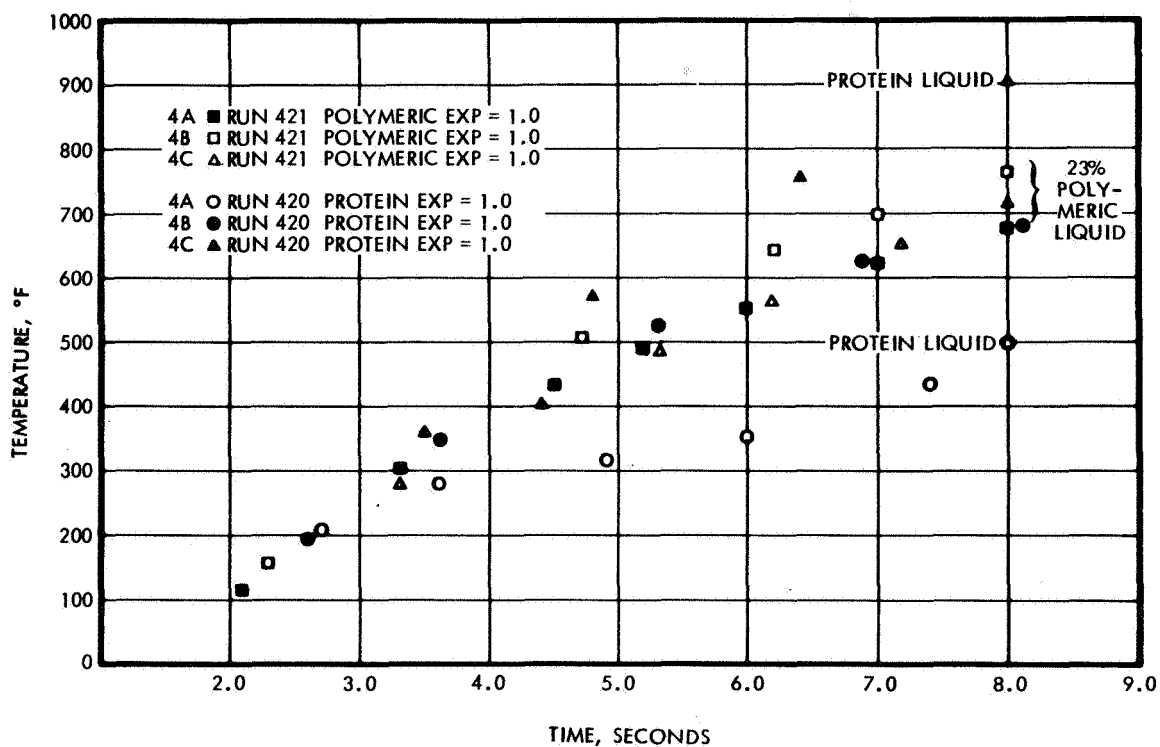
Figure 75. Copper Plug Temperature-Time Traces Showing Difference
between Protein and Polymeric Liquids

101
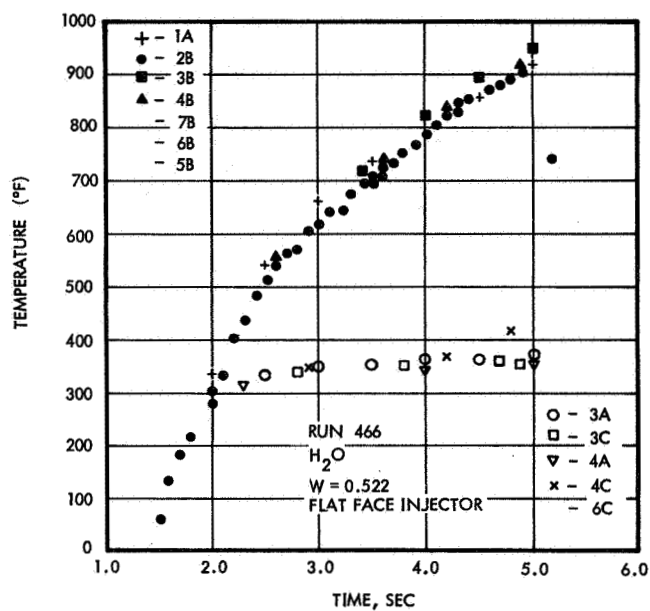
Figure 76

Chamber Temperature-Time
Traces for Water Illustrating
Susceptibility to Streaking
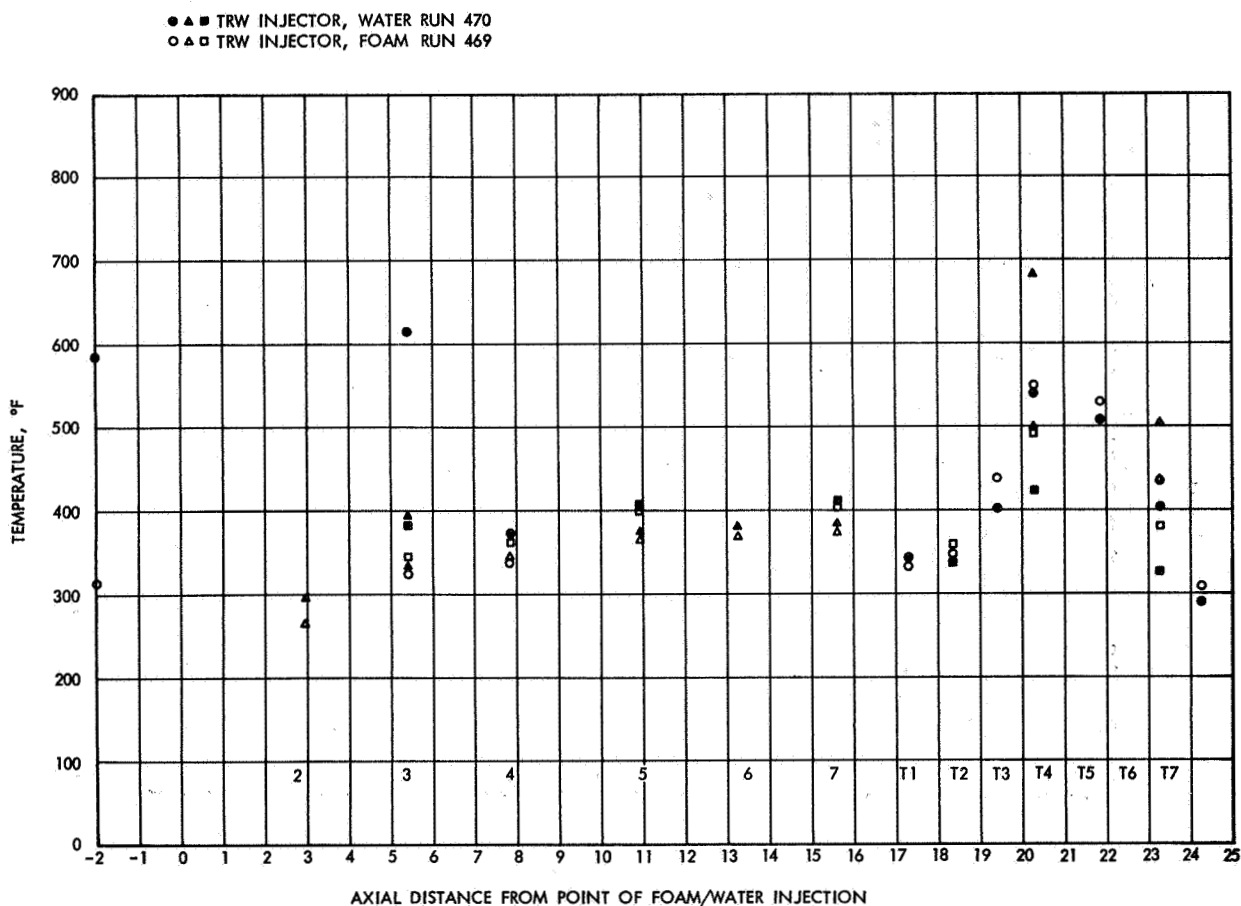
Figure 77. Comparison of Axial Temperature Traces for Water
and Protein Foam

102

5.4 COMBUSTION ROUGHNESS INTERACTION

It was readily apparent that general combustion roughness had some influence upon the results. The UDMH data clearly illustrates a superiority over that from the N_2H_4 data. A possible basic capability of the foamed liquids is that they may possess some damping characteristics. The unstable flat face injector case is worth examining in this respect.

A summary of oscillograph results of the single test with the flat face injector is given in Table 16. When these results are viewed simultaneously with the motion pictures of the test, a complete description of the test can be formulated. The start-up and early part of the run was characterized by stable, smooth combustion with "perfect" foam film cooling through the entire engine. A longitudinal pop occurred, but the engine temporarily recovered. During the pop the foam film was seen to cease flowing. A second pop occurred later and shortly thereafter the combustion was seen to go into a coupled chugging and swirling instability. During the low pressure cycle of the chugging mode, foam builds up in a "pile" underneath the point of foam injection. Then, during the upswing pressure cycle, the foam is recompressed and flows along the chamber wall. However, when the point of swirling combustion is reached, the foam is sheared from the wall, although the boundary layer remains "cloudy" through the throat. It is considered quite remarkable and a testimony to the cooling ability of foam that the acrylic engine could be run for approximately 3 seconds in this mode without any significant hardware damage.

That the first recovery from the pop was due to acoustic damping is certainly not proven; however, the possibility exists. At the second pop, the foam flow was completely disrupted and was not fed into the zone of maximum turbulence. Therefore, if it were a damper, it had been removed from the zone of effectiveness, and at the low injection velocities, could not force itself into the zone of maximum sensitivity.

Table 16. Summary of Run Data for Run 460 Flat Face Injector with Acrylic Engine

Time from Start (seconds)	
0.650	First significant pop, P_c 240, 100 cycle/sec, 40 psi
0.865	Very bad fuel oscillation, 79 cps, 74 psi peak-to-peak
1.0	Maximum chamber pressure 300.66 psia, $\Delta P_{fuel} = 112$ psi, $\Delta P_{ox} = 68$ psia
1.26	Start engine roughness (chugging and swirling)
2.44 to 2.73	Engine roughness seems to subside
3.9	Shutdown, $P_c = 189$ psia

5.5 PERFORMANCE SUMMARY

Although not of specific task interest to this program, it is of interest to examine the effect on performance with the introduction of the foamed coolants. Both theoretical and experimental performance calculations were made to determine the effect of coolant flow rate and expansion ratio upon overall performance.

Experimental performance calculations were made every one-fourth second of the run by a computer according to the following sequence of formulas.

$$P_{CD} = P_{CH}(0.991)$$

$$C^* = \frac{P_{CD}(A_t g)}{\dot{W}_p}$$

$$F_{CORR} = F_m + P_a A_E$$

$$C_F = \frac{F_{CORR}}{P_{CD} A_t}$$

$$I_{SP} = \frac{F_{CORR}}{\dot{W}_p}$$

Calculated values of C^* and I_{sp} were adjusted for the coolant flow rate by multiplying by the following factor:

$$\frac{\dot{W}_p}{\dot{W}_p + \dot{W}_c}$$

where $\dot{W}_c = \dot{W}_{H_2O} + \dot{W}_{N_g}$ (GN_2 was used as the carrier gas here.)

No other corrections were made to the data, other than the indicated standard momentum with heat addition correction. This provides a ready means of normalizing the data for comparison purposes.

Theoretical results for the characteristic velocity are given in Figure 78 for various percentages of water (the nitrogen addition has a minor effect on the results). Temperature data are given in Figure 79.

Since the primary effect is one of heat loss to the coolant, the interest should be focused on the contribution of the coolant back on performance. The raw reduced data are summarized in Table 17 for both the N_2H_4 and UDMH runs. The reduced plot of the data is given in Figure 78.

104

Table 17. Summary of Performance

Run	I_{sp}	C^*	C_F	$\dot{W}_C/\dot{W}_p$ *	L/D	$\dfrac{C^* \text{ With Coolant}}{C^* \text{ Without Coolant}}$
417	260	5445	1.53	0.0	1.31	1.0
418	263	5506	1.54	0.0	1.31	1.0
419	263	5334	1.54	0.0	1.31	1.0
420	244	5060	1.545	0.133	1.31	.934
421	236	4910	1.545	0.183	1.31	.905
422	240	4980	1.555	0.183	1.31	.917
423	217	4595	1.54	0.300	1.31	.846
424	--	4660	--	0.283	1.31	.859
425	219		1.535	0.273	1.31	.848
426	220	4610	1.53	0.267	1.31	.850
427	--	--	1.542	0.263	1.31	--
428	217	4600	1.525	0.342	1.31	.848
429	221	4610	1.54	0.337	1.31	.85
430	216	4460	1.55	0.382	1.31	.823
431	202	4240	1.537	0.366	1.31	.808
446	244	5080	1.573	0.168	2.62	
447	258	5500	1.51	0.126	2.62	
448	247	5250	1.528	0.152	2.62	
449	270	5700	1.525	0.0279	2.62	
450	247	5260	1.515	0.147	2.62	
451	247	5260	1.516	0.146	2.62	
452	248	5210	1.536	0.148	2.62	
453	248.5	5290	1.538	0.123	2.62	
454	258	5410	1.535	0.0585	2.62	
455	257.5	5380	1.542	0.087	2.62	
456	259	5400	1.54	0.0894	2.62	
457	238	4990	1.54	0.207	2.62	
458	235	4940	1.528	0.21	2.62	
459	239.5	5050	1.527	0.194	2.62	
460	235	5040	1.50	0.205	1.31	

FUEL PROPELLANT CHANGE TO UDMH

Run	I_{sp}	C^*	C_F	$\dot{W}_C/\dot{W}_p$ *	L/D	$\dfrac{C^* \text{ With Coolant}}{C^* \text{ Without Coolant}}$
461	258.6	5420	1.535	.0	2.62	1.0
462	258	5460	1.515	.0	2.62	1.0
463	239	5060	1.524	0.14	2.62	.935
464	250	5280	1.525	0.066	2.62	.972
465	246	5200	1.52	0.104	2.62	.951
466	249	5280	1.525	0.0579	2.62	.975
467	253	5350	1.521	0.0184	2.62	.985
468	228	4840	1.52	0.216	2.62	.89
469	226	4970	--	0.182	2.62	.91
470	240	5010	1.54	0.192	2.62	.915
471	252	5340	1.525	0.102	2.62	.975

* $\dot{W}_C = \dot{W}\ \text{Liquid} + \dot{W}\ N_2\ \text{Gas}$

$\dot{W}_p = \dot{W}\ \text{Fuel} + \dot{W}\ \text{Oxidizer}$
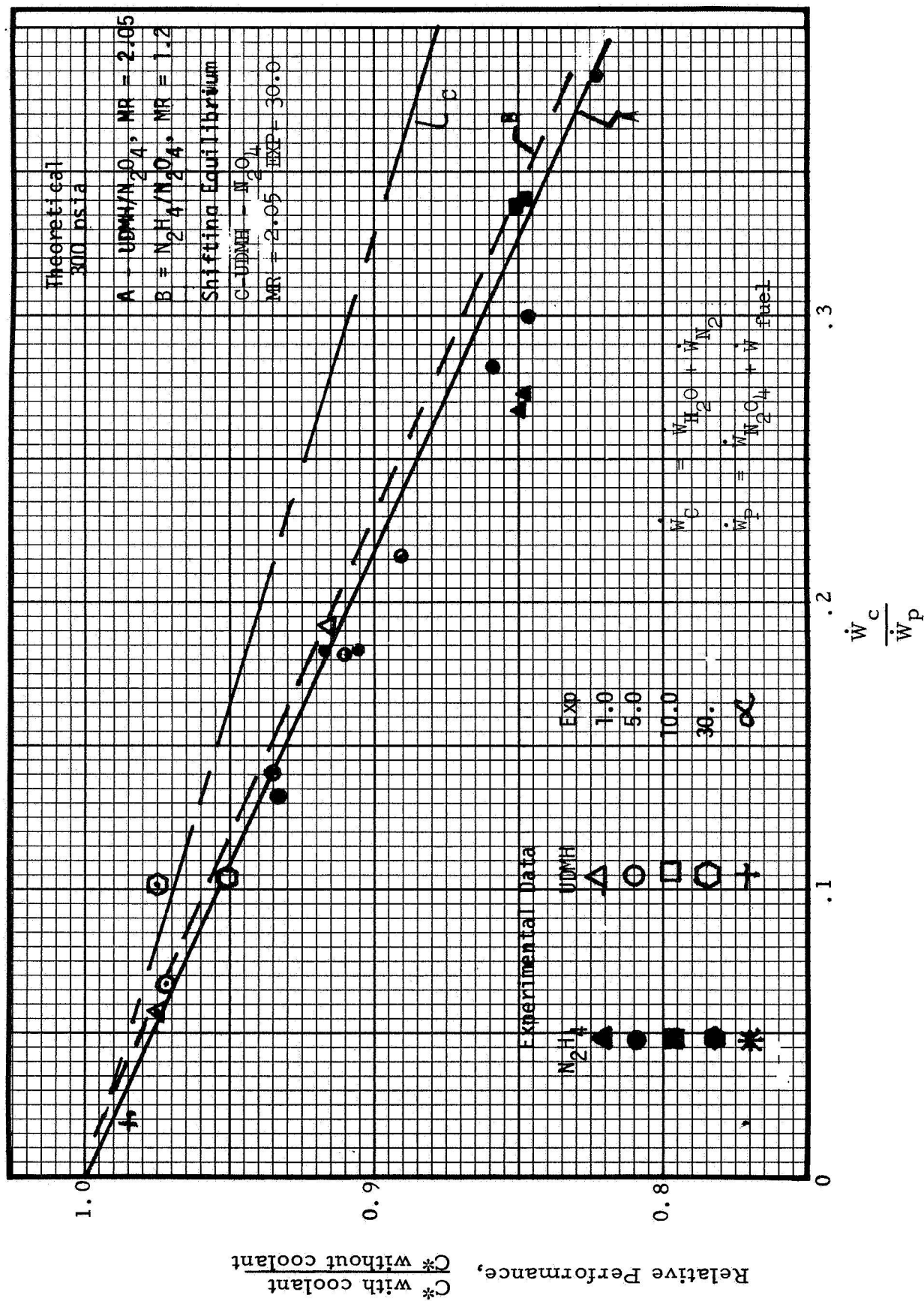
Figure 78. Relative Comparison of Theoretical and Actual Performance Without Coolant to Theoretical and Actual Performances With Coolant
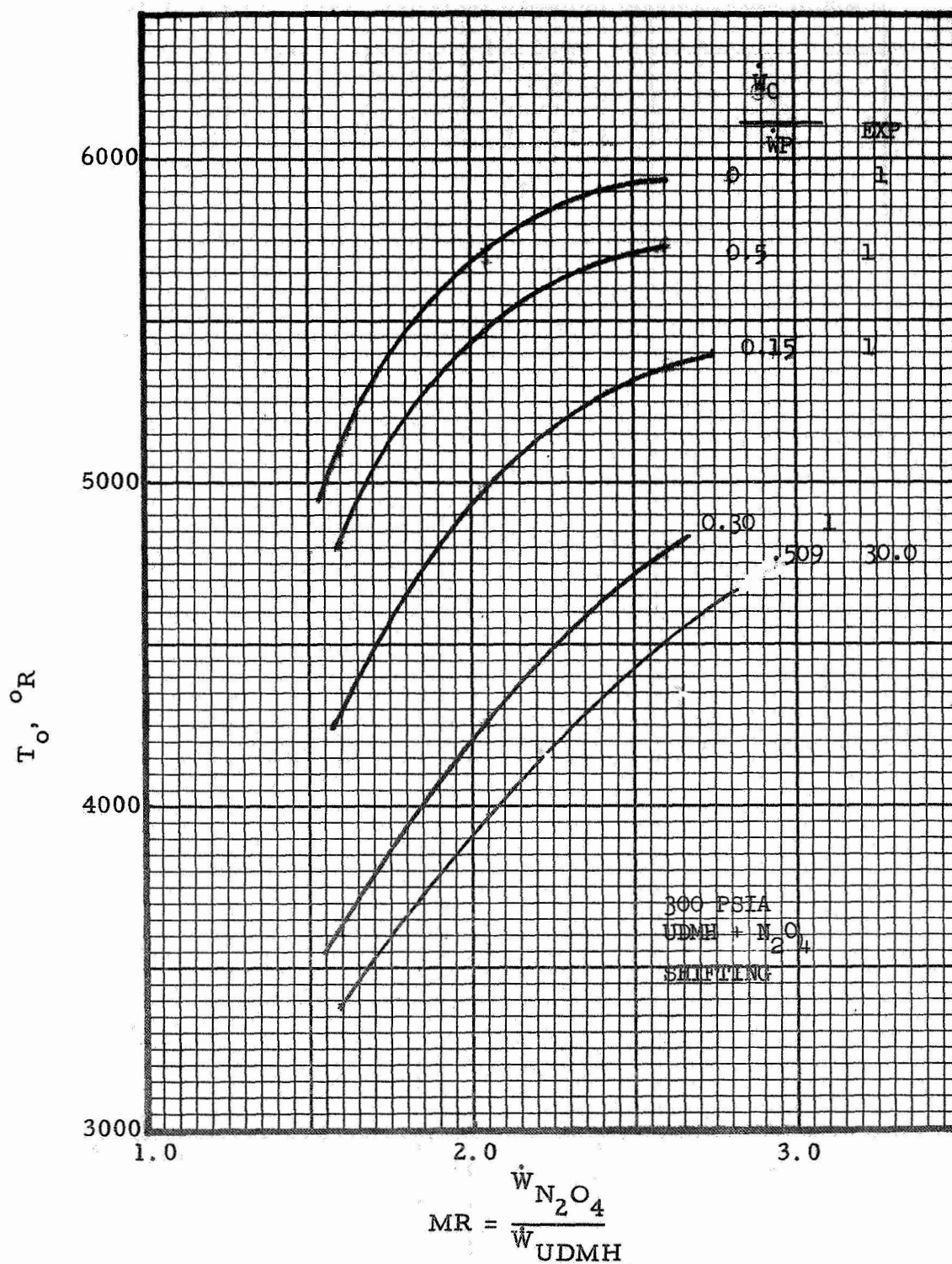
Figure 79. Theoretical Combustion Temperature As A
Function of MR for Various Coolant Fractions
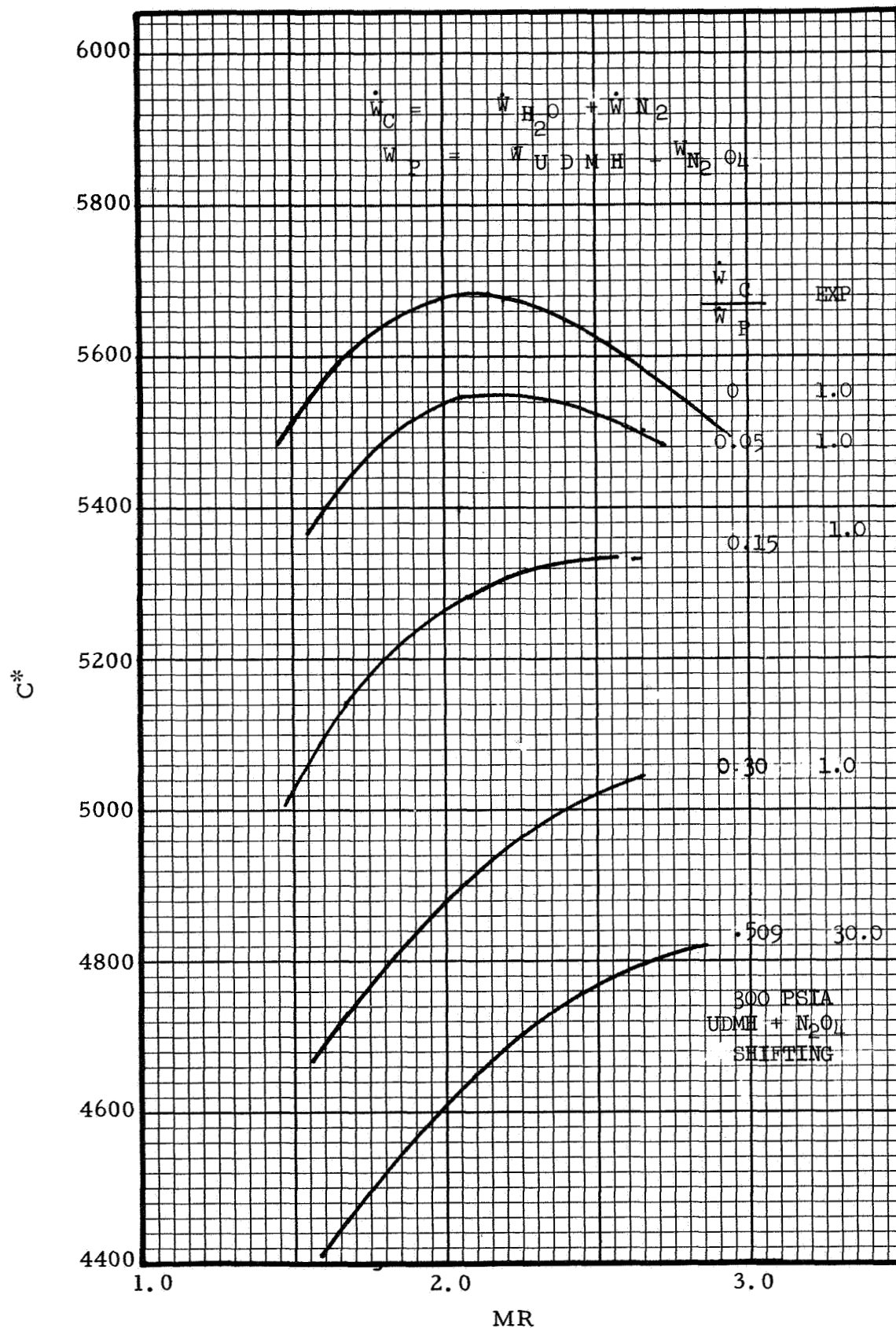
Figure 80. Theoretical Performance Versus MR for
Several Coolant Fractions

108

This relative performance figure was prepared from the data of Table 17, by plotting the ratio of performance with coolant to that without coolant versus the fraction coolant $\dot{W}_c/\dot{W}_p$. The gas flow rate was included in the coolant flow rate and becomes a significant portion at expansion ratios near 30. Data for runs 446 through 460 were not included in the correlation because no baseline run was made with this L/D. The chart shows that, in general, the performance of the coolant is ~1/2 of that for the main propellant combination, and that the performance enhancement increases with expansion ratio. The solid and dashed lines represent relative theoretical performance and UDMH + N_2O_4 for varying fraction of coolant at nominal MR's of 1.2 and 2.05, respectively. As indicated on the graph, the theoretical effect of the addition of N_2 is to increase the performance over that for the unfoamed liquid. In general, the agreement between theory and experiment is quite good.

The analysis presented in the preceeding paragraphs illustrates a potentially attractive feature of direct film cooling with foamed liquids. Further performance optimization by the use of foamed reactive coolants such as N_2H_4 may lead to nearly "free" cooling of an engine with only a slight increase in weight and complexity in an actual system.

5.6 GENERALIZED CORRELATION TO LARGER ENGINES

As a part of the analysis effort an approach to generalizing the results for design purposes was developed. The sketches given below show a simplified view of the model.

coolant   saturated
liquid   vapor

T_o — Recovery/Combustion Temperature

T_s — Saturation Temperature of Coolant

Driving force for heat transfer

TEMP
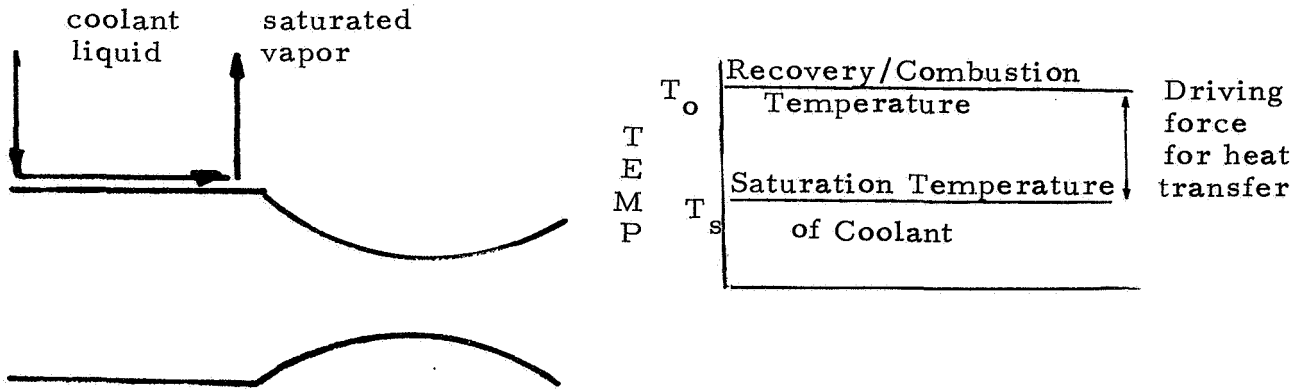
The model is constructed with the following restrictions:

(1) It deals with only the chamber wall

(2) It considers only saturation cooling, i.e., ignores super-heating of vapor

(3) An ideal case where no liquid stripping occurs.

With this simple model the quantity of coolant required to maintain the chamber wall at the saturation temperature is straightforwardly given by:

$$\dot{W}_C = \frac{\text{heat transferred to wall}}{\text{cooling capacity of liquid}} = \frac{hA\Delta T}{\Delta H_C} = \frac{h\pi DL(T_o - T_s)}{\Delta H_C}$$

where

h - heat transfer coefficient hot gas to chamber wall

A - area of chamber wall

D - diameter of chamber

L - length of chamber

T_o - combustion or recovery temperature

T_s - saturation temperature of coolant

ΔH_C - cooling capacity of liquid, heat of vaporization plus sensible heat of liquid

If the flow through the nozzle is given by the classical equation for one dimensional flow of an ideal gas:

$$\frac{\dot{W}_p}{A^*} = \sqrt{\frac{k}{R}\left(\frac{2}{k+1}\right)\exp\frac{k+1}{k-1}}\ \frac{P_o}{\sqrt{T_o}} = K\frac{P_o}{\sqrt{T_o}}$$

where

$\dot{W}_p$ = propellant flow rate

R = universal gas constant

k = ratio of specific heats

A^* = throat area

P_o = chamber pressure

T_o = stagnation temperature or combustion temperature

Then the ratio of coolant flow to propellant flow is:

$$\frac{\dot{W}_c}{\dot{W}_p} = \frac{h\frac{\Delta T}{\Delta H}\pi D L}{K\frac{P_o}{\sqrt{T_o}}A^*}$$

Approximating ΔT by T_o and multiplying and dividing by $4D/4D$ the first approximation is reached.

$$= \frac{h}{KP_o\Delta H}\ (T_o)\sqrt{T_o}\ \frac{\pi D}{A^*}\ \left(\frac{D}{L4}\right)\ \left(\frac{4L}{D}\right)$$

$$= \frac{h}{KP_o\Delta H}\ (T_o)^{3/2}\ \frac{A}{A^*}\ 4\frac{L}{D}$$

$$= \frac{h}{KP_o\Delta H}\ (T_o)^{3/2}\ (CR)\ \left(4\frac{L}{D}\right)$$

where

$$CR\ (contraction\ ratio) = \frac{chamber\ flow\ area}{throat\ area}$$

111

At this point any applicable substitution for the film coefficient, h, can be made. For simplicity, a generalized pipe flow type relationship is used

$$\frac{hD}{\lambda} = C \left[(\frac{\rho VD}{\mu}) (Pr) \right]^n$$

For rocket engines fairly good correlation in the downstream part of the combustion can be obtained with C ⁓ 0.027 to 0.030 and n of 0.75 to 0.80. Starting with the Reynolds number first, simplifications can be made as follows:

$$N_{RE} = \frac{D(\rho V)}{\mu} = \frac{D}{\mu} (\dot{W}/A) = \frac{D}{A\mu} \left(\frac{KA*P_o}{\sqrt{T_o}} \right) = \frac{DK}{\mu} \frac{1}{A/A*} \frac{P_o}{\sqrt{T_o}} = \frac{DK}{\mu} \frac{1}{CR} \frac{P_o}{\sqrt{T_o}}$$

Substitution of this relationship into the equation for heat transfer coefficient and rearrangement leads to:

$$h = C \frac{\lambda}{D} \left[\left(\frac{KP_o/\sqrt{T_o}}{CR} \frac{D}{\mu} \right) \left(\frac{C_p\mu}{\lambda} \right) \right]^{0.75}$$

$$= \left[C_p K \frac{P_o}{\sqrt{T_o} \, CR} \right]^{0.75} \left(\frac{\lambda}{D} \right)^{0.25}$$

Further substitution of this relationship into the equation for the coolant percentage leads to:

$$\frac{\dot{w}_c}{\dot{w}_p} = C \frac{\left[C_p K \dfrac{P_o}{\sqrt{T_o} \, CR} \right]^{0.75} (\frac{\lambda}{D})^{0.25}}{KP_o \Delta H} T_o^{3/2} \quad (CR) \quad (4 \frac{L}{D})$$

$$= 0.0364 \left[C_p^{0.75} (\frac{\lambda}{K})^{0.25} T_o^{1.125} \right] \left[\left(\frac{CR}{P_o D} \right)^{0.25} (4 \frac{L}{D}) \right] \frac{1}{\Delta H_c}$$

$$\begin{bmatrix} \text{Properties} \\ \text{of} \\ \text{Flowing Fluid} \end{bmatrix} \qquad \begin{bmatrix} \text{Chamber} \\ \text{Conditions} \end{bmatrix} \begin{bmatrix} \text{Coolant} \\ \text{Properties} \end{bmatrix}$$

Since the term K is related to the characteristic exhaust velocity, C*:

$$C* = \sqrt{\frac{gT_o}{\frac{k}{R}(\frac{2}{k+1})^{\frac{k+1}{k-1}}}} = \frac{(gT_o)^{1/2}}{K}$$

The equation for fraction of coolant can be further related to conventional rocket engine parameters accordingly:

$$\frac{\dot{w}_c}{\dot{w}_p} = \frac{C}{(g)^{0.125}}\left[C_p^{0.75}(\lambda C*)^{0.25}T_o\right]\left[\left(\frac{CR}{P_oD}\right)^{0.25}(4\frac{L}{D})\right]\frac{1}{\Delta H_c}$$

Interestingly, this equation says that T_o, L/D, and ΔH_c play the most important roles in determining $\dot{w}_c/\dot{w}_p$. $C*$, CR, P_o, and D are accordingly secondary parameters.

The formulas developed in the preceding paragraphs can be used to directly predict the fraction of coolant for increased engine sizes, or, more practically, to scale known results to other engine sizes by using the same propellant:

$$\%(FP)_1 = \% FP_0 \left(\frac{CR_1}{CR_0}\right)\left(\frac{D_o}{D_1}\right)^{0.25}\left(\frac{L/D_1}{L/D_0}\right)$$

Table 18 presents the results of scaling calculations using a known data point, Run 471, and a high value of C of 0.0364 for the 50K and 250K operating engines.

The results in the table show how $\dot{w}_c/\dot{w}_p$ decreases with engine size. Calculations based on predicted Q/A confirm the scaling technique.

Based upon the simplified cooling model which assumes that the coolant does not mix with the reacted propellant, a simplified performance analysis was undertaken to estimate the performance contribution of the coolant. Shown in Figure 81 are computer-calculated performances for steam at 1500° and 860°R for a range of expansions. This plot shows, in general, that the performance of the coolant is ~1/2 of that for the reactive propellants, confirming the experimental data shown in Figure 78.

These preliminary calculations which predict a very reduced coolant fraction flow with increasing engine sizes and the experimental performance results indicating negligible performance degradation with coolant may combine to make this an extremely attractive low-cost method of cooling a rocket engine.

113

Table 18. Summary of Scaling Calculations

NOMINAL THRUST	CHAMBER DIAMETER	THROAT DIAMETER	CHAMBER LENGTH	C.R.	L/D	Q/A	$\dot{\omega}_P$	$\dot{\omega}_C$	$\dot{\omega}_C/\dot{\omega}_P(100)$*	$\dot{\omega}_C/\dot{\omega}_P(100)$** Theoretical
3K	6.0	2.71	7.85	4.9	1.31	1.75 (Run 471)	8.65 (Run 471)	.52 (Run 471)	6.0 (Run 471)	3.0
50K	24.0	12.25	12, 18, 24	3.84	0.5, .75, 1.0	1.5 (est from thr)	220	3.3, 5.1, 7.0	1.5, 2.3, 3.2	.61, .92, 1.2
250K	39.0	26.	22, 34	2.25	0.564, 0.871	2.0 (est)	1000	13, 21	1.3, 2.1	.54, .84
2000K	118	79.	103	2.25	.871	1.5 (est)	80 00	131	1.63	.72

*% F.P. $= 6.0 \left(\frac{C.R.}{4.9}\right)^{0.25} \left(\frac{6.0}{D}\right)^{0.25} \left(\frac{L/D}{1.31}\right)$

**% F.P. $= \frac{(\pi DL)}{\dot{\omega}_P} \frac{(Q/A)}{\Delta H_c}$; $\Delta H_c \cong 1000 \frac{Btu}{lb}$
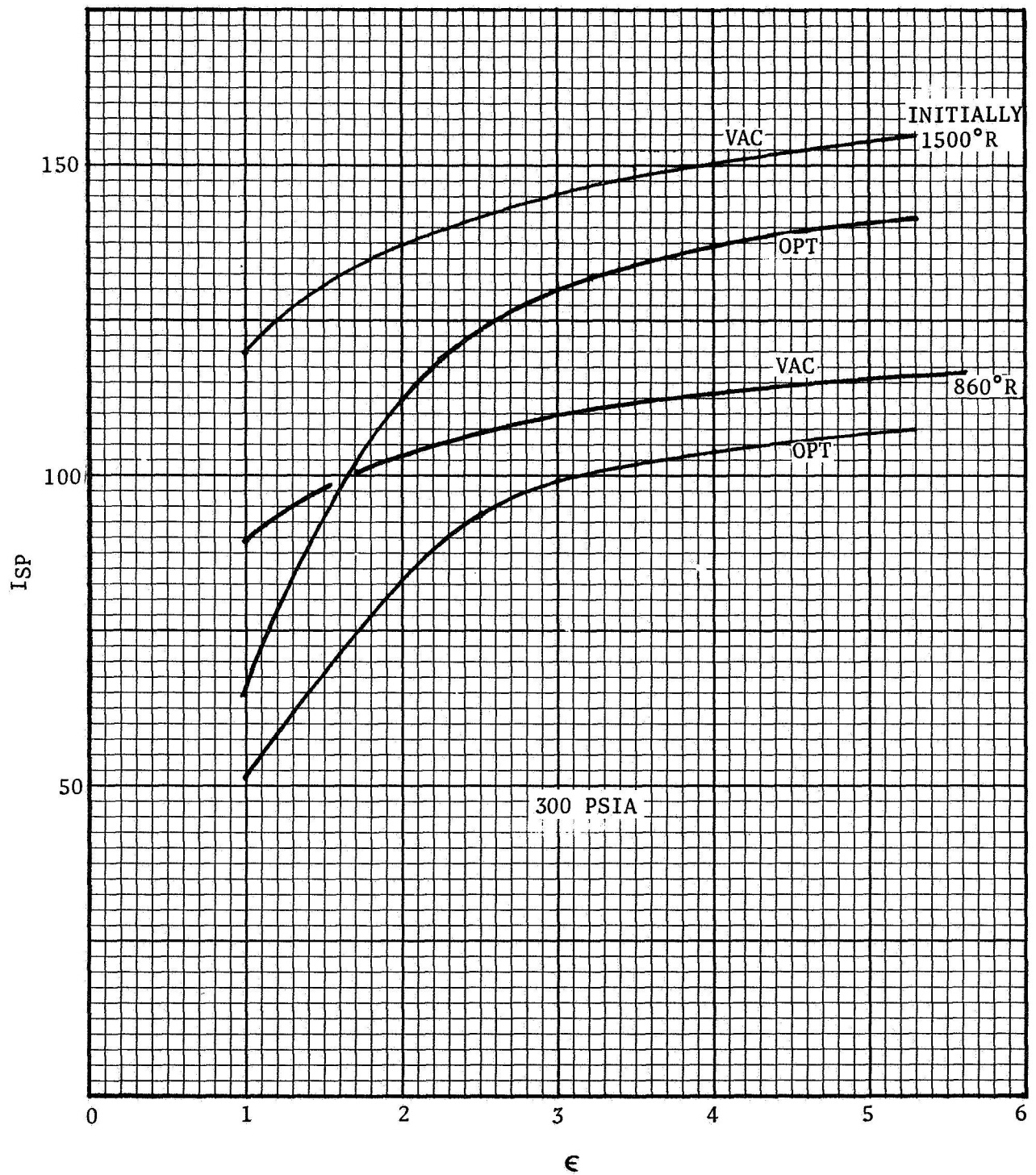
Figure 81. Steam Performance for Two Selected Temperatures

Multiple injection points have not been evaluated as yet; however, theoretical considerations show that the effectiveness can only improve. The actual need for multiple injection with foams has, of course, not been determined as yet.

6. CONCLUSIONS

An experimental-analytical study has been conducted to evaluate the feasibility of foam liquids as potential film coolants in a rocket engine. The evaluation consisted of pressure evaluation of foam on a laboratory scale, and a rocket engine heat transfer evaluation. The following conclusions were reached in the pressure evaluation of foams:

- Water fire-fighting foams made with protein or polymeric or detergent surface active agents and a N_2H_4 foam made with the polymeric agent were found to exist to pressures of at least 300 psia.

- Visual observations were made of water and N_2H_4 foam under the influence of flowing, high-pressure N_2 gas in a glass venturi 25 inches long. All foams were observed to persist in the subsonic, sonic, and trans sonic flow regimes, confirming high resistance to shear stripping.

- Satisfactory high pressure foam generation methods and rocket engine foam injection techniques were developed and proven.

Forty-one heat transfer tests conducted in heat sink and acrylic rocket engines capable of chamber length, injector, propellant combination and coolant property variations led to the following:

- Confirmation of the existence of foam in a hostile combustion and pressure environment

- That high coolant efficiencies of at least 70 percent were possible for propellant combinations having good combustion characteristics

- That foamed liquids exhibit superior cooling capacity and antistreaking characteristics to their parent liquids

- That the highest cooling efficiency was obtained for a protein foam at an expansion ratio of 20 to 30

- That cooling efficiencies were approximately halved when the injector chamber designs are not properly matched. In such instances wide coolant property variations seemed to have little effect on cooling efficiency. The point of foam injection seemed to be a significant parameter, though.

A generalized correlation was developed to show how the ratio of coolant to propellant flow markedly decreases with engine size. Coolant flows near 1 percent were predicted from actual data. The small coolant flows plus some enhanced performance drived from the coolant make the film coolant concept attractive.

117

In conclusion, the feasibility of the concept has been established and additional parametric evaluations and improvements of the foams through chemistry studies as well as injector design are warranted.

APPENDIX A

PERFORMANCE CHARACTERISTICS FOR PROPELLANT
COMBINATIONS USED IN
ADVANCED ROCKET ENGINE COOLING CONCEPT STUDY
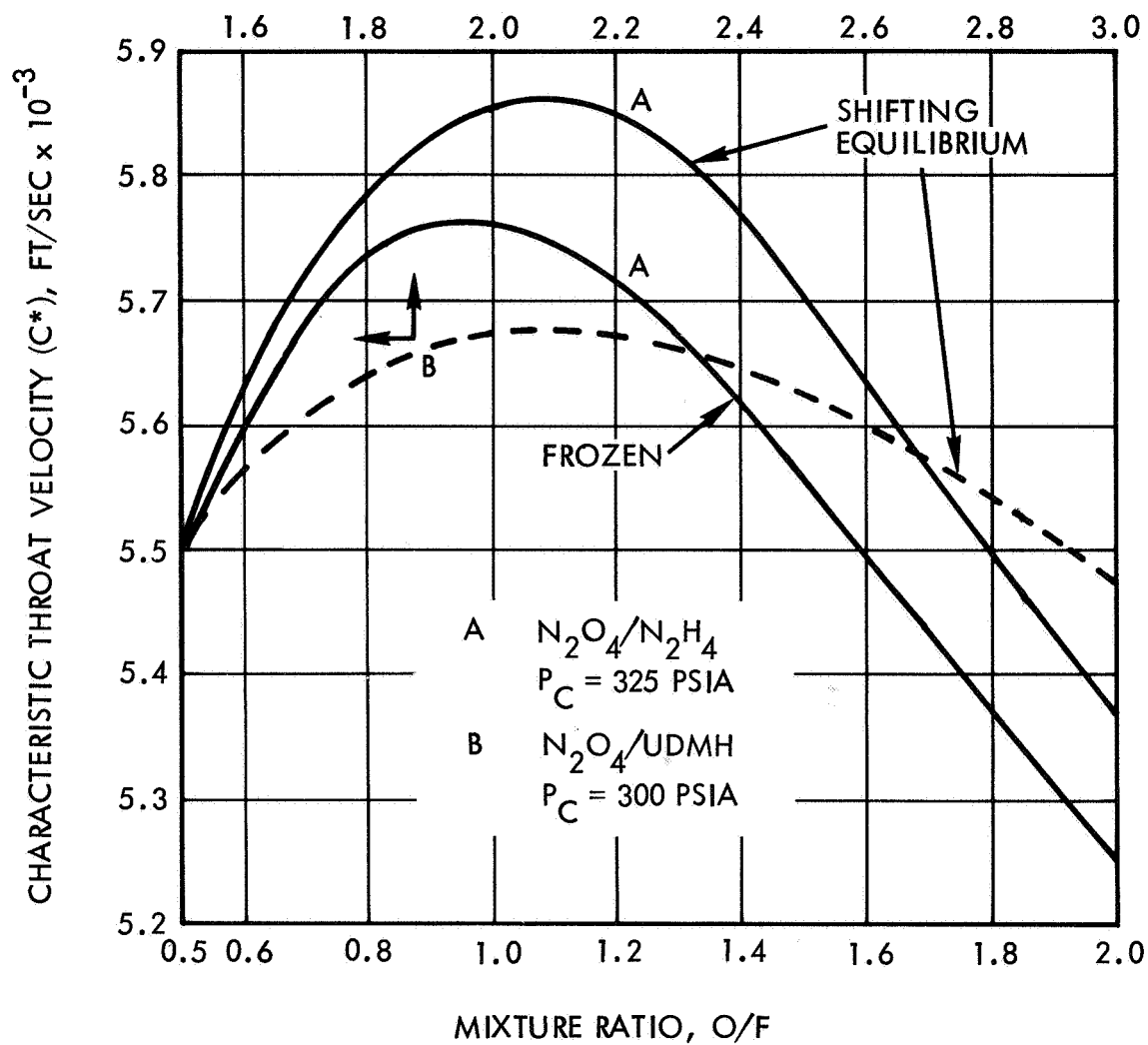
Figure A-1. Characteristic Velocity as a Function of Mixture Ratio for N_2O_4/N_2H_4
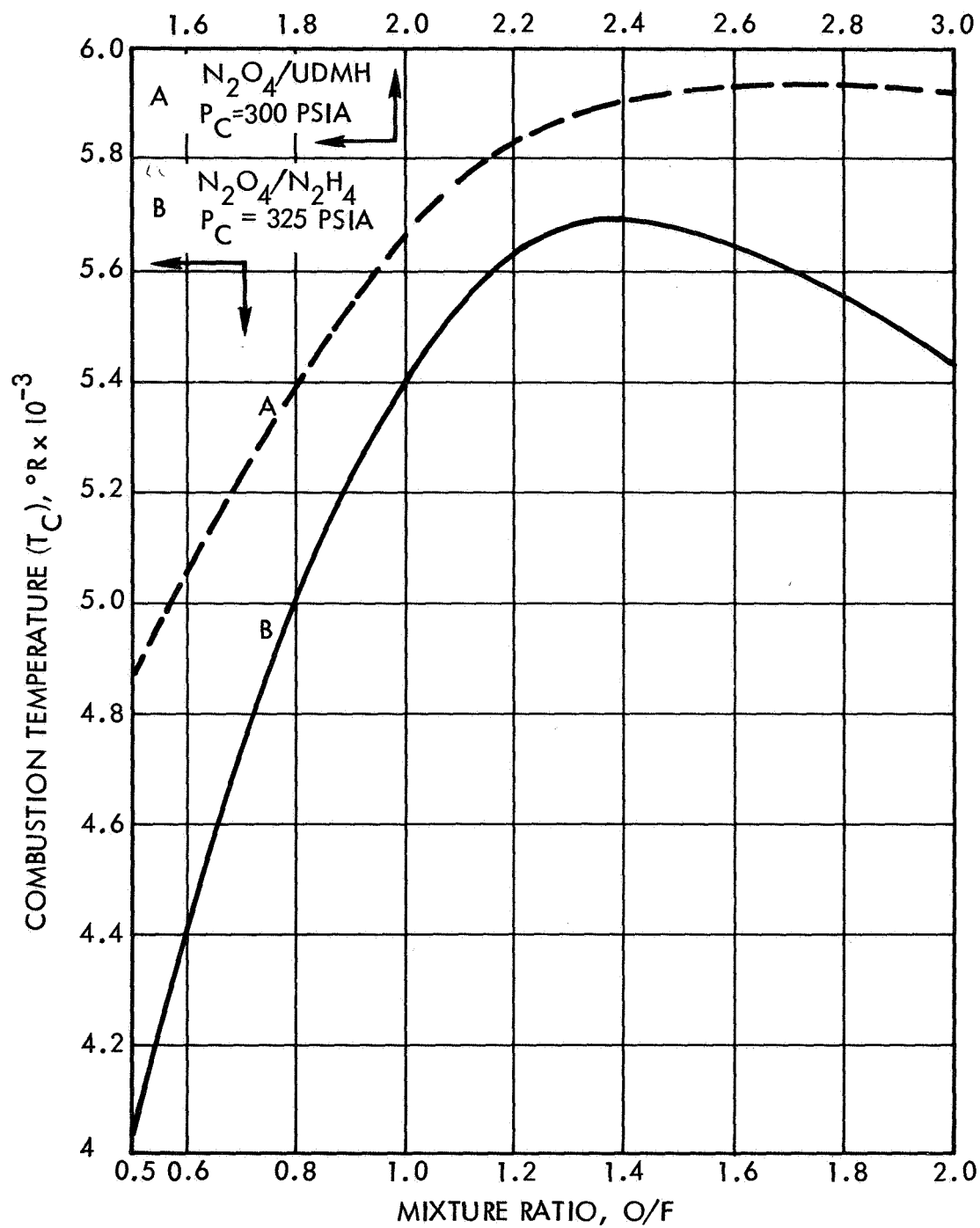
Figure A-2. Combustion Temperature Versus Mixture Ratio

NOMENCLATURE

A — Area

A^* — Throat Area

C — General constant

C_F — Thrust coefficient

CR — Contraction ratio

C_P — Heat capacity

C^* — Performance, ft/sec

D — Diameter

d — Depth of foam sample

Exp — Expansion ratio of foam, $\dfrac{V_g + V_L}{V_L}$

F — Force

F' — Applied radiation flux

Gg — Mass velocity

g — Gravitational constant

H_s — Total Enthalpy

h' — Relative Heat Resistance, $\dfrac{\theta F\ Exp}{d\rho\ H_s}$

h   Heat transfer coefficient

K — $\sqrt{\dfrac{k}{R}\left(\dfrac{2}{k+1}\right)\ exp\ \left(\dfrac{k+1}{k-1}\right)}$

k — Specific heat ratio

λ — Thermal conductivity

L — Length

MR — Mixture Ratio

P — Pressure

Q/A — Heat flux

122

R	-	Gas constant
t	-	Thickness
T	-	Temperature
V	-	Velocity
$\dot{V}$	-	ft^3/sec
$\dot{W}$	-	lb/sec
x	-	Distance
y	-	Distance
ΔH_{fg}	-	Heat of vaporization
ΔP	-	Pressure difference
ΔT	-	Temperature change
N_{Re}	-	Reynolds Number, $\dfrac{D\nu\rho}{\mu}$
Pr	-	Prandtl Number $\dfrac{C_p\mu}{\lambda}$
FP	-	Fraction Propellant
η	-	Cooling efficiency
σ	-	Surface tension
α	-	Thermal diffusity, $\dfrac{\lambda C_p}{C_p}$
τ	-	Time constant
μ	-	Viscosity
ρ	-	Density
θ	-	Measured destruction time of foam

Subscripts

S	-	Saturation
i	-	Injection
r	-	Recovery

C   -   Coolant; chamber

W   -   Wall

CD   -   Chamber down

CH   -   Chamber head

P   -   Reactive propellant

O   -   Stagnation, oxidizer

f   -   fuel

t   -   Throat

g   -   Gas

L   -   Liquid

1   -   Condition 1

2   -   Condition 2

V   -   Vaporization

VP   -   Vapor pressure

a   -   Ambient

m   -   Measured

Corr   -   Corrected

REFERENCES

1. J.S. Bikerman, Foams: Theory and Industrial Applications, Reinhold Publishing Corporation, New York, 1953.

2. S. Berkman and G. Egloff, Emulsions and Foams, Reinhold Publishing Corporation, New York, 1941.

3. A.M. Schwartz and J. W. Perry, Surface Active Agents, Vol. I, Interscience Pub. Inc., New York, 1949.

4. A.R. Aidun and C.S. Grove Jr., "Novel Uses for Aqueous Foams," Chem. Engr., 71, 4, 17 February 1964.

5. G. Morrell, "Rocket Thrust Variation with Foamed Liquid Propellants," NACA RM E56K27, February 1957.

6. R.F. Tangren, C.H. Dodye, and H.S. Seifert, "Compressibility Effects in Two-Phase Flow," J. Applied Physics, 20, 7, July 1949.

7. Rubin and E. L. Gaden Jr., "Foam Separation," New Chemical Engineering Separation Techniques Ch. 5, Ed. H.M. Schoen, Interscience Publ., New York, 1962.

8. C.S. Grove Jr., G.E. Wise, Jr., W.C. Maish, and J.B. Gray, "Viscosity of Fire-Fighting Foam," Ind. and Eng. Chem., 43, 5, May 3, 1951.

9. R. Drouhin, "La Formation des Lits de Mousse et Leur Application au Transfert de Chaleur et de Matiere," Genie Chimique, 85, 1, January 1961.

10. N.O. Clark, "Fire-Fighting Foams," Chem. and Ind., January 10 1948.

11. R.J. French, "The Resistance of Fire-Fighting Foams to Destruction by Radiant Heat," J. Appl. Chem. 2, February 1952.

12. P.H. Thomas, "The Absorption of Radiant Heat by Fire-Fighting Foam," J. Appl. Chem, 9 Part 5, May 1959.

13. D.N. Meldrum, J.R. Williams, and C.J. Conway, "Storage Life and Utility of Mechanical Fire-Fighting Foam Liquids," Fire Technology 1, 2, May 1965.

14. J.F. Fry, and R.J. French, "A Mechanical Foam-Generator For Use in Laboratories," J. Appl. Chem., 1, October 1951.

15. J. F. Fry and R. J. French, "A Laboratory Method of Comparing the Efficiencies of Fire-Fighting Air-Foams," J. Appl. Chem., I, October 1951.

16. C. R. Viswanadham, S. Singh, and U. Ranganathan, "Laboratory Test Methods For Foam Making Compounds Used in Fire Fighting," J. Sci. and Ind. Res, 19A, 10, October 1960.

17. L. A. Eggleston, "Fire Fighting Foam—Its Development and Progress," Fire Engineering, 118, No's 1, 2, 3, and 4, January 1965, pp. 38-40, February 1965, p. 34-6, March 1965, p. 46-7, 75-6 April 1965, p. 58-9, 92-3.

18. J. R. Williams, "A New Foam For Polar Solvents," Nat. Fire Protection Association Quarterly, 58, 1, July 1964.

19. D. N. Meldrum, J. R. Williams, and D. Gilroy, "Foam Fire Protection of Liquid Propellants," Fire Tech., 2, 3, August 1966.

20. C. Cunningham and G. Falkenstein, "Evaluation of Three Film-Cooling Methods in Thin-Wall, Stainless-Steel, Radiation-Cooled Thrust Chambers," Rocketdyne Research Dept. No. 65-13, April 1965.

21. G. R. Kinney, A. E. Abramson, and J. L. Sloop, "Internal-Liquid-Film Cooling Experiments with Air-Stream Temperatures to 2000°F in 2- and 4-Inch Diameter Horizontal Tubes," NACA Report 1087, 1952.

22. W. B. Powell, and T. W. Price, "A Method for the Determination of Local Heat Flux from Transient Temperatures," Vol. 3, No. 3, ISA Transactions 1964.

23. S. Bell, Final Report on Air Force Contract F04611-68-C-0054, in Preparation.

DISTRIBUTION

Report Copies	Recipient	Designee
	National Aeronautics and Space Administration Lewis Research Center 21000 Brookpark Road Cleveland, Ohio 44135 Attn:	
5	Liquid Rocket Technology Branch, MS 500-209	
1	Technical Report Control Office, MS 5-5	
1	Technology Utilization Office, MS 3-16	
2	AFSC Liaison Office, MS 4-1	
2	Library	
1	Office of Reliability and Quality Assurance, MS 500-111	
1	D. L. Nored, Chief, LRTB, MS 500-209	
3	E. A. Edelman, Project Manager, MS 500-209	
1	E. W. Conrad, MS 500-204	
2	Chief, Liquid Experimental Engineering, RPX Office of Advanced Research and Technology NASA Headquarters Washington, D. C. 20546	
2	Chief, Liquid Propulsion Technology, RPL Office of Advanced Research and Technology NASA Headquarters Washington, D. C. 20546	
1	Director, Launch Vehicles and Propulsion, SV Office of Space Science and Applications NASA Headquarters Washington, D. C. 20546	

Report Copies	Recipient	Designee
1	Director, Advanced Manned Missions, MT Office of Manned Space Flight NASA Headquarters Washington, D. C. 20546	
6	NASA Scientific and Technical Information Facility P. O. Box 33 College Park, Maryland 20740	
1	Director, Technology Utilization Division Office of Technology Utilization NASA Headquarters Washington, D. C. 20546	
1	National Aeronautics and Space Administration Ames Research Center Moffett Field, California 94035 Attn: Library	
1	National Aeronautics and Space Administration Flight Research Center P. O. Box 273 Edwards, California 93523 Attn: Library	
1	National Aeronautics and Space Administration Goddard Space Flight Center Greenbelt, Maryland 20771 Attn: Library	Merlund L. Moseson, Code 620
1	National Aeronautics and Space Administration John F. Kennedy Space Center Cocoa Beach, Florida 32931 Attn: Library	Dr. Kurt H. Debus
1	National Aeronautics and Space Administration Langley Research Center Langley Station Hampton, Virginia 23365 Attn: Library	Ed Cartwright, Director
1	National Aeronautics and Space Administration Manned Spacecraft Center Houston, Texas 77001 Attn: Library	J. G. Thiobodaux, Jr. Chief, Propulsion and Power Division

2

Report Copies	Recipient	Designee
1	National Aeronautics and Space Administration George C. Marshall Space Flight Center Huntsville, Alabama 35812 Attn: Library	Keith Chandler, Hans G. Paul, Leon J. Hastings, James Thomas
1	Jet Propulsion Laboratory 4800 Oak Grove Drive Pasadena, California 91103 Attn: Library	Henry Burlage, Jr. Duane Dipprey
1	Defense Documentation Center Cameron Station Building 5 5010 Duke Street Alexandria, Virginia 22314 Attn: TISIA	
1	Office of the Director of Defense Research and Engineering Washington, D. C. 20301 Attn: Office of Asst. Dir. (Chem. Technology)	
1	NASA Pasadena Office 4800 Oak Grove Drive Pasadena, California 91103 Attn: F. A. Abbott	
1	RTD (RTNP) Bolling Air Force Base Washington, D. C. 20332	
1	Arnold Engineering Development Center Air Force Systems Command Tullahoma, Tennessee 37389 Attn: Library	Dr. H. K. Doetsch
1	Advanced Research Projects Agency Washington, D. C. 20525 Attn: Library	D. E. Mock
1	Aeronautical Systems Division Air Force Systems Command Wright-Patterson Air Force Base, Dayton, Ohio Attn: Library	D. L. Schmidt Code ARSCNC-2

3

Report Copies	Recipient	Designee
1	Air Force Missile Test Center Patrick Air Force Base, Florida Attn: Library	L. J. Ullian
1	Air Force Systems Command Andrews Air Force Base Washington, D. C. 20332 Attn: Library	Capt. S. W. Bowen SCLT
1	Air Force Rocket Propulsion Laboratory (RPCC) Edwards, California 93523 Attn: Don McGregor	
1	Air Force Rocket Propulsion Laboratory (RPRRE) Edwards, California 93523 Attn: Library	
1	Air Force FTC (FTAT-2) Edwards Air Force Base, California 93523 Attn: Library	Donald Ross
1	Air Force Office of Scientific Research Washington, D. C. 20333 Attn: Library	SREP, Dr. J. F. Masi
1	Director (Code 6180) U. S. Naval Research Laboratory Washington, D. C. 20390 Attn: Library	H. W. Carhart J. M. Krafft
1	Picatinny Arsenal Dover, New Jersey 07801 Attn: Library	I. Forsten
1	Air Force Aero Propulsion Laboratory Research and Technology Division Air Force Systems Command United States Air Force Wright-Patterson AFB, Ohio 45433 Attn: APRP (Library)	R. Quigley C. M. Donaldson
1	Electronics Division Aerojet-General Corporation P. O. Box 296 Azusa, California 91703 Attn: Library	W. L. Rogers

Report Copies	Recipient	Designee
1	Space Division Aerojet-General Corporation 9200 East Flair Drive El Monte, California 91734 Attn: Library	S. Machlawski
1	Propulsion Division Aerojet-General Corporation P. O. Box 15847 Sacramento, California 95803 Attn: Technical Library 2484-2015A	R. Stiff
1	Aeronutronic Division of Philco Ford Corp. Ford Road Newport Beach, California 92663 Attn: Technical Information Department	D. A. Carrison Dr. L. H. Linder
1	Aerospace Corporation 2400 E. El Segundo Blvd. Los Angeles, California 90045 Attn: Library-Documents	J. G. Wilder
1	Arthur D. Kittle, Inc. 20 Acorn Park Cambridge, Massachusetts 02140 Attn: Library	A. C. Tobey
1	Astropower Laboratory McDonnell-Douglas Aircraft Company 2121 Paularino Newport Beach, California 92163 Attn: Library	Dr. George Moc Director Research
1	Astrosystems, International 1275 Bloomfield Avenue Fairfield, New Jersey 07007 Attn: Library	A. Mendenhall
1	ARO, Incorporated Arnold Engineering Development Center Arnold AF Station, Tennessee 37389 Attn: Library	Dr. B. H. Goethert

Report Copies	Recipient	Designee
1	Susquehanna Corporation Atlantic Research Division Shirley Highway and Edsall Road Alexandria, Virginia 22314 Attn: Library	Dr. Ray Friedman
1	Battelle Memorial Institute 505 King Avenue Columbus, Ohio 43201 Attn: Report Library, Room 6A	
1	Beech Aircraft Corporation Boulder Facility Box 631 Boulder, Colorado Attn: Library	Douglas Pope
1	Bell Aerosystems, Inc. Box 1 Buffalo, New York 14205 Attn: Library	T. Reinhardt W. M. Smith
1	Bendix Systems Division Bendix Corporation 3300 Plymouth Street Ann Arbor, Michigan Attn: Library	John M. Brueger
1	Boeing Company Space Division P. O. Box 868 Seattle, Washington 98124 Attn: Library	J. D. Alexander C. F. Tiffany
1	Chemical Propulsion Information Agency Applied Physics Laboratory 8621 Georgia Avenue Silver Spring, Maryland 20910	Tom Reedy
1	Chrysler Corporation Missile Division P. O. Box 2628 Detroit, Michigan Attn: Library	John Gates
1	Chrysler Corporation Space Division New Orleans, Louisiana Attn: Librarian	

Report Copies	Recipient	Designee
1	Fairchild Stratus Corporation Aircraft Missiles Division Hagerstown, Maryland Attn: Library	J. S. Kerr
1	General Dynamics/Convair P. O. Box 1128 San Diego, California 92112 Attn: Library	Frank Dore R. Roberts
1	Missiles and Space Systems Center General Electric Company Valley Forge Space Technology Center P. O. Box 855 Philadelphia, Pa. 190101 Attn: Library	F. E. Schultz F. Meger
1	Grumman Aircraft Engineering Corporation Bethpage, Long Island, New York Attn: Library	Joseph Gavin
1	Hercules Powder Company Allegheny Ballistics Laboratory P. O. Box 210 Cumberland, Maryland 21501 Attention: Library	
1	Honeywell Inc. Aerospace Division 2600 Ridgeway Road Minneapolis, Minn. Attn: Library	Gordon Harris
1	IIT Research Institute Technology Center Chicago, Illinois 60616 Attn: Library	C. K. Hersh
1	Kidde Aero-Space Division Walter Kidde and Company, Inc. 567 Main Street Belleville 9, New Jersey Attn: Library	R. J. Hanville
1	Ling-Temco-Vought Corp. P. O. Box 5907 Dallas, Texas 75222 Attn: Library	Warren G. Trent

Report Copies	Recipient	Designee
1	Lockheed Missiles and Space Company P. O. Box 504 Sunnyvale, California 94087 Attn: Library	V. C. Lee J. Guill
1	Lockheed-California Company 10445 Glen Oaks Blvd. Pacoima, California Attn: Library	G. D. Brewer
1	Lockheed Propulsion Company P. O. Box 111 Redlands, California 92374 Attn: Library, Thackwell	H. L. Thackwell
1	Marquardt Corporation 16555 Saticoy Street Box 2013 - South Annex Van Nuys, California 91409	W. D. Boardman, Jr. Howard McFarland
1	Martin-Marietta Corporation Baltimore Division Baltimore, Maryland 21203 Attn: Library	John Calathes C. E. Thomas
1	Denver Division Martin-Marietta Corp. P. O. Box 179 Denver, Colorado 80201 Attn: Library	Dr. Morganthaler F. R. Schwartzberg I. W. Murphy
1	Orlando Division Martin-Marietta Corp. Box 5827 Orlando, Florida Attn: Library	J. Fern
1	Western Division McDonnel Douglas Aircraft Company, Inc. 3000 Ocean Park Blvd. Santa Monica, California 90406 Attn: Library	R. W. Hallet G. W. Burke Paul Klevatt
1	Northrop Space Laboratories 3401 West Broadway Hawthorne, California Attn: Library	Dr. William Howard

Report Copies	Recipient	Designee
1	Purdue University Lafayette, Indiana 47907 Attn: Library (Technical)	S. Fairweather
1	Rocket Research Corporation Willow Road at 116th St. Redmond, Washington 98052 Attn: Library	Fy McCullough, Jr.
1	Rocketdyne Division of Rockwell North American Rockwell Inc. 6633 Canoga Avenue Canoga Park, California 9134 Attn: Library, Department 596-306	Dr. R. J. Thompson S. F. Iacobellis
1	Space and Missile System Organization Air Force Unit Post Office Los Angeles, California 90045 Attn: Technical Data Center	
1	Office of Research Analyses (OAR) Holloman Air Force Base New Mexico 88330 Attn: Library	Major R. E. Bracken, Code MDGRT
1	U. S. Air Force Washington, D. C. Attn: Library	Col. C. K. Stambaugh, Code AFRST
1	Commanding Officer U. S. Army Research Office (Durham) Box CM, Duke Station Durham, North Carolina 27706 Attn: Library	
1	U. S. Army Missile Command Redstone Scientific Information Center Redstone Arsenal, Alabama 35808 Attn: Document Section	Dr. W. Wharton
1	Bureau of Naval Weapons Department of the Navy Washington, D. C. Attn: Library	J. Kay, Code RTMS-41
1	Commander U. S. Naval Missile Center Point Mugu, California 93041 Attn: Technical Library	

Report Copies	Recipient	Designee
1	Commander U.S. Naval Weapons Center China Lake, California 93557 Attn: Library	W. F. Thorm Code 4562
1	Commanding Officer Naval Research Branch Office 1030 E. Green Street Pasadena, California 91101 Attn: Library	
1	Stanford Research Institute 333 Ravenswood Avenue Menlo Park, California 94025 Attn: Library	Thor Smith Dr. Gerald Marksman P. R. Gillette
1	Thiokol Chemical Corporation Reaction Motors Division Denville, New Jersey 07834 Attn: Library	A. Sherman Dwight S. Smith
1	Thiokol Chemical Corporation Redstone Division Huntsville, Alabama Attn: Library	John Goodloe
1	TRW System Group 1 Space Park Redondo Beach, California 90278 Attn: STL Tech. Lib. Doc. Acquisitions	G. W. Elverum
1	TRW Incorporated TAPCO Division 23555 Eucild Avenue Cleveland, Ohio 44117	P. T. Angell
1	United Aircraft Corporation Corporation Library 400 Main Street East Hartford, Connecticut 06108 Attn: Library	Dr. David Rix Erle Martin
1	United Aircraft Corporation Pratt and Whitney Division Florida Research and Development Center P. O. Box 2691 West Palm Beach, Florida 33402 Attn: Library	R. J. Coar Dr. Schmitke

Report Copies	Recipient	Designee
1	Rohm and Hass Company Redstone Arsenal Research Division Huntsville, Alabama 35808 Attn: Librarian	
1	United Aircraft Corporation United Technology Center P. O. Box 358 Sunneyvale, California 94088 Attn: Librarian	Dr. David Altman
1	North American Rockwell, Inc. Space and Information Systems Division 12214 Lakewood Boulevard Downey, California 90241 Attn: Technical Librarian	H. Storms
	Chemical Propulsion Information Agency Applied Physics Laboratory 8621 Georgia Avenue Silver Spring, Maryland 20910	Tom Reedy